INFORMATION TO USERS

This manuscript has been reproduced from the microfilm master. UMI films the text directly from the original or copy submitted. Thus, some thesis and dissertation copies are in typewriter face, while others may be from any type of computer printer.

The quality of this reproduction is dependent upon the quality of the copy submitted. Broken or indistinct print, colored or poor quality illustrations and photographs, print bleedthrough, substandard margins, and improper alignment can adversely affect reproduction.

In the unlikely event that the author did not send UMI a complete manuscript and there are missing pages, these will be noted. Also, if unauthorized copyright material had to be removed, a note will indicate the deletion.

Oversize materials (e.g., maps, drawings, charts) are reproduced by sectioning the original, beginning at the upper left-hand corner and continuing from left to right in equal sections with small overlaps. Each original is also photographed in one exposure and is included in reduced form at the back of the book.

Photographs included in the original manuscript have been reproduced xerographically in this copy. Higher quality 6" x 9" black and white photographic prints are available for any photographs or illustrations appearing in this copy for an additional charge. Contact UMI directly to order.

UMI®

Bell & Howell Information and Learning
300 North Zeeb Road, Ann Arbor, MI 48106-1346 USA
800-521-0600

Flow Phenomena in Horizontal Axially Rotated Partially-filled Cylinders

by

KADIR BULENT BELIBAGLI

A Thesis Submitted to the
Faculty of Engineering
in Partial Fulfilment of the Requirements
for the Degree of

DOCTOR OF PHILOSOPHY

Major Subject: Food Science and Technology

APPROVED:

[redacted]
Dr. Feridun Hamdullahpur (Co-Supervisor)

[redacted]
Dr. Allan T. Paulson (Co-Supervisor)

[redacted]
Dr. Marvin A. Tung

[redacted]
Dr. R. Alex Speers

[redacted]
Dr. M. Andy Rao (External examiner, Cornell University)

DALHOUSIE UNIVERSITY, DALTECH

Halifax, Nova Scotia 1998

DALTECH, DALHOUSIE UNIVERSITY

"AUTHORITY TO DISTRIBUTE MANUSCRIPT THESIS"

The above library may make available or authorize another library to make available individual photo/microfilm copies of this thesis without restrictions.

Full Name of Author: KADIR BULENT BELIBAGLI

Signature of Author: 

Date: Sept. 15th /98

TABLE OF CONTENTS

LIST OF TABLES

LIST OF FIGURES

LIST OF SYMBOLS AND ABBREVIATIONS

A	area	m^2
A_A	frequency factor in Arrhenius relationship	l/s
a	number of cells in the initial population	cfu/mL
b	number of cells in the final population	cfu/mL
C_p	heat capacity	J/kg K
D	can diameter	m
D_f	optical fringe spacing	m
D_r	retort diameter	m
D_{ro}	diameter of the rotation	m
D_{re}	decimal reduction time at retort temperature	min
d	distance	m
$\boldsymbol{E}$	electric vector	___
E	height of headspace	m
E_A	activation energy in Arrhenius relationship	kJ/kg
e	photodetector output voltage	V
F_o	equivalent sterilization time at 121.1 °C for z = 10 C°	min
F_d	measured Doppler frequency	MHz
F_{shift}	frequency shift	MHz
f	frequency	Hz
f_D	Doppler frequency	Hz
g	acceleration due to gravity (= 9.80)	m/s^2
h	heat transfer coefficient or film coefficient	W/m^2K
I	intensity	W/m^2
J	light flux	W
k	thermal conductivity	W/mK
k	wave number	m^{-1}
L	length	m

L_c	characteristic length	m
m	consistency coefficient for a power-law non-Newtonian fluid	Ns^n/m^2
N	rotation speed	1/s, rpm
n	flow behaviour index for a power-law non-Newtonian fluid	___
n_p	refractive index of particle	___
n_w	refractive index of water	___
P	pressure	N/m^2
$\hat{p}$	polarization direction	unit vector
Q_{ii}	Eulerian correlation tensor	___
q	heat transfer rate	W
R	universal gas constant (= 8.314)	J/kgK
$\hat{r}$	position in the far field	____
r	radial position	m
r_b	equivalent bubble radius	m
S_B	Stefan-Boltzman constant (= 5.669×10^{-8})	W/m^2K^4
$\hat{s}$	propagation direction	____
T	temperature	K
t	time	s
t_{rl}	time for one full reel rotation	s
t_{rr}	time during a reel rotation, in which cans rotate	s
t_s	time, during a reel rotation, in which can does not rotate	s
U	overall heat transfer coefficient	W/m^2K
U	average velocity	m/s
u	velocity	m/s
V	velocity	m/s
V_c	volume of can	m^3
v	velocity	m/s
x	position, distance	m

y	distance	m
z	number of Celsius degrees required for thermal destruction curve to traverse one log cycle	C°
z	distance	m

Subscripts

c	can
D	Doppler
f	fluid
h	headspace
i	initial
l	scattered beam
ol	ith illuminating beam
r	retort
s	surface
w	evaluated at wall temperature

Greek letters

α	thermal diffusivity	m^2/s
β	volume coefficient of expansion	1/K
ρ	density	kg/m^3
Φ	phase	____
Σ	kinetic energy	J
ϵ_m	emissivity	____
σ	shear stress	N/m^2
σ	scattering coefficient	____
σ	standard deviation	____
η	apparent viscosity	Pa.s
η_b	apparent viscosity at bulk temperature	Pa.s
η_w	apparent viscosity at wall temperature	Pa.s
λ	wavelength	m
κ	half angle between illuminating beams	rad
$\dot{\gamma}$	shear rate	s^{-1}
μ_a	kinematic viscosity	mPa.s
μ_r	relative refractive index	____
τ	time burst	s
ω	angular velocity (= 2 π N)	1/s
ϖ	circular frequency	rad/s

Dimensionless Groups

Gr	Grashof number	$Gr = \frac{\rho^2 g \beta D^3 \Delta T}{\eta^2}$
Fr	Froude number	$Fr = \frac{r\omega^2}{g}$
Re	Reynolds number	$Re = \frac{L_c V_v \rho}{\eta}$
Re_r	Rotational Reynolds number based on diameter of rotation	$Re_r = \frac{D_r^2 N \rho}{\eta}$
Re_g	Rotational Reynolds number based on bubble diameter	$\mathrm{Re}_g = \frac{\omega r_b^2}{\nu}$
GPr	Generalized Prandtl number	$GPr = \frac{C_p m 8^{n-1}(3n+1)^n}{kN^{1-n}(4n)^n}$
Gre	Generalized Reynolds number	$G\mathrm{Re} = \frac{D_c^2 N^{2-n} \rho}{8^{n-1} m \left(\frac{3n+1}{4n}\right)^n}$
Nu	Nusselt number	$Nu = \frac{h L_c}{k}$
Pr	Prandtl number	$\mathrm{Pr} = \frac{\rho C_p}{k}$
We	Weber number	$We = \frac{w^2 L_c^2 \pi D}{\tau}$

ACKNOWLEDGEMENTS

I would like to thank my present co-supervisors, Dr. Allan T. Paulson and Dr. Feridun Hamdullahpur, and my former supervisor Dr. Marvin A. Tung for advice, encouragement, assistance, moral support and undying great patience during the duration of this study. Their high professional standards and skills with people have been an inspiration to me.

I would like to thank my guiding committee: Drs. Paulson, Hamdullahpur, Rao, Tung and Speers for guidance and their advice.

Sincere thanks to my friend Murat Koksal for his time to review my thesis and to make useful comments.

I would like to thank all staff members in the Department of Food Science and Technology for their assistance.

I would like to thank my friends; Ali, Selcuk, Caner, Merih, Burak, Levent, Indrasena, Yulai, Bill, Julian, Lisbeth, Fa, Alberto, Surender and Sjofn, Dihui, Clare, Roberta and all fellow students in our department for their help, friendship and support.

I would like to thank to the entire Department of Food Science and Technology, especially John Thompson, Doug Singer and Gerry Morello.

I sincerely appreciate Ian Britt's contribution in the design and construction of the flow device to simulate steady and intermittent axial rotation.

Special thanks to Arzu, for her unwavering support and encouragement throughout the years for making all this possible.

I would like to acknowledge the financial support from Gaziantep University, Turkey, and the Natural Sciences and Engineering Research Council of Canada.

Finally, I would like to thank my parents and my family for their moral support. These have perhaps been the most difficult years. To them I owe more than words can say; it is to my family this work is dedicated.

ABSTRACT

Velocity fields in a partially-filled rotating horizontal cylinder were determined by a Laser Doppler Velocimeter as a measuring device. Two types of rotation were used: 1) Continuous rotation, 2) Sterilmatic™ simulation. To simulate the Sterilmatic™ motion, an optically transparent container was rotated at quasi-constant speed and stopped periodically in order to approximate the movement of a cylindrical metal can travelling in a helical path along the inside of a large diameter horizontal retort shell. In such systems, cans of food roll when in contact with the retort shell in the lower portion of travel in the spiral track, but remain stationary when carried by the rotating reel along the upper portion of travel along the track.

Velocity data were obtained for two Newtonian and two non-Newtonian fluids at different concentrations. The fluids were: water, 25, 50 and 80% (w/w) glycerol/water solutions, carboxymethylcellulose (CMC) aqueous suspensions, a 2% low molecular weight CMC, 2% medium molecular weight CMC and 1.5% high molecular weight CMC, and 0.10 and 0.15% xanthan polymer in water. Three different rotational speeds (200, 300 and 350 rpm) and headspaces (0.25 cm (2.53% by v/v), 0.50 cm (5.06% by v/v), and 1.5 cm (10.12% by v/v)) were studied.

Contour plots of the velocity profiles and visual observations made during the experiments revealed that the inertial (centrifugal), gravitational and viscous forces determined the flow structure inside the cylinder together with agitative motion of the headspace bubble. The large scale motion inside the can was found to be governed by the centrifugal and gravitational forces whereas small scale motion was dependent mostly on the apparent viscosities of the liquids.

The following results were found from the experiments conducted to investigate the influence of the rotational speed, headspace and viscosity on the characteristics of flow inside the cylindrical container. The magnitude of the mean radial velocities and tangential turbulence intensities were found to be larger than the mean tangential velocity and the radial turbulence intensity for all liquids studied. The standard

deviation of the tangential velocity component was found to be 1-400% of the mean velocity obtained. However, the standard deviation values of the radial component of the velocity was much lower than that of the tangential component. An increase in the rotational speed significantly increased the mean radial component of velocity along the radial direction and the turbulence intensities for both Newtonian and non-Newtonian liquids. The mean velocity profiles were not affected by changes in the headspace volume, whereas the radial tangential intensities were augmented with the increase in the headspace volume.

An increase in the apparent viscosity of fluids significantly suppressed turbulence inside the cylindrical container by decreasing both radial and tangential intensities.

Time-velocity plots displayed periodic fluctuations which may be attributed to inherent features of the liquid motion. However, the response to changes was not the same at different locations within the fluids.

The mixing characteristics of the system were correlated with rotational Reynolds number which comprised all the parameters relating the hydrodynamics of flow inside the container namely, the viscosity, rotational speed and headspace. The results showed that mixing in the system can be characterized in two different regions, a low rotational Reynolds number region in which the mixing in both radial and axial directions increased very sharply with increasing rotational Reynolds number, and the other region in which mixing was slightly improved or unaffected by the increase in rotational Reynolds number.

CHAPTER 1

INTRODUCTION

I. Concepts of Food Preservation in Cans

Traditional thermal processing of foods involves filling foods into containers which are then sealed hermetically and thermally processed until the contents become microbially shelf stable. The major aim of thermal processing is to render the food free from spoilage and pathogenic organisms, which may grow and/or produce toxins. Therefore adequate control of the sterilization process is essential to ensure the safety of heat processed foods.

Heat transfer to food products can be accomplished by conduction, convection and radiation. Heat transfer to homogeneous liquid foodstuffs is mostly by convection; however, fluid foods containing particulates have two different heat transfer mechanisms; convection, and conduction, a slower heating mechanism. In canned food containing particulates, sufficient heat must be taken up by both phases in order to ensure the desired destruction of microorganisms. Depending on particle size and thermophysical properties, there is a lag time for the temperature to rise at the center of particles, therefore oversterilization of the liquid phase is carried out in order to ensure particulates are sterilized.

Various heating systems have been used to ensure sterilizing of foods. Still batch-type retorts (i.e., non-agitating) are widely used because of their low cost and ability to process a wide variety of convection and conduction heating products in a range of container sizes. Different kinds of agitating retorts are used when food contents can be made to flow, because agitation will increase the rate of heating which will result in shorter process times and normally improve food quality. Commonly, agitation induces flow of contents within a container, usually by means of moving the containers in end-over-end (EOE) or axial rotation. Various other thermal processing systems have been developed which are beyond the scope of this study.

Axial rotation is an effective way to achieve agitation while providing for continuous travel of cylindrical metal cans in a spiral track through a horizontal pressure vessel. This is known as the Sterilmatic™ retort system. For conduction-heating solid food products, process calculations could be carried out using conduction theory, however, convection-heated products are more complex. Temperature histories at the slowest heating point in axially rotated cylindrical containers depend strongly on convection currents which cause product movement inside the container. For this reason, it is first necessary to understand the fluid dynamics in axially rotating cylindrical containers in order to gain deeper knowledge of heat transfer in such food processing systems.

This study has been limited to experimental investigation of the flow in axially rotating cylinders to describe the flow phenomena which will provide a sound basis for future studies on heat transfer relevant to Sterilmatic™ thermal processing systems.

1.2. Thermobacteriology of Canned Food

The extent of thermal processing depends on the relative heat resistances of microorganisms present and composition of the food. *Clostridium botulinum* is a spore forming obligative anaerobe which is capable of producing a deadly neurotoxin, and may be present in foods, thus the destruction of botulinum spores is generally accepted as a minimum requirement for achieving safe thermal processing of foods.

In order to specify the capability of a heat process to reduce the number of viable microorganisms present in a food, the F-concept has been introduced. The F-value is derived from an end-point thermal death time experiment (Stumbo, 1973) in which the thermal death time (TDT) is determined over a range of lethal temperatures (T) to obtain a straight line plot of log (TDT) vs. T. From this relationship, the TDT at the chosen reference temperature, usually 121.1°C (250°F) is defined as the F-value in minutes. The F-value may be used to compare the resistance of microorganisms to sterilization at the reference temperature. A second thermobacteriological property determined from the TDT plot is related to the slope of the line. The z-value refers to

the temperature difference in the lethal range for the thermal death time curve to traverse one log cycle of thermal death time, thus it provides information on the relative sensitivity of an organism to different lethal temperatures.

When considering the lethal effect of a thermal process for a food, the temperature history in the food is related to lethal effects shown in the TDT curve. Process lethality is defined by the F_o value where F_o is the lethal effect of a processing temperature history at the center point or cold spot of a food in a process when the reference TDT behavior is expressed as F=1.0 minutes at a temperature of 121.1 °C and the TDT curve has a slope represented by a z value of 10 C° (18 F°). The F_o for a convection heating product in which the entire contents of the container experience the same temperature history can be calculated from the relationship.

$$F_o = D_{re}(\log a - \log b) \tag{1}$$

where a is the initial spore population, b is the final population after processing and D_{re} is the decimal reduction time, the time required to destroy 90% of the organisms at the reference temperature (121.1°C).

The 12-D concept was introduced for determination of process lethality requirements. The 12-D concept is arbitrary and implies that the minimum heat process should reduce the probability for survival of *Clostridium botulinum* spores to 10^{-12} of the original contamination level. Although the 12-D concept has been in use for many years, Pflug (1982) has confirmed its validity as the preservation specification for low-acid (pH>4.6) foods with respect to achieving safety with respect to mesophilic spore-forming pathogenic bacteria, specifically, *Clostridium botulinum*.

Although the goal in thermal processing is to produce shelf stable foods which are free from viable toxin-producing microorganisms, the focus of this study is restricted to achieving and understanding flow phenomena in axially rotated partially-filled horizontal cylinders, which will impact upon convective heat transfer of canned foods. Thus, this study will represent a stepping-stone toward prediction of heat transfer

in axially rotated cylindrical food containers.

1.3. Modes of Heat Transfer

The mechanism by which heat is transferred in a container can be a very complex process. Although there are three distinct types of heat transfer processes, temperature distribution in any medium is often controlled by combined effects of these three modes of heat transfer are discussed below.

1.3.1. Conduction

Conduction is the mode of heat transfer in which "energy exchange takes place by the kinetic motion or direct impact of molecules, as in the case of fluid at rest, and by the drift of electrons, as in the case of metals" (Ozisik, 1985). Conduction takes place in solids, liquids or gases. The basic law governing heat conduction is known as Fourier's law and is given by the following equation:

$$q = -k\left(\frac{dT}{dx}\right) \tag{2}$$

1.3.2. Convection

Convection is a transport process and can be defined as the transport of mass and energy by potential gradients and by gross fluid motion (Kays and Crawford, 1980). Convection is the most important heat transfer mechanism between a solid surface and a fluid. If the fluid motion is induced artificially by some external means such as motion of the solid surface or by pumping of the fluid past the solid, the process is called forced convection. In contrast, if fluid motion is set up by buoyancy effects resulting from density gradients caused by mass concentration and/or temperature differences in the fluid, heat transfer is said to be by free or natural convection. Newton defined the rate of heat transfer between a solid and fluid by the equation (Whitaker, 1976):

$$q = hA(T_s - T_f) \tag{3}$$

where A = heat transfer area, T_s= surface temperature, T_f= fluid temperature

1.3.3. Radiation

Radiation is also one of the mechanisms for energy transport and takes place through electromagnetic waves emitted from one body to another. Radiation is not regarded as a substantial mode of heat transfer in thermal processing except in flame sterilization. The heat flux from a surface is expressed by the following equation

$$q = S_B A \varepsilon_m T^4 \tag{4}$$

where S_B = Stefan-Boltzman constant and ϵ_m= emissivity

1.4. Thermal Properties of Foods

Thermal properties of food materials must be known in order to carry out calculations of heat transfer. These are regarded as thermal conductivity, k, specific heat capacity, C_p, and thermal diffusivity which is defined by the ratio, α.

$$\alpha = \frac{k}{\rho C_p} \tag{5}$$

Thermal conductivity of a substance is a physical property which is an inverse measure of resistance to heat flow. Specific heat is the quantity of heat that can be absorbed for a stated change in temperature. Thermal diffusivity reflects the ability of a substance to change temperature during unsteady state heat transfer.

Thermal properties of a material depend on its chemical composition, physical structure, phase, temperature and pressure. The models described later for the prediction

of heat transfer parameters (viz., process time) require these parameters. In such calculations, thermal properties are usually considered as constant although it is well known that this is a reasonable assumption only for a modest range of temperature change.

1.5. Types of Retorts

Various types of retorts are used in the canning industry and are discussed by Lopez (1987a). Non-agitating vertical or horizontal batch type-retorts are the oldest systems and are still used widely because of their relatively low cost and versatility, as different products can be processed at different times and temperatures on subsequent runs in the same vessel. Some disadvantages of these retorts are their high labor costs and low energy efficiencies.

Agitating batch-type retorts have several advantages over non-agitating retorts for liquid and multi-component (liquid and solid) foods. These are:

a) Improvement of heat penetration rates by the movement of a headspace bubble inside the container. If particulates are present, they may act as turbulent flow promoters that also improve heat transfer rates,
b) Fast heating and cooling are often possible,
c) Since the overall process time may be shorter, the quality and nutrient retention of the food may be improved,
d) Various container sizes can be processed in batch-type retorts because of flexibility in time and temperature of processes,
e) More viscous products may be processed in large containers without overcooking,
f) Agitation can delay the tendency for separation of some starchy products and syrups,
g) Shorter times for the sterilization cycle may increase production rate,
h) Savings in steam consumption and therefore, lower energy costs may be obtained.

Various types of agitating retorts using live steam, water immersion or steam-air

mixtures as heating media are currently used in the canning industry (Eisner, 1988). In the past fifteen years, considerable effort has been focussed on studies of heat transfer in rotating sterilization systems.

1.6. Rheological Properties of Foods in Thermal Processes

Rheological properties of fluid foods are important in design of agitated thermal processes because of their effects on mixing and heat transfer. For our purposes, fluid foods may be classified into two main categories; Newtonian and non-Newtonian.

1.6.1. Newtonian Fluids

In flow, Newtonian fluids exhibit a direct proportionality between shear stress and shear rate. Newtonian behavior is generally found in gases and simple solutions of low molecular weight solutes such as water, sugar syrups, salt brines and most oils. Newtonian flow behavior can be described by:

$$\sigma = \eta\dot{\gamma} \tag{6}$$

where σ is the shear stress, η is the coefficient of viscosity and $\dot{\gamma}$ is the shear rate. However, most fluid food systems do not exhibit Newtonian behavior because they are usually not simple liquids.

1.6.2. Non-Newtonian Fluids

Resistance to flow in non-Newtonian fluids is influenced by both temperature and shear rate or rate of flow. Non-Newtonian behavior can be divided into three broad categories (Tung, 1989):

a) Time independent flow in which the resistance to flow (apparent viscosity) is a function of the shear rate and/or shear stress,
b) Time dependent flow in which flow properties are also influenced by the time of

flow.

c) Viscoelastic behavior which simultaneously displays both elastic and viscous properties.

1.6.3. Time Independent non-Newtonian Fluids

Some time independent non-Newtonian fluids can be further described as follows:

a) Bingham or non-Bingham materials:

Plastic substances will not flow unless a critical yield stress is exceeded. At stresses above the yield stress, a linear relation between stress and shear rate would characterize a Bingham material. Non-linear rheograms indicating a yield stress would be exhibited by non-Bingham plastics.

b) Pseudoplastic fluids:

Many non-Newtonian foods fall into this classification. Pseudoplastic fluids exhibit shear rate thinning, in which apparent viscosity decreases with increasing shear rate. Concentrated fruit juices, colloidal suspensions, protein concentrates, and fruit and juice purees are some examples of this type of behavior.

c) Dilatant fluids:

Dilatant flow behaviour is the opposite to that of pseudoplastics; i.e., apparent viscosity increases with increasing shear rate (shear thickening). This shear thickening behaviour has been observed in cooled starch suspensions (Bagley and Christianson, 1982).

Non-plastic flow behaviour of time independent non-Newtonian fluids can described in many cases by a simple model called the power law:

$$\sigma = m\dot{\gamma}^n \tag{7}$$

where m and n are the consistency coefficient and flow behavior index, respectively.

The flow behavior index, n, identifies shear thinning ($n<1$) and shear thickening ($n>1$) flow behaviour. Several other models have been developed to describe the flow behavior of non-Newtonian fluids (Tung, 1989).

Since thermally processed foods are first heated and then cooled during sterilizing preservation treatments, the influence of temperature on rheological behavior is important. Viscosity of most fluids depends strongly on the temperature. Temperature dependence of fluids may often be expressed by the Arrhenius relationship:

$$\eta = A_A \, exp\left(\frac{E_A}{RT}\right) \tag{8}$$

where A_A is the frequency factor, E_A is the activation energy for viscous flow, R is the universal gas constant and T is temperature in absolute units (K).

The viscosity of Newtonian fluids generally decreases with increasing temperature. For non-Newtonian fluids whose viscosity depends on both shear rate and temperature, temperature dependence becomes more complex. The combined effects of temperature and shear rate have been proposed by different models considering the power law and Arrhenius equations (Christiansen and Craig, 1962; Speers and Tung, 1986).

1.6.4. Time Dependent non-Newtonian Fluids

Time dependent non-Newtonian fluids can be divided into two groups depending on whether the shear stress increases or decreases with time at a fixed shear rate and temperature. The former fluids are termed antithixotropic and the latter, thixotropic, provided that the time dependent effect is reversible.

1.7. Factors Affecting Heat Penetration

Factors which affect the heat penetration rate into food containers are listed below (Lopez, 1987b):

1. Retort temperature,
2. Agitation of containers during sterilization,
3. Container orientation during sterilization,
4. Size and shape of container,
5. Material of which the container is made,
6. Headspace or the presence of air within the container,
7. Fill weight,
8. Product preparation,
9. Ratio of solids to liquid in the product,
10. Type, size, shape and arrangement of particles,
11. Consistency of the product,
12. Initial product temperature,
13. Retort temperature deviations,
14. Particle interactions,
15. Vacuum,
16. Heating medium.

Some of these factors are discussed below.

a. Headspace

It is noteworthy that headspace is extremely important during the rotation of canned products (Berry et al., 1985; Teixeira Neto, 1982), as the agitation of the can contents was reported to be mainly brought about by the movement of the "headspace bubble". The headspace volume affects the flow patterns inside the can. Berry et al. (1985) found unusual results for cheese ravioli in brine in 603 x 700 cans processed in a Steritort™ which is a pilot-scale simulator for Sterilmatic™ processing. At 20 rpm with 100 ravioli portions, increasing headspace decreased the heating rate. Quast and Siozawa (1974) also studied the effect of headspace in axially rotating cans. The heat transfer coefficient (h) decreased slightly for water in 1 kg cans with increasing headspace. They used very high rotational speeds (80 to 280 rpm). For 1% CMC

solutions, the heat transfer coefficient increased with increasing headspace except at 80 rpm for which it first increased and later decreased. With flow visualization, they observed that the headspace bubble remained at the upper part of the can at speeds up to 150 rpm. At 280 rpm the headspace bubble was dispersed in the form of small air bubbles which moved randomly in the water. They concluded that lower heat transfer rates at larger headspaces were probably due to less favorable agitation. The amount of headspace within a rotating can is one of the most critical factors affecting the heat transfer coefficient. Berry et al., 1979 and Berry and Bradshaw, 1982 reported that the rate of heat penetration decreased with decreased headspace in cream-style corn and sliced mushrooms in brine, respectively. Naveh and Kopelman (1980) indicated that 2% headspace significantly increased the heat transfer coefficient in 84° brix glucose syrup; however, further increases in headspace, up to 10%, scarcely improved the heat transfer coefficient. Conley et al. (1951) showed that a decrease in the headspace caused a reduction in the cooling efficiency in water, tomato juice, orange concentrate and corn syrup during end-over-end rotation.

No significant change in the heat transfer coefficient was observed during end-over-end (EOE) rotation for a headspace volume from 3% to 9% of the can volume, whereas less than 3% headspace decreased the heat transfer coefficient (Anantheswaran, 1984). He used the following Newtonian and non-Newtonian liquids in his study: water; 30, 50, 60 % sucrose solutions; glycerine; 0.4, 0.5 and 0.75% guar gum solutions.

b. Reel and can speed

For Sterilmatic™ systems, a rotating reel system propels cans along the helical path down the length of the horizontal cylindrical retort shells. Depending on the rotational speed, as well as the shell diameter and can diameter, cans will roll at a certain speed when in contact with the helical track through the lower part of the turns in the track.

Higher reel speeds (5 to 8 rpm) provided effective axial agitation, increased sterilization value and decreased heating rate indices in cream-style corn processed in

303 x 406 cans (Berry et al., 1979). However, further increases of the reel speed had a limited influence on the rate of heat penetration (Berry and Dickerson, 1981; Berry and Bradshaw, 1982). Peralta and Merson (1982) indicated that the speed of can rotation did not greatly affect the heat transfer rate in axial rotation during flame sterilization in a pilot-scale Steriflamme™ simulator. They concluded that when the can peripheral velocity increased to about twice the cross flow velocity, the can rotation had a significant effect on the heat transfer rate.

Effective agitation in EOE systems was provided by increasing reel speeds up to a certain speed (Clifcorn et al., 1950; Naveh and Kopelman, 1980), beyond which no change in heat transfer rate in the EOE system was observed and further increase in speed brought about a decrease in the heating rate due to excess centrifugal forces acting on the can (Clifcorn et al., 1950). The optimal speed would provide sufficient time in each half rotation to allow the headspace bubble to travel from one end of the container to the other.

Clifcorn et al. (1950) defined a come-up time for his work which was the time taken by the product inside the can to reach a temperature 1 F° below the retort temperature. Slower rotational speeds were required at greater radii of rotation in order to minimize the come-up time. Conley et al. (1951) indicated that there was an "optimal rotation" speed for a given can radius of rotation.

Naveh and Kopelman (1980) reported that for EOE rotation, moving the axis of rotation from the center of the can to off-axis improved the heat transfer coefficient. In another study using a laboratory sterilizer 60 cm in diameter and 56 cm long, the heat transfer coefficient in EOE rotation was found to be independent of the radius of rotation and the size of the can (Anantheswaran, 1984).

Zaman et al. (1991) studied the influence of container movement in Steritort™ and Sterilmatic™ processing systems. The Steritort™ studies indicated there was an exponential decay in the lethality with decreased can rpm. They also found that commercial operators used slower can rotations than corresponding pilot scale experiments. This could be a dangerous situation if lethality results from pilot scale

cookers are applied to commercial retorts.

c. Retort temperature deviation

Houtzer and Hill (1977) studied the effect of temperature drops on the process lethality in rotary sterilizers. The retort temperature was lowered by 20 F°, the reel was stopped, and the retort temperature was then raised to the original operating temperature after a set time. Since in lethality calculations based on formula methods (e.g., Stumbo, 1973) retort temperature is considered as a constant, a drop in temperature results in understerilization of the can contents if the calculations are based on these formula methods.

d. Fill weight

An increase in the particle fill weight of sliced mushrooms packed in brine caused a decrease in the heating rate of the product (Berry and Bradshaw, 1982), presumably due to reduced convective effects in the over-filled cans. A study by Jones et al. (1980) showed the effect of fill weight on the F-value delivered to cans of green beans in a Sterilmatic™ retort. Their results indicated that as the fill weight increased, the F_o value decreased and f_h value (heating rate index) increased. The same phenomenon was observed in cream-style corn and whole kernel corn processed in a Steritort™ (Berry et al., 1979; Berry and Dickerson, 1981; Berry and Bradshaw, 1982). Berry et al. (1985) also indicated that overfilling of ravioli in brine and in tomato sauce could result in underprocessing.

e. Particle interactions

If the fluid contains particulates, then during rotation two or more moving particles may collide and touch one another. This phenomenon may result in conduction heat transfer through the contact area of the particles if there is a temperature difference among these particles. However, due to the small contact area and short impact duration this contribution is normally neglected in heat transfer calculations.

f. Product consistency

The rate of heat transfer generally decreases with an increase in its non-Newtonian viscosity or consistency. Since consistency indicates the product's resistance to flow and is influenced by the size and amount of particulates (Berry et al., 1979), it follows that products with solids content are likely more resistant to flow. Javier et al. (1985) studied the effect of viscosity of Newtonian fluids on the heating rate parameter in an agitating retort simulator. A decrease in heating rates was found with increasing viscosity at a given rotational speed.

Consistency was reported to have a significant effect on the rate of heat transfer in EOE systems (1985b Ball and Boyd as cited by Ball and Olson, 1957; Anantheswaran and Rao). High consistency caused a decrease in the bubble velocity (Naveh and Kopelman, 1980).

g. Solid particulates

The presence of particulates affects the rate of heating. Hiddink (1975) determined the temperature profiles for water and silicone fluids containing differently sized spherical particles in a non-agitating system. The presence of small particles (3 mm in diameter and porosity = 0.37) reduced the convective heating rate. On the other hand, the presence of large particles (18 mm diameter, porosity = 0.41) in moderately viscous liquids did not reduce convection patterns.

h. Particle size, shape and density

Shape factor is also an important factor in heat transfer to particles in suspension. For example, non-spherical particles have more surface area as compared to spherical particles of the same volume. In addition, non-spherical particles provide more sharp edges and thus may create more turbulent flow. Therefore, particle shape and size may change the flow pattern. Smaller particles (less than 0.31 cm) have been treated as homogeneous system (de Ruyter and Brunet, 1973). The effect of the density of particles may be quite large since it may affect particle movements in agitated systems,

but it has not been studied in thermal processing of foods in cans.

i. Can size

Can aspect ratio affects the convection patterns set up in the product. Naveh and Kopelman (1980) found that an increase in viscosity and in the container size caused a decrease in heat transfer coefficient in agitated systems. Lenz and Lund (1978) and Anantheswaran (1984) found that the convective heat transfer coefficient was independent of the container size in an EOE system.

j. Vacuum

Berry and Dickerson (1981) studied the effect of vacuum on sterilization value for whole kernel corn in a Steritort™ retort. A slight influence was detected, which also varied with the can size. A slight decrease in the sterilization value at low vacuums for 603 x 600 cans was observed, while no change was observed for 307 x 306 cans.

k. Container material

Rotstein et al. (1988) showed that can rotation in axially rotating systems was affected by lid material and can material. They found that electroplated tin cans rotated more than tin-free steel cans when processed in the same cooker.

1.8. Dimensionless Numbers

Dimensionless parameters emphasize our understanding of fluid flow phenomena and heat transfer. Most of the dimensionless parameters may be viewed as a ratio of a pair of forces such as fluid forces, the relative magnitude indicating the relative importance of one of the forces with respect to the other. If some forces in a particular situation are very much larger than the others, it is then possible to neglect the effect of the smaller forces and treat the system as if it is completely determined by the major forces. In rotating systems, forced convection is the major mode for the heat transfer.

Arpaci and Larsen (1984) viewed forced convection as analogous to conduction in moving media which involve inertial and viscous forces. The resulting fluid flow brings about enthalpy flow which is known as convective heat transfer. The following dimensionless numbers are of importance in correlating experimental data in forced convection: Reynolds number, pressure coefficient, Froude number, Weber number, Mach number, Prandtl number, Grashof number and Nusselt number.

The Reynolds number is the ratio of inertial forces to viscous forces in a fluid. A critical Reynolds number distinguishes among flow regimes, such as laminar or turbulent, and is expressed as:

$$Re = \frac{inertial\ forces}{viscous\ forces} = \frac{L_c V \rho}{\eta} \tag{9}$$

Therefore, a low value of the Reynolds number means that viscous forces are large in comparison with inertial forces.

Nusselt number, *Nu*:

$$Nu = \frac{convection}{conduction} = \frac{hL_c}{k} \tag{10}$$

Nusselt number represents heat transfer coefficent in dimensionless form. It can also be interpreted as a measure of boundary layer thickness.

Froude Number, *Fr*:

$$Fr = \frac{inertial\ forces}{gravity\ forces} = \frac{r\omega^2}{g} \tag{11}$$

Froude number represents free-surface effects.

The Prandtl number is the ratio of molecular diffusivity of momentum to molecular diffusivity of heat. It is found in all convective heat transfer coefficients.

$$Pr = \frac{\rho C_p}{k} \tag{12}$$

The Grashof number, *Gr*, contains the coefficient of volumetric expansion and temperature difference and is employed when natural convection occurs.

$$Gr = \frac{\rho^2 g \beta D^3 \Delta T}{\eta^2} \tag{13}$$

The other dimensionless parameters one could consider are geometric ratios, flux ratios, apparent viscosity ratios, dimensionless radial or axial position, relative volume, or others.

Many food properties such as viscosity are temperature dependent. In a non-dimensional equation, these values are evaluated either at bulk temperature or at the average of bulk and surface temperature. Watson and Harper (1987) suggested that the use of an arithmetic average of bulk and surface temperatures to evaluate these properties was reasonable because most of the heat transfer resistance was located in a film which is intermediate in temperature between the surface and the bulk temperatures.

The viscosity of non-Newtonian fluids depends on both temperature and the shear rate resulting from agitation during processing. It is very difficult to account for the effect of shear rate in solving partial differential equations in heat transfer calculations due to the very complicated nature of agitation. However, this can be correlated with dimensionless numbers. For example, Anantheswaran (1984) used generalized rotational number, *GRe*,

$$GRe = \frac{D_r^2 N^{2-n} \rho}{8^{n-1} m \left(\frac{(3n+1)}{4n} \right)^n} \tag{14}$$

In many cases, depending on the nature of the system, the dimensionless

parameters can be modified. For example, in agitation problems, a rotational Reynolds number, Re_r may be used.

$$Re_r = \frac{L_c^2 N \rho}{\eta} \tag{15}$$

where L_c = characteristic length or impeller diameter, N = rate of rotation.

1.9. Studies of Heat Transfer to Fluids in Rotating Systems

Various studies have been conducted for agitation systems considering several factors affecting heat transfer rates. Rao and Anantheswaran (1988) have reviewed the convective heat transfer to cans in non-agitating and agitating systems. Some of the previous work is briefly explained below.

Quast and Siozawa (1974) studied the heat transfer during heating of rotated canned model solutions of sucrose and carboxymethylcellulose (CMC) in a pilot plant spin cooker. Two to four times higher heating rates were obtained with agitation. For sucrose solutions, the following correlation was found:

$$Nu = \frac{UD_{ro}}{k} = 0.55\, Re_r\, Pr^{1/3} \left(\frac{L}{E}\right)^{1/3} \tag{16}$$

Later, Merson et al. (1980) revised this correlation as:

$$Nu = 0.17\, Re_r^{0.52}\, Pr^{1/3} \left(\frac{L}{E}\right)^{1/3} \tag{17}$$

for $600 < Re_r < 250{,}000$, $6 < Pr < 375$, $6 < L/E < 35$

Naveh and Kopelman (1980) studied the effect of some processing parameters on heat transfer coefficients in a rotating retort. These parameters were headspace, reel speed, and mode of rotation (EOE and axially). They used 70° DE glucose syrup in a 105 x 122 mm brass cylinder. Higher heat transfer coefficients were obtained with end-over-end rotation than those of the other systems (see Table 1). Table 1 shows the maximum overall heat transfer coefficients for different modes of heat transfer.

Javier et al. (1985) studied the convection heating rate parameters of model solutions (Newtonian oils) in different agitating systems. The working parameters were viscosity, rotation speed, and rotation mode. Highest heating rates were obtained with EOE rotation, and the lowest with the stop-and-go mode of rotation.

Table 1. Overall heat transfer coefficients for different modes of heat transfer (Naveh and Kopelman, 1980).

Mode of Heat Transfer	U_{max} (cal/m^2 s °C)
End-over-end	45.00
End-over-end-centrally	43.80
Axial rotation	48.80
Natural convection	6.20
Conduction	3.25

Soule and Merson (1985) developed a dimensionless correlation for Newtonian liquids in axially rotated liquids. They used distilled water and silicone oils at different viscosities having one cm headspace in three different sizes of cans. The correlation was:

$$Nu = \frac{UD}{k} = 0.434 Re_r^{0.571} Pr^{0.278} \left(\frac{L}{D}\right)^{0.356} \left(\frac{\eta_b}{\eta_w}\right)^{0.154} \quad (18)$$

for $12 < Re_r < 44200$, $2.2 < Pr < 2300$, $1.1 < L/D < 1.61$, $1.22 < \eta_b / \eta_w < 1.78$

where

$$Re_r = \frac{\rho N L_c^2}{\eta} \quad (19)$$

where L_c = characteristic length or D_c.

They used can diameter as a characteristic dimension. The internal heat transfer coefficient was also given as

$$h = \frac{U}{(0.9359 \pm 0.0363)} \quad (20)$$

As mentioned previously, the heat transfer rate in agitated systems depends on the velocity profiles, size, shape and density of solid particles, viscosity of fluids, thermophysical properties of both phases, geometry of the can, rotational speed, and a number of other factors. Due to the large number of variables and the complexity of their influences on heat transfer, empirical correlations which have been proposed for heat transfer coefficients are generally valid within the limits of experimental conditions.

In order to calculate process variables for a thermal process in which the can contains particulates, it is necessary to know temperatures of both the fluid and the particulates. The measurement of fluid temperature involves little difficulty. However,

the temperature measurement of moving particulates within a can is a very difficult process. In general, the particle temperature can be estimated in terms of heat transfer coefficient between the particulate and fluid. Some of the work considered only wall-to-fluid heat transfer coefficients instead of fluid-particulate convective heat transfer coefficient.

Various solutions of the energy equation for the heating of the fluid with particulates have been presented (Carslaw and Jaegar, 1959; de Ruyter and Burnet, 1973; Lenz and Lund, 1978; Hassan, 1984; Chang and Toledo, 1989; Stoforos and Merson, 1990).

1.10. Studies Involving Rotation

In end-over-end rotation, cans rotate around a circle in a vertical plane. The headspace changes its position along the length of the can during the rotation and this in turn provides mixing of the can contents.

Clifcorn et al. (1950) studied heat transfer in EOE rotation. The heat transfer increased rapidly at low rotations until it reached a critical value above which little or no increase in the rate of heat transfer was observed. This optimal speed decreased with increasing consistency. These authors also studied the forces acting in a can during EOE rotation; centrifugal and gravitational forces were considered. Centrifugal forces, [(mass x velocity^2)/radius] increased with increasing rotational speed and opposed gravitational forces, (mass x gravitational acceleration).

Clifcorn et al. (1950) found that when the average centrifugal force was equal to the weight of the contents of the container, the headspace volume traversed through the center of the contents. This gave the optimal rotational speed. This optimal rotational speed provided maximum turbulence within the container, resulting in the maximal heat penetration rate. Beyond a certain speed, centrifugal forces became greater than gravitational forces and the contents of the container were forced out to the other end of the container and remained there. This provided no mixing and heat transfer took place through conduction.

A study done by Ball and Boyd (quoted by Ball and Olson, 1957) indicated that besides the speed of rotation, consistency significantly affected the rate of heat penetration. Movement of the headspace bubble depended upon the viscosity of the product.

Conley et al. (1951) found that speed and radius of rotation were extremely important factors which affected the heat transfer rate in an EOE rotary retort. The effect of the headspace and radius on cooling of 307 x 409 cans of orange concentrate was studied in a 1.168 m diameter laboratory retort. At the largest radius (0.406 m) a decrease in heat transfer rate at very high speeds was observed. Increased headspace improved the efficiency of cooling. However, beyond 0.006 m of gross headspace a reduced effect on cooling rate was observed. They also concluded that there was an optimum speed of rotation for each radius. The effect of viscosity was also pronounced in this study.

Parchomchuk (1977) conducted heat penetration tests using a 5% (w/w) bentonite suspensions in a 1.067 m diameter horizontal retort. Maximum heating rates in 603 x 700 cans with 0.013 m headspace was accomplished between 40 and 80 rpm. Above 80 rpm, it was observed that the heating rate decreased. At 144 rpm (inertial forces were 8.2 times gravitational forces), broken heating curves were obtained due to inhibition of the motion in the contents of the container.

Naveh and Kopelman (1980) calculated the heat transfer coefficients for an 84 Brix glucose syrup within rigid brass cylindrical cans with EOE and axial rotation methods. Heat transfer coefficients were much higher in end-over-end rotation than in axial rotation. Increasing headspace volume beyond 2% did not improve the heat transfer coefficients proportionally.

Duquenoy, 1980 (cited by Anantheswaran, 1984) studied water, toluene, ethylene glycol, aniline, sugar solutions, ethanol, and sodium chloride solutions at different concentrations. The following correlation was obtained.

$$Nu = 17x10^{-5}\, Re^{1.449}\, Pr^{1.19}\, We^{-0.551} (D/2L_c)^{0.932} (V_p/V_c)^{0.28} \qquad (21)$$

The characteristic length in Nu and Re was the radius of the can, where in the Weber number it was the half height of the can.

Hotani and Mihori (1983) investigated the mode of headspace bubble movement in axial and vertically rotating cans and measured experimentally the temperature distribution in still and rotated cans. They used a 5-6% CMC solution as a model. They stated that "the dynamic forces acting on the bubble are its buoyancy and the centrifugal force exerted on the can contents", Drag force, which was related to the liquid velocity gradient in the boundary layer, was governed by the viscosity of the liquid. Temperature distribution studies indicated that, in a vertical rotating can, there was a temperature difference between the center and near the end walls. This temperature difference decreased with increasing rotational speed. They also conducted an experiment in which the direction of EOE rotation was reversed in 15 and 45 seconds. This method increased the heating speed and provided more uniform temperature distribution throughout the can.

Anantheswaran (1984) and Anantheswaran and Rao (1985a,b) studied the heat penetration to model fluids in cans during EOE rotation. The fluids were Newtonian; consisting of sucrose/water and glycerol/water solutions at various concentrations, or non-Newtonian with various concentrations of guar gum/water. A lab sterilizer (60 cm diameter and 56 cm long) was used. Firstly, an energy balance was written and solved numerically, and then instantaneous and time averaged heat transfer coefficients were evaluated.

Their experimental findings are summarized below:

a) The heat transfer coefficient was found to be independent of the radius of rotation and the size of the can. That is, increased radius of rotation did not significantly enhance the heat transfer rate,
b) The rate of heat transfer increased with the rotational speed of the can, and
c) The following correlations were developed;

For Newtonian fluids,

$$Nu = 2.9\,Re^{0.436}\,Pr^{0.237} \tag{22}$$

for 83 <Re<2.1x10^5 and 2.8<Pr<49

and non-Newtonian fluids,

$$Nu = 1.41G\,Re^{0.482}\,GPr^{0.355} \tag{23}$$

where GPr is the generalized Prandtl number defined as:

$$GPr = \frac{C_p m 8^{n-1}(3n+1)^n}{kN^{1-n}(4n)^n} \tag{24}$$

anad GRe is the generalized Reynolds number,

$$GRe = \frac{D_r^2 N^{2-n}\rho}{8^{n-1} m\left(\frac{(3n+1)}{4n}\right)^n} \tag{25}$$

d) Significant fluctuations were observed at the can center temperature,
e) Headspace volume between 3 and 9% did not affect the heat transfer coefficient for Newtonian liquids, and
f) The rates of heat transfer for highly viscous glycerol and 0.75% guar gum were not improved by the EOE rotation system.

Javier et al. (1985) studied the heating rate properties of Newtonian fluids in

different cans and at different modes; axial, EOE and reciprocating axial. Heating rates were higher in EOE rotation than in the other modes. A significant decrease in f_h with increasing rotational speed (up to 100 rpm) was determined.

Lekwauwa and Hayakawa (1986) developed a computerized model for the prediction of thermal responses and lethality in particle-fluid systems. The reliability of their model was tested by conducting heat penetration tests for potatoes-in-brine in a pilot plant Stock Rotor-900 water immersion agitated retort (EOE). Good agreement between experimental and predicted temperature profiles was obtained.

CHAPTER 2

FLUID DYNAMIC ASPECTS

2.1. Flow Patterns

The mechanism of convection heating can be obtained by studying temperature profiles and flow patterns. There are few studies for visualizing flow patterns in convection heating-type products. Dye injection, particle streaking and generation of bubbles are the methods mostly used. In the particle streak method, small glittering particles are suspended in the liquid, then the particles are illuminated by a flat narrow beam of light, and photographed. Fagerson and Esselen (1950) studied flow patterns and temperature profiles in 1% bentonite suspensions in glass jars. Flow patterns were visualized by adding methylene blue to water in glass jars. They observed an upward flow starting from the center of the bottom of the container. Blaisdel (1963) also studied the flow patterns in water and 50% sucrose solutions, and discussed the formation of eddies during the heating processes. The author postulated that the cold point was located on the central axis where eddies and downward core flow met, and this cold point would shift downward during heating with time.

Gavish et al. (1978) studied the flow visualization in axially rotating cans. They used viscous glycerol and photographed the flow behavior in the presence of very small air bubbles dragged by the fluid along streamlines. They also determined the radial and angular position of the bubble as a function of the speed of rotation.

Most studies have not considered the effect of free convection on calculating heat transfer calculations which could be negligible when rotational speed was high. However, in some cases where the fluid velocity was small or the temperature difference between the container and surrounding heating medium was large, the influence of buoyancy forces and the associated free convection could significantly affect heat and mass transfer.

2.2. Application of Laser Doppler Velocimetry in the Food Industry

The first application of Laser Doppler Velocimetry (LDV) in this field was reported by Hiddink (1975) who studied velocity profiles in a boundary layer during natural convection heating of liquids. The author used a cylindrical container (half of which was made of brass), the back of which was polished to reflect the forward scattered light. Because of the necessity to include scattering particles, milk was added to water and a centrifuged suspension of "Mearlwhite" was added to silicone liquid (F111/100, medium viscosity) to provide particle sizes of 5 to 10 μm as seeding materials. Several factors affected the measurement, for example, brass expanded upon heating, thus the measurement points varied. The results showed that the boundary layer flow was essentially laminar.

Karwe and Sernas (1996) measured the tangential and axial velocities inside the screw channel of a twin-screw extruder using a two dimensional argon ion LDV. Heavy corn syrup with naturally occurring particles was used. Measured tangential velocity gradients were slightly higher than numerically predicted values for Newtonian fluids. Measured tangential velocity was at a maximum before and after the screw flight and a minimum in the middle of the screw channel. Tangential velocity gradients at the barrel were lower in the middle of the screw channel. The scatter in the data for axial velocity with angular position was much larger than the scatter for tangential velocity. It was concluded that velocity measurements can be used to quantify mixing in extruders.

Applications of LDV in fermenters have been demonstrated by Koutsakos and Nienow (1989) who measured tangential and radial velocities in different fluids with different impeller geometries. They showed that it was possible to have regions of laminar and turbulent flow in a mixing tank at the same time. The occurrence of a distinct flow reversal beneath the impeller at the point off-bottom clearance has been shown (Jaworski et al., 1991). The effect of shear rate on various parameters and processes has been well known. Increasing the shear rate increases certain transport properties such as heat and mass transfer. Elias et al. (1995) have used LDV to study the

effect of shear stress on mammalian cell culture. The Brabender Farinograph has been used extensively in dough mixing studies and its shearing action is known to be non-homogeneous. Recently, LDV was used to determine velocity gradients in the Brabender Farinograph and local shear rates and shear rate distributions were calculated (Parakash, Ph.D. thesis, quoted by Chandrasekaran et al., 1997). This study indicated that the degree of mixing was location dependent with higher shear rates for non-Newtonian fluids and in the region near the blades.

In a recent study (Marcroft MS thesis, quoted by Chandrasekaran et al., 1997), LDV was used to measure velocity distribution in a commercial hot-air impingement oven used to cook various food products such as pizzas, breads, and chickens. Dry-ice fog was used to generate small particles for velocity measurement. Velocity measurements in air jets impinging on a flat surface of food products such as on pizza were made. The authors plotted contours of axial velocities. Different regions of velocities such as negative axial velocities were determined. From these, it was concluded that the local heat transfer rates, which were dependent on the velocity profiles would not be constant within the jet impingement oven. Therefore, these data can be used to develop appropriate heat and mass transfer models for evaluating cooking in these ovens.

Recently, Chandrasekaran et al. (1997) reviewed the applications of LDV in food process operations. They indicated that the measurement of local fluid velocities is needed for the validation and improvement of mathematical models which are used to simulate transport phenomena and to estimate some process parameters such as local shear rates and residence time distributions for the purpose of evaluation or optimization of equipment performance. They stated that the degree of thermal processing received by food materials depends on fluid velocity, which can affect the safety and quality of the final product.

2.3. Similar Problems in Other Fields of Technology

Considerable effort has been focussed on fluid flow and heat transfer in rotating

machines. Flow in horizontally rotated cylinders has been examined both theoretically and experimentally by a number of investigators in diverse contexts, (e.g., Greenspan, 1976; Singler, 1989). Rapidly rotating cylinders with differentially rotating endcap, spin up/down of filled containers, and rimming flow have been extensively studied.

However, most of these studies involved rapidly rotating cylinders in which the fluid was held out against the wall by centrifugal forces that dominated the flow field. If there was a headspace at high rotational rates, the liquid would take an annular shape bounding the cylindrical headspace When body forces such as buoyancy, centrifugal or coriolis forces act in a direction normal to the main flow, hydrodynamic instabilities may arise in the form of vortices. Examples are Taylor vortices in two concentric infinite cylinders with the inner cylinder rotating and the outer at rest, and longitudinal vortices in plane Poiseuille flow subjected to spanwise rotation. These forces also cause secondary flows normal to the main flow, examples of which are secondary flows caused by buoyancy forces in heated cooled tubes and centrifugal forces in curved pipes. Because of destabilizing effects, boundary layers can be turbulent. Centrifugal instability may cause higher magnitudes of the velocity fluctuations in the boundary level and result in more turbulent intensities. In rotating cylinders, the cylinder ends also play an important role in flow. Wedemeyer (1964) studied flow in the boundary layers near end walls. The fluid within the boundary layer was thrown radially outwards by centrifugal forces, and created slow secondary flows. Due to secondary flow transport of momentum from the walls to the interior, this accomplished convection rather than diffusion. In this case, the source of instability is the adverse angular momentum gradient. Whereas convection in a heated layer is brought about by buoyant forces becoming large enough to overcome the viscous resistance, the convection in a Couette flow is generated by the centrifugal forces being able to overcome the viscous forces.

Axially rotating partially filled systems are involved in some other technologies. (Bien and Penner, 1970, as well as Ladeinde and Torrance, 1991). The majority of these studies involved rapidly rotating cylinders (Phillips, 1960 and Greenspan, 1974). A few of them are involved partially-filled systems (Singler, 1989). Kawashima and Yang

(1988) used LDV to study unsteady flow in a hollow drum filled with liquids. They determined the effect of side walls and fluid viscosity on the transient flow response.

Ladeinde and Torrance (1991) mathematically analyzed the convection heat transfer driven by radial and normal gravitational forces in a rotating horizontal system. Their work was intended to assist heat transfer calculations for axially rotating systems. However, they did not consider the effect of headspace. They found that when radial gravity dominated the flows tended to be multicellular. On the other hand, when normal gravity dominated, the flows were bicellular. They also concluded that flows driven by radial gravity were more efficient at transporting heat than flows driven by normal gravity. If radial and normal gravitational forces were comparable, large rates of fluid circulation and heat transfer were observed due to complex time dependent motions with large shear. Yang et al. (1988) studied the effect of rotation on natural convection in a horizontally rotating cylinder heated differentially on the two ends. They reported that Coriolis forces dominated at low rotational speeds. Increasing the speed provided more uniform temperature distribution.

Heat transfer has also been studied in different rapidly rotating systems. Kuo et al. (1960) studied the heat transfer in flow through rotating ducts and concluded that it was a complex mechanism that could not be treated in terms of conventional parameters, and it requires a better understanding of wave and vortex phenomena. They found that the heat transfer coefficient was independent of temperature difference. Rotational speed was an important factor in their experimental conditions (rotational speed: 100-246 rpm, water flow rate: 76.9-210.6 kg/h and ΔT: 2 to 20 C°).

2.4. The Equations of Motion

The flow and heat transfer characteristics of rotating systems are of practical importance and also theoretical interest. Flow characteristics in rotating sterilization systems affect convective heat transfer. Fluid mechanics tries to understand the motion of fluids and the mechanisms which cause the motion. Newton's law may be locally applied to describe the motion of the fluid, and for an incompressible fluid, Newton's

second law may be written:

$$\rho\left(\frac{D\vec{V}}{Dt}\right) = -\nabla p - \nabla.\sigma + \rho g \qquad (25)$$

where the left hand side is the product of mass and acceleration and the right hand terms are the pressure, shear and gravitational forces causing the motion. This equation is obtained from a momentum balance. The shear stress, σ, can be related to velocity gradients by Newton's law of viscosity. Then

$$\rho\left(\frac{D\vec{V}}{Dt}\right) = -\nabla p - \mu\nabla^2\vec{V} + \rho g \qquad (26)$$

This is known as the Navier-Stokes equation.

Navier-Stokes equations are nonlinear partial differential equations. Exact solutions are obtained for laminar flow and very simple geometries. Approximate, numerical, and statistical solutions have been developed for some complex systems using proper initial and boundary conditions.

Most flows taking place in nature and physical processes are turbulent. Some of the characteristics of turbulent flow are that they are random, irregular, rotational, and three dimensional and originate as an instability of laminar flow. Turbulent flows are dissipative and need a continuous supply of energy to make up for losses such as viscous losses. The common source of energy for turbulent velocity fluctuations is shear in the mean flow. Turbulent flow is a continuum phenomenon. Another characteristic of turbulence is diffusivity that causes rapid mixing and increased rates of momentum, heat and mass transfer.

2.5. Statistical Description of Turbulent Motion

Turbulence is a very complex phenomenon from both measurement and analysis points of view. Because of its random variation in space and time, much analysis relies on statistical approaches. The theory of turbulent flow involves statistics per se which are based on the equations of fluid motion. The statistical description of the fluid flow starts with describing the velocity and pressure in two parts: mean and fluctuating components.

Most of the information that we obtain for flows come from experimental works. Some of the parameters used in statistical theory can be measured experimentally, and formulated in terms of average values. Various averaging techniques are applied (Chen and Jaw, 1998), in which time averaging is generally used. Velocities for turbulent flow can be represented as average value $(\bar{u} \text{ or } \bar{v})$ plus a fluctuating component $(u' \text{ or } v')$.

$$u = \bar{u} + u' \tag{27}$$

$$v = \bar{v} + v' \tag{28}$$

where u is the x-component of the velocity and v is the y-component of velocity. This representation of velocity components can be substituted into the relevant continuity and Navier-Stokes equations, respectively.

$$div(\mathbf{U} + u) = 0 \tag{29}$$

or

$$U\frac{\partial U}{\partial x} + V\frac{\partial U}{\partial y} = -\frac{1}{\rho}\frac{\partial P}{\partial x} + \mu\frac{\partial^2 U}{\partial y^2} - \frac{\partial}{\partial y}(\bar{uv}) \tag{30}$$

where U indicates the mean motion of fluid. Statistically, velocity fluctuations are also given by other average quantities, such as mean square fluctuation, $\overline{u}^2$ .The expression $(\overline{u}^2)^{1/2}$ is known as the intensity of the turbulence component. Also,

$$\left(\overline{q}^2\right)^{1/2} = \left(\overline{u}^2 + \overline{v}^2 + \overline{w}^2\right) \tag{31}$$

is known as the intensity of turbulence.

The fluctuation velocities account for much of the dissipation of energy, mass and heat transfer in turbulent systems. Therefore it is very important to know some information about these parameters.

The intensity of turbulence is directly related to the kinetic energy per unit volume associated with the velocity fluctuations,

$$\Sigma = \frac{1}{2}\rho\overline{q}^2 \tag{32}$$

where Σ is turbulence kinetic energy per unit volume. Writing the last two terms of above equation 30 as:

$$\frac{1}{\rho}\frac{\partial}{\partial y}\left(\mu\frac{\partial U}{\partial y} - \rho\overline{uv}\right) \tag{33}$$

shows that the velocity fluctuations produce a stress on the mean flow. A gradient of this produces a net acceleration of the fluid in the same way as a gradient of the viscous stress. The quantity $\left(-\rho\overline{uv}\right)$ is called a Reynolds stress which arises from the correlation of two components of the velocity fluctuations at the same point. A non-zero value of this correlation implies that the two components are not independent of one

another. For example, if $\overline{uv}$ is negative, then at moments when u is positive, v is more likely to be negative than positive, and vice versa. The Reynolds stresses account for the enhanced mixing observed in turbulent flows. The introduction of the Reynolds stress tensor adds six additional unknowns to the momentum equations.

Turbulence closure requires modelling of the fluctuating terms in momentum or energy equations such as in equation 30. Different techniques have been applied for closure such as algebraic eddy viscosity models (mixing length models), one or two equation models and Reynolds stress models (Marvin, 1983).

The correlation coefficient is a statistical measure of the relationship between two sets of quantities. In this instance values in the correlation equation could be simultaneous values of the same component of the velocity at two different points or two different components of the velocity at a single point. Their values indicate whether or not, or to what degree of fluctuating velocity, components are statistically dependent. In terms of flow this will indicate the relative amount of structured (contained in organized eddies) versus random turbulence that is present. Values of the correlation coefficient can range from -1 to +1. The "-1" indicates a negative correlation, on the other hand "+1" indicates the quantities are directly related. Values of zero indicate that the quantities being tested are not related. The concept of correlation can be extended to higher orders such as $\overline{u_1 u_2 u_3}$.

Most turbulence studies have been based on the energy cascade model in which energy is transported from large to small eddies. The smallest eddies are limited to a finite size by viscous dissipation at high shear rates. The largest eddies are limited in size by the boundaries of the system and are able to interact with the main flow and the boundaries to extract energy through the Reynolds stresses. It is assumed that smaller eddy sizes are due to inertial vortex stretching.

In analyzing turbulence, some measure of the distribution of the turbulent kinetic energy between various eddy sizes is required. It is possible to estimate the size of the turbulent eddies by correlating the fluctuating velocity components in the flow system. The Eulerian correlation tensor is written as:

$$Q_{ii}(r) = \overline{\sqrt{u_i^2(x)}\sqrt{u_i^2(x+r)}} \tag{34}$$

which is defined as the time averaged product of the root mean square (RMS) fluctuations at each point.

The Eulerian correlation will decrease from a maximum value as the separation distance increases. The shape of the correlation curve provides information about the average size of the eddies. It may be transformed from physical space to wave number space by taking the Fourier transform of the correlation tensor. The energy spectrum function is defined as;

$$E(k) = \frac{1}{n}\int_1^\infty kr \sin krQ(r)dr \tag{35}$$

where the wave number, k, is related to the wavelength;

$$k = \frac{2\pi}{\lambda} \tag{36}$$

The energy spectrum function defines the way in which the turbulent energy is distributed among the various sizes of eddies.

If a fluid bounded by a solid wall, presence of viscosity affects the motion near the wall. Physical considerations suggest that the velocity profile near the wall depends on only the parameters relevant near the wall and does not depen on the free-stream velocity or the thickness of flow. The inner part of the wall layer (consists of 3 layers: viscous sublayer, buffer layer, and logarithmic layer), right next to the wall, is dominated by viscous effects and is called the viscous sublayer. Reynolds stresses are small and still found there. Because of the thinness of the viscous sublayer, the stress can be taken as uniform within the layer and equal to the wall shear stress. The region where the velocity distribution is neither linear nor logarithmic is called the buffer layer. Neither the viscous stress nor the Reynolds stress is negligible here. The next layer is

called the logarithmic layer where the flow is still dominated by the wall, but the turbulence develops sufficiently to render the viscous stress negligible. The mean velocity varies nearly logarithmically in this region. The last region is the turbulent core, in which the largest scales of motion are independent of viscosity.

2.6. Laser Doppler Velocimetry

Laser Doppler Velocimetry (LDV) is a non-intrusive flow measurement technique using electro-optical devices which may be applied to measuring velocities in various liquid and gas systems. To date it is one of the most accurate flow measuring techniques, as compared to hot film anemometer and others. In LDV, very small particles moving with the fluid are illuminated with a focussed laser beam and become sources of scattered light. The velocity of these particles is then determined from the change in frequency (Doppler shift) of the scattered light due to the movement of the particles. LDV has many advantages for measurement of velocities compared to other methods:

a) it is a non-intrusive technique because no probe is placed in the flow which would cause disturbance in the flow,
b) no calibration is required,
c) flow velocity is measured directly, and is not strongly dependent on the temperature, density or composition of the medium,
d) there is a small sensing region,
e) it has the ability to measure more than one velocity component at the same time.

Applications of LDV range from low velocity measurements such as natural convection flows (Plattern et al., 1986) to complex flows such as in rotating machines (Elder and Forster 1984), flames (Cheng and Ng, 1983), supersonic flows, etc. It is possible to determine velocity of flows close to moving surfaces, vibrating surfaces, and in combustion and separated flows, multi-phase flows (Drain, 1980). In addition,

size distributions of particles can be determined by this technique.

2.6.1. Doppler Shift Phenomenon

The change in the frequency of wave motion owing to the relative motion of the source and the receiver is known as the Doppler shift. The Doppler shift phenomenon is shown in Figure 1.

Doppler shift is explained by electromagnetic wave theory. Electromagnetic waves consist of travelling electric and magnetic waves that vary sinusoidally in space and time. The magnetic component is not very important in optics. In a wave of well defined and constant intensity, the electric field at a point varies sinusoidally with time at the defined frequency. The phase of motion varies with distance, x, along the direction of propagation. Thus at any given time, variation of the electric field with x is also sinusoidal.

The basic principle of Laser Doppler Velocimetery is primarily concerned with the frequency shift of light scattered from a moving object. In Figure 1 where the *i*th particle located at $x_i(t)$ scatters the light wave with complex vector E_{li} from the incident illuminating beam E_{ol}. We assume that the illuminating wave is a plane wave (in reality it is a spherical wave at the beam waist, which is then taken as a plane wave), linearly polarized in the spatial region, with frequency ω_{ol} in the direction of propagation $\hat{s}_1$ (unit vector), wave number $k=2\,\Pi/\lambda$, intensity I_{ol} (W/m^2) and direction of linear polarization $\mathbf{p_1}$. The incident wave may be represented by the complex wave (only the real part is shown)

$$E_{ol} = \sqrt{I_{ol}(X)}\, e^{\,i\Phi_{ol}(x)} p_1 \qquad (37)$$

where $\Phi_{ol}(X) = \omega_{o1} - k s_1 \; x$.

The particle scatters a light wave from E_{ol} in all directions and a point **r** is said

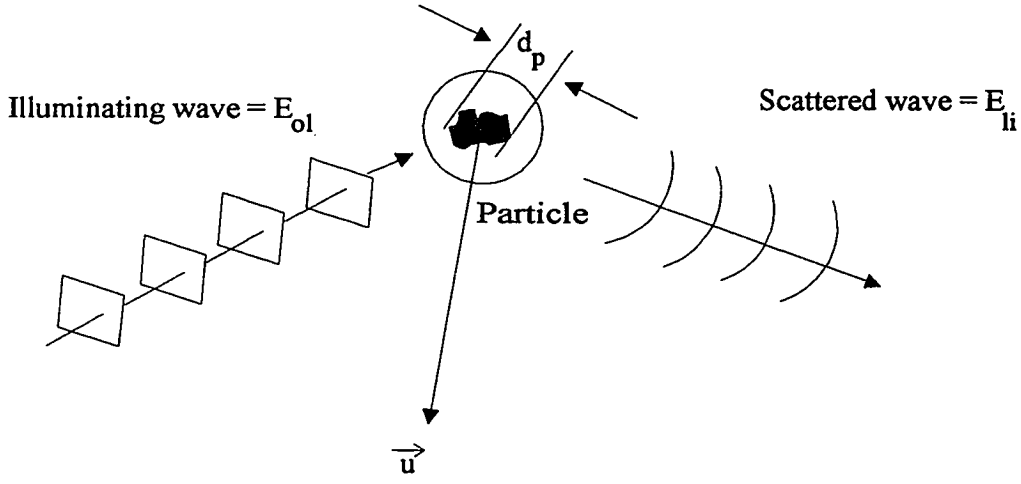

Figure 1. Light scattered by a moving particle.

to be in the far field of the particle. In the far field the light is scattered by the particle in all directions in a spherical manner, and its electric vector is given by,

$$E_{li} = \sqrt{I_{ol}(X_i)}\frac{\sigma_{li}}{k|r-x_i|}e^{j[\varpi_{ol}(x)-k|r-x_i|} \tag{38}$$

By considering the far field approximation $|X| << |r|$, the vectors r-x_i and r are considered to be nearly parallel, and by simple geometry $|r-x| \approx r - x_i.r$. Then the phase factor Φ_{ol} becomes

$$\Phi_{ol} = \varpi_{ol}^{t-kr+kX_i(\hat{r}-\hat{s}_l)} \tag{39}$$

and the electric field becomes,

$$E_{lo} = \sqrt{I_{ol}}\frac{\sigma}{kr}e^{j\Phi_{li}} \tag{40}$$

Equation 40 implies that the scattered wave is approximately a spherical wave whose wave depends on the particles position (term $k\,X_i.s_l$)

The frequency is now defined as the time derivative of its phase. From equation 40:

$$\Phi_{li} = \varpi_{ol} + kV_i(t)(\hat{r}-\hat{s}) \tag{41}$$

where $V_i(t)$ is the particle velocity. Equation 41 gives the frequency in radians per second. In units of Hertz the frequency will be:

$$V_{li} = \frac{\Phi_{li}}{2\Pi} = V_{ol} + \frac{V_i(\hat{r} - \hat{s})}{\lambda} \qquad (42)$$

where V_{ol} is the frequency of the illuminating beam, in Hertz. Equation 42 is the basic formula of the Doppler shift phenomenon. This equation implies that the Doppler shift is the sum of the shifts associated with the particle's component of velocity away from the incident wave, $-v_I \hat{s}_I$ and the particle's components of velocity toward the observer at r, $v_I \hat{r}_I$. Note that the doppler shift has a sign, so that the flow in the positive shift direction can be distinguished from a negative one. The maximum Doppler shift in the frequency occurs where at $\hat{r} = -\hat{s}$ and its maximum value is $\Delta f_{max} = 2 \mid v \mid / \lambda$, so that $\Delta f_{max}/v = 2/\lambda$. For a typical value of $\lambda = 480\ nm$, the maximum frequency difference is *4* MHz. Usually **r** is more nearly parallel to $\hat{s}$, and a typical value is 0.4 MHz/(m.s^{-1}). Thus for a velocity of 0.5 m/s the shift would be around 0.2 MHz.

If the Doppler shift of the scattered light is large enough, it may be measured directly. However, in most systems, LDV measurement gives very low Doppler shifts, in the range of 10 kHz -10 MHz, which are too low for direct measurement. Therefore, most laser systems use optical beating. The basic frequency of the light used is about 10^{14} Hz. Thus 10 kHz or even 30 MHz cannot be detected unless they are added to the basic light frequency. The method used in all Laser Doppler Velocimetry is to subtract the basic light frequency from the total frequency by the technique called optical heterodyne detection or optical mixing. This is accomplished at the surface of a photomultiplier by combining two light waves. The mixed output then contains sum and difference frequencies and harmonics.

A normal optical detector is non-linear in an electrical sense since its output is proportional to the intensity of the incident light, (i.e., the square of the optical electrical field). Since a photomultiplier is a square-law device, the output will be of the following form (e.g., two sine waves coming in):

form (e.g., two sine waves coming in):

$$(\sin \sin \varpi_1 t + \sin \varpi_2 t)^2 = \sin^2 \varpi_1 t + \sin^2 \varpi_2 t + 2 \sin \varpi_1 t \sin \varpi_2 t$$

$$= \sin^2 \varpi_1 t + \sin^2 \varpi_2 t + [\cos (\varpi_1 + \varpi_2) t + \cos (\varpi_1 - \varpi_2) t] \quad (43)$$

Three methods which are commercially available combine the Doppler shift phenomenon and the heterodyne detection. These are, dual beam, reference beam, and dual-scattered beam anemometers. In the reference beam method, light from a laser source is divided by a beam splitter, most of the light being focussed by a lens to a measuring point. Light scattered by particles moving with the fluid is received by a photomultiplier tube. The weaker beam from the beam splitter, unshifted reference is directed to the detector by a mirror. The output from the photomultiplier contains a signal of the difference frequency between the two beams (incident beam, $\hat{s}$ and the reference beam, $\hat{r}$). In the dual-scattered system, the scattered light is collected from two directions and $\hat{r}_1$ and $\hat{r}_2$ are heterodyned. Dual beam velocimeters are used most often. The scattered light from two incident beams $\hat{s}_1$ and $\hat{s}_2$ is heterodyned. Two beams of equal intensity are focussed at the measuring point. The scattered light from the measuring point is focussed onto a photomultiplier. In this method large collection apertures can be used to produce strong signals without violating coherence requirements. In the dual beam LDV, a scattering particle is illuminated with two plane waves E_{o1} and E_{o2}. The particle scatters two waves E_1 and E_2 with frequencies

$$f_1 = f_{01} + \left(\frac{\nu(\hat{r} - \hat{s}_1)}{\lambda} \right) \quad (44)$$

$$f_2 = f_{02} + \left(\frac{\nu(\hat{r} - \hat{s}_2)}{\lambda} \right) \quad (45)$$

since $f_{o1} = f_{o2}$

$$\Delta f = \frac{v(\hat{s}_2 - \hat{s}_1)}{\lambda} \tag{46}$$

The difference is independent of the scattering direction $\hat{r}$, so that the heterodyne frequency is independent of the detector location and is the same at every point on the photodetector.

$$\delta f_D = \frac{2(\sin\kappa)v}{\lambda} \tag{47}$$

The equation can be written simply as:

$$\Delta f_D = \frac{2(\sin\kappa)v}{\lambda} \tag{48}$$

where 2κ is the angle between incident beams. This is the general equation used for the LDV. The system measures the velocity component, where it is perpendicular to the bisector of the two illuminating beams and is in the same plane as the beams.

2.6.2. LDV System

A schematic diagram of the Laser Doppler Velocimeter set-up used in the present study is shown in Figure 2. The laser and optical components are mounted on a vibration free optical base. Each component of the LDV system used is briefly described in the materials and methods and the appendix.

A laser light is generated and passes through the beam collimator which ensures the laser beam is collimated along its entire length. Then it passes through a polarization rotator, and after being linearly polarized, the laser passes through an attenuator and dispersion prism that splits the incoming beam into 3 strong beams (the blue beam at

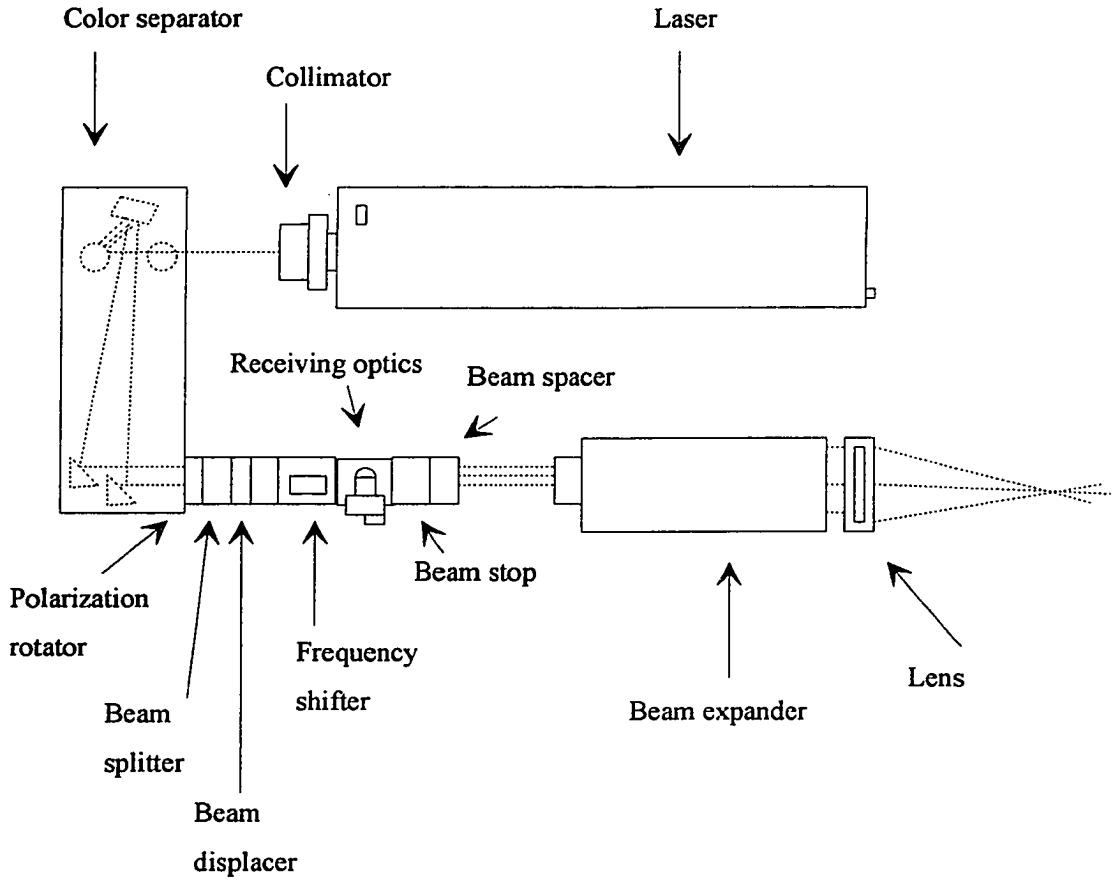

Figure 2. Layout of the laser Doppler Velocimeter system.

488 nm, the green beam at 514 nm and the violet beam at 476.5 nm) and several very weak beams. With the help of two mirrors, the blue and green beams are selected and are set parallel to each other and the base. After passing through the polarizing rotator, the beams enter the beam splitter that splits the green and the blue beam into two beams in the vertical and horizontal planes, respectively. The frequency shifter optics module is placed after the polarizing rotator. Then beams are adjusted by the beam splitting and steering so that the beams are 25 mm away from the center. After leaving the frequency shifter, the beams pass through focussing and receiving optics, where they are focussed at the exit aperture after passing through color separators. Photomultiplier apparatuses are then attached. After the receiving lens, the four beams pass through a beam spacer and beam expander and finally a focussing lens. Beams cross at a focal length of 480 mm.

During an experiment, the light is collected by a set of lenses and focussed down to a pinhole aperture and then it goes to the photomultiplier. The optical mixing of laser beams then takes place at the surface of the photomultiplier. The illuminating beams are blocked from going into the photomultiplier, since they would swamp the scattered light. The photodetector also receives some optical noise such as background room light, light from flares and reflections from different objects. The lens pinhole system is so designed that it will reject most of these extraneous light sources and the pinhole is smaller than the measuring volume, which increases the signal to noise ratio. The measuring volume can be seen schematically in Figure 3.

The laser used was a Lexel Ar-ion laser, with output power of 2W and an on-axis backscatter optical system. Other features were: a focal length of 480 mm; beam diameter of 1.2 mm; beam expander ratio of 3.75; beam spacing of 131.25 mm, and half angle of 7.78 degrees. The resulting probe volume (see Figure 3) formed where the two beams intersect was approximately ellipsoidal in shape with the following dimensions:

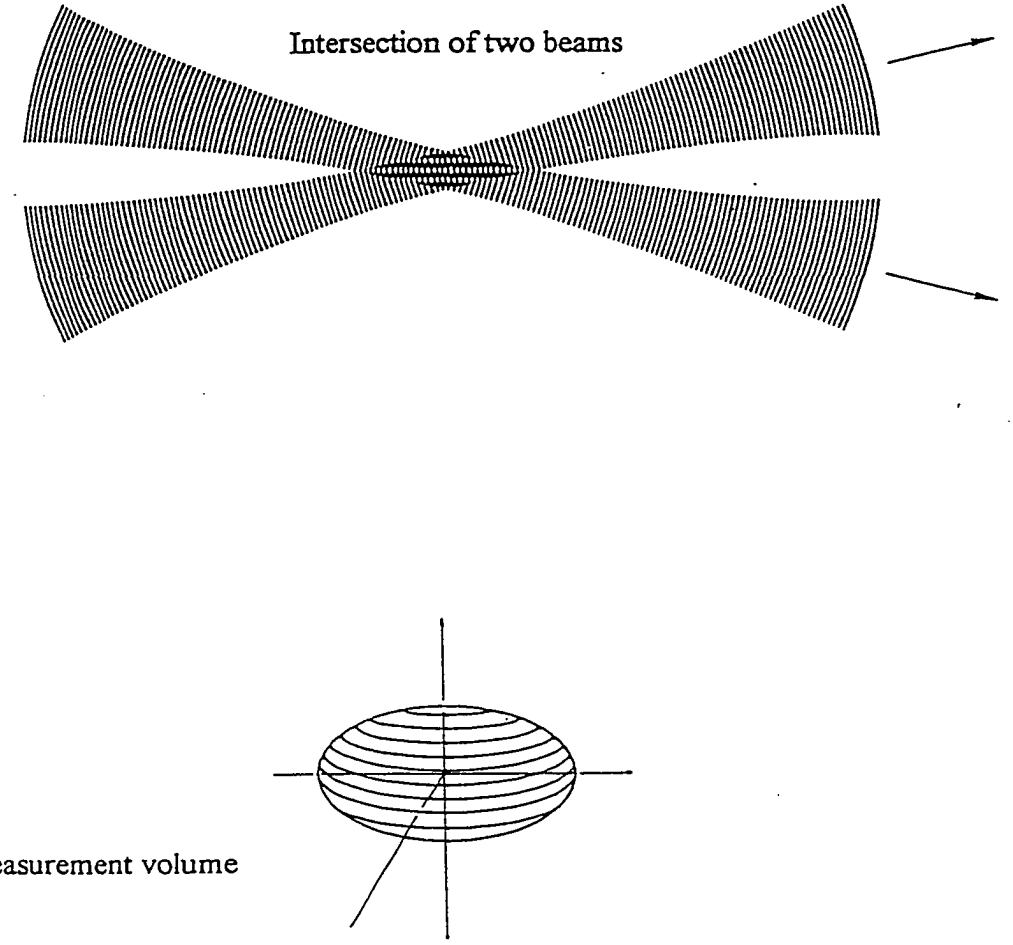

Figure 3. Measurement volume shown as the intersection of the laser beams.

	Green Beam	Blue Beam
diameter	69.87 μm	66.27 μm
height	70.50 μm	66.81 μm
length	516.33 μm	489.54 μm

The measuring volume is at the intersection of the beams, and when a particle passes through the measuring volume, it scatters light. A particle moving in the control volume produces a signal proportional to the modulated component of the intensity distribution of fringe amplitude. The major axis of the probe volume was oriented parallel to the axis of the rotating cylinder. The x and y components of the velocity were measured simultaneously.

2.6.3. Data Processing

Once the signal processor converts the signal from a frequency to a voltage or a number that is proportional to the velocity, the next step is to analyze the data for the desired information. Along with mean velocity information, the following information is often of interest:

a) amplitude information such as rms, Reynolds stress, high order moments,
b) temporal information (correlation with time delay, power spectrum), and
c) spatial information (two-point spatial correlation).

Data processing is the last step in the LDV measurement, after the signal processor converts the incoming signal to an analog output or a number. Data processing depends on the signal processor and the quality of the signal such as burst and data densities. Low data density may cause some problems. One such difficulty arises from the fact that for a fluctuating velocity field more particles pass through the measuring volume per unit of time at high velocities than at low velocities. This will

cause a distortion of both data average and time average toward higher velocities. This phenomenon is called velocity bias (McLaughlin and Tiederman, 1973). Fringe biassing is also a potential problem in LDV measurements, which occurs when the signal processor requires a minimum number of cycles to make a measurement, however, some particles may fail to pass this minimum requirement. If particles that pass from the center of the measuring volume are crossing more fringes that pass near the edges of the volume at oblique angles, this means that resulting data are biassed toward samples from perpendicular velocities. Fringe bias correction has not been well studied. Frequency shifting adds cycles to a Doppler burst by moving the fringes with respect to the fluid.

The flow velocity is related linearly to the measured Doppler frequency by the fringe spacing which is a constant. Fringe space is the distance between the light fringes in the interference pattern of the measurement volume.

$$Velocity = F_d \times D_f \tag{49}$$

If frequency shifting is used, then,

$$Velocity = \left(F_d - F_{shift}\right) \times D_f \tag{50}$$

where

F_d = measured Doppler frequency, D_f = optical fringe spacing, and F_{shift} = frequency shift.

The software FIND (version 4.03, TSI Inc., St. Paul, MN) uses transit time weight to correct for velocity bias.

2.6.4. Equations for Calculating Various Parameters from LDV Data

This section describes the equations that are used to compute velocity statistics. The Data-processing software calculates the following parameters as

$$Velocity\ mean\left(\bar{V}\right)=\frac{\Sigma V\tau}{\Sigma\tau} \tag{51}$$

where τ is total burst time.

$$Standart\ Deviation\ (\sigma_v)=\sqrt{\left(\frac{\Sigma V^2\tau}{\Sigma\tau}-\bar{V}^{\,2}\right)} \tag{52}$$

$$Turbulence\ intensity=\frac{\sigma_v\ x\ 100}{\bar{V}}=\frac{\sqrt{\bar{V}^{\,2}}}{\bar{V}} \tag{53}$$

$$Third\ moment=\frac{\Sigma V^3\tau}{\Sigma\tau}-\left((3x\frac{\Sigma V^2\tau}{\Sigma\tau}x\bar{V})+2(\bar{V})^3\right) \tag{54}$$

$$Skewness\ coefficient=\frac{3^{rd}\ moment}{2(\sigma_v)^3} \tag{55}$$

$$4^{th}\ m=\frac{\Sigma V^4\tau}{\Sigma\tau}-\left(4x\frac{\Sigma V^3\tau}{\Sigma\tau}x(\bar{V})\right)+\left(6x\bar{V}^{\,2}\ x\frac{\Sigma V^2\tau}{\Sigma\tau}\right)-3\bar{V}^{\,4} \tag{56}$$

where $4th\ m$ = fourth moment

$$Flatness\ coefficient = \frac{4^{th}\ moment}{(\sigma_v)^4} \tag{57}$$

$$Reynolds\ stress = \overline{uv} - \bar{u} \times \bar{v} \tag{58}$$

$$Correlation\ coefficient = \frac{(Reynolds\ stress)}{\sigma_i \sigma_j} \tag{59}$$

2.7. Objectives

A review of the literature revealed that very limited qualitative and quantitative information is available to describe flow phenomena in axially rotating partially filled cylindrical containers.

The objective of this thesis was, therefore, to investigate the flow behavior in model systems in order to better understand the complex hydrodynamics of fluid foods in axially rotating cans in a retort. The investigation focussed on the effects of some critical parameters such as the headspace, rotational speed and viscosity of the fluid on the overall hydrodynamics of the flow. Specifically, the following tasks were undertaken to achieve the overall objective:

a) to design and build an experimental set-up capable of conducting studies within the range of parameters involved,
a) to select and modify a system capable of performing non-intrusive in-situ measurements of flow properties,
b) to conduct measurements of the fluid velocity field as a function of the critical parameters,
c) to provide an appropriate definition of the flow Reynolds number and use it to determine the relevant flow domain
d) to carry out a statistical analysis to determine the effects of different factors and their interactions on velocity,
e) to determine the energy and power spectra of the velocity fluctuations and turbulent energy transport mechanisms, and
f) to apply this knowledge to facilitate understanding the heat transfer in axially rotating cans.

CHAPTER 3

MATERIALS AND METHODS

3.1. Methodology and Materials

The heat transfer rate is a direct function of the temperature difference between the can surface and the fluid, material properties and, most importantly, the flow structure, (i.e., turbulent mixing of the fluid inside the can). While the effect of the temperature difference and the material properties can be confidently predicted from existing knowledge available in the literature, the effect of flow structure remains to be determined.

In rotating systems, the flow structure inside the can is controlled mainly by three major parameters (Eisner, 1988); (a) the rotational speed of the can; (b) the apparent viscosity of fluid in the can and (c) the headspace between the free surface of the fluid and the inner surface of the can.

In thermal processing the axial rotation of partially filled cans is an effective way of increasing the rate of heat transfer. This is achieved mostly due to forced convection currents. Any factor that affects convection currents will, in turn, affect the heat transfer rate to the contents of the cans. The heat transfer rate also depends on various factors such the food consistency, retort rotational speeds, headspace volume, particle content, initial product temperature, retort temperature, properties of the container and others. Of these factors, three have been found to have pronounced effects on convection currents in the container: apparent viscosity, headspace, and rotational speed. Indeed, the rate of heat transfer to highly viscous food products may not be improved by agitation because they may behave as solid-like materials which transfer heat mainly by conduction. The amount of headspace controls the bubble movement that again affects the convection currents. Rotational speeds also affect the convection pattern set up inside the container.

Therefore, within the scope of this study, these three factors were selected as the

experimental variables. The ranges of the variables are shown in Table 2.

Table 2. Experimental variables used in this study.

	Solution (w/w)	Rotation type	Rotational velocity (rpm)	Headspace height (cm)
Newtonian fluids	Water	continuous	200, 300, 350	0.25, 0.5, 1
	Water	stop-go*	200, 300, 350	0.25, 0.5, 1
	Glycerol, 25%	continuous	200, 300, 350	0.25, 0.5, 1
	Glycerol, 25%	stop-go	200, 300, 350	0.25, 0.5, 1
	Glycerol, 50%	continuous	200, 300, 350	0.25, 0.5, 1
	Glycerol, 50%	stop-go	200, 300, 350	0.25, 0.5, 1
	Glycerol, 80%	continuous	200, 300, 350	0.25, 0.5, 1
	Glycerol, 80%	stop-go	200, 300, 350	0.25, 0.5, 1
Non-Newtonian fluids	CMC-L, 2.0%	continuous	200, 300, 350	0.25, 0.5, 1
	CMC-L, 2.0%	stop-go	200, 300, 350	0.25, 0.5, 1
	CMC-M, 2.0%	continuous	200, 300, 350	0.25, 0.5, 1
	CMC-M, 2.0%	stop-go	200, 300, 350	0.25, 0.5, 1
	CMC-H, 1.5%	continuous	200, 300, 350	0 25, 0.5, 1
	CMC-H, 1.5%	stop-go	200, 300, 350	0.25, 0.5, 1
	Xanthan, 0.15%	continuous	200, 300, 350	0.25, 0.5, 1
	Xanthan, 0.25%	stop-go	200, 300, 350	0.25, 0.5, 1
	Xanthan, 0.15%	continuous	200, 300, 350	0.25, 0.5, 1
	Xanthan, 0.25%	stop-go	200, 300, 350	0.25, 0.5, 1

* stop-go indicates Sterilmatic™ simulated rotation

The Newtonian and non-Newtonian liquids were chosen to simulate food products with a wide range of apparent viscosities. The selection of rotational speed is a critical factor in simulating the retort operation. The methodology used to determine rotational speed is explained later in section 3.5. Two different modes of rotation were used: continuous and stop-go. While continuous rotation is the typical mode of operation for flame-type sterilizers (although rotational speeds are different); the stop-go mode is more appropriate to simulate the Sterilmatic™ retort operation.

Measurement of headspace and viscosity were conducted prior to each experimental run. For continuous operation, the rate of revolution was recorded after the steady-state speed was obtained, whereas for stop-go operation, it was monitored continuously.

For each set of experimental conditions the following velocity components were measured. The vertical component was measured using green laser light while horizontal velocity was measured using blue light. The velocity components obtained in the Cartesian coordinate domain were converted into the cylindrical coordinate domain using the conversion methodology given in section 3.7.2. The converted velocity data were then used to obtain velocity contours inside the container.

Measurement points are shown in Figure 4. Note the holes or places lacking data in Figure 4. "Gridding" is therefore applied to calculate the values at these locations using the data points. Gridding also provides regularly spaced data for use in creating surface representations. Gridding attempts to interpolate a "z" value at the intersection of each row and column of grid lines. The equation used in inverse distance gridding was:

$$Z = \frac{\sum_{i=1}^{n}\left(\frac{z_i}{d_i}\right)^2}{\sum_{i=1}^{n}\left(\frac{1}{d_i}\right)^2} \qquad (60)$$

where z_i = a neighbouring point, d = distance and n = number of z elements.

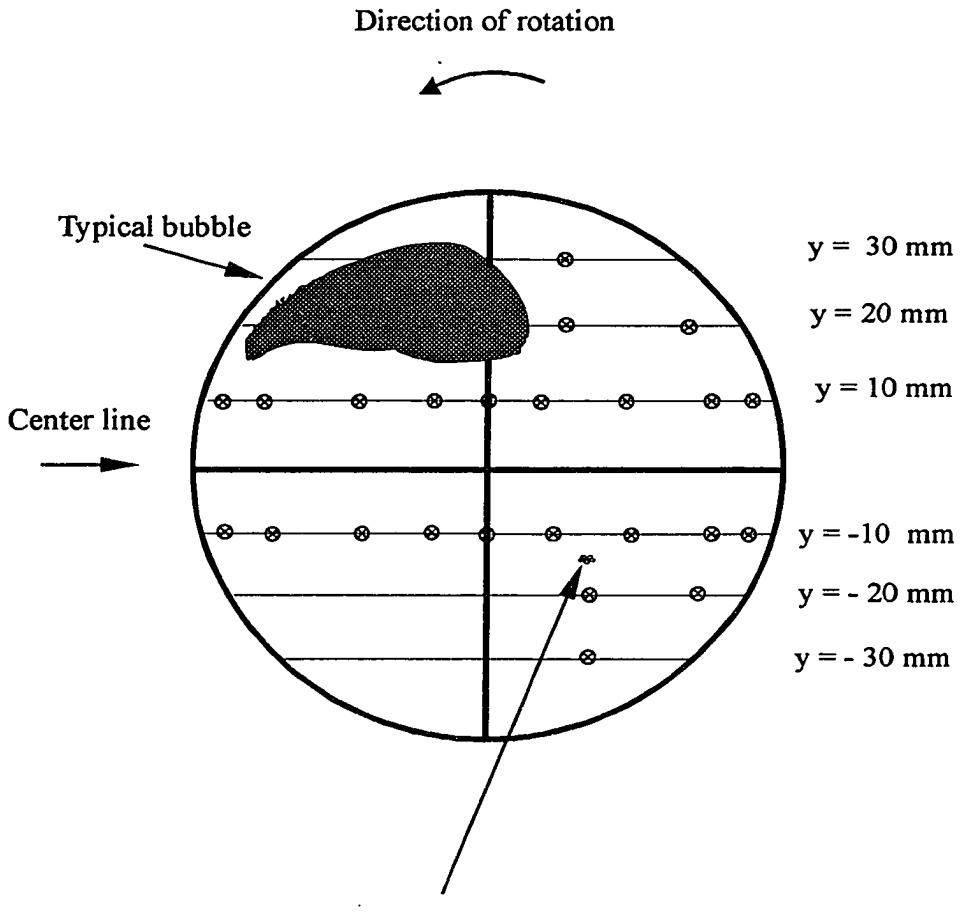

Figure 4. Location of measurement points shown in an end view of the horizontal cylinder.

A contour map is a plot of three values of which the first two are (x,y) coordinates and the third (z) is defined by lines of equal values generated by a gridding method. The area between two adjacent contours contains points having values which lie only within the range defined by enclosing lines.

The contours represent the motion of the fluid inside the can. They can also show the size, motion, break-up and coalescence pattern of the bubbles formed as a result of headspace. In addition to the graphical representation of the velocity data in the form of velocity contours, the turbulence intensity, correlation coefficient and Reynolds stresses were calculated. The calculated turbulence parameters were then used to quantify the effect of independent parameters (rotational speed, headspace and apparent viscosity) on the overall behaviour of the fluid motion as well as their specific mixing patterns.

3.2. Solutions Used in Experiments

Several Newtonian and non-Newtonian solutions were used in the experimental investigation. The Newtonian liquids used were water and solutions of glycerol at different concentrations to achieve a range of viscosities. The non-Newtonian fluids were aqueous carboxymethylcellulose (CMC) and xanthan polymer solutions. They were prepared at various mass fractions to obtain desired viscosities. Xanthan polymer was selected initially because of its thermal stability. However, because of its poor optical properties (i.e., not being fully transparent to allow for LDV measurement). CMC was chosen as it provided much better optical clarity and covered a wider viscosity range.

3.2.1. Preparation of Xanthan Polymer Dispersion

The xanthan polymer used was obtained as a powder from the NutraSweet Kelco Company, San Diego, CA (Keltrol, # 77375 A). The polysaccharide was used without purification. However, a long centrifugation was applied to remove debris. The xanthan powder was sprinkled onto the sides of a vortex of double-distilled water

formed in a high speed blender (Waring 7011, Model: 31BL92, New Hartford, CT) and mixed for 5 min. The dispersions were centrifuged at 10,000 rpm (13750 x g) for 3 h to remove entrapped air bubbles and debris. The xanthan polymer concentration in the stock solution after centrifuging was determined by measuring the solids content by drying in an oven. Then the solutions were allowed to remain at room temperature (22°C) and were used within 16 h.

3.2.2. Preparation of CMC Solutions

The CMCs (specifically CMC-7LF, CMC-7MF, and CMC-HF used for different viscosity ranges) were obtained from Aqualan Company (Wilmington, DE). Three different products, CMC-7LF, CMC-7MF, and CMC-HF, were labelled as CMC-L, CMC-M, and CMC-H, respectively. The CMC was dissolved as described for xanthan polymer. The dispersions were left at room temperature for 6 h to remove entrapped air bubbles.

3.2.3 Preparation of Glycerol

Glycerol (99%) obtained from Merck and Co, (Whitehouse Station, NJ) was used to prepare 25, 50 and 80% (w/w) solutions by dilution with double-distilled water.

3.3. Viscosity Measurements

Rheological measurements of the solutions were carried out using two different viscometers, Brookfield models LVT and HB (Brookfield Inc. Stoughton, MA) and Bohlin VOR viscometer (Bohlin Instruments Inc. Cranbury, NJ). All measurements were made at 25.0°C. Standard oils (Cannon Ins. Company, State College, PA) of known viscosity were used to calibrate the viscometers. Viscosities of less viscous solutions of glycerol were measured using a Brookfield model LVT viscometer fitted with an Ultra-low (UL) adapter. Rheological measurements of the non-Newtonian solutions were carried out with the Bohlin VOR viscometer.

The power law model was used to characterize the flow behaviour of non-

Newtonian solutions,

$$\sigma = m\dot{\gamma}^n \tag{61}$$

where σ (N/m^2) is the shear stress, m ($Pa.s^n$)is the consistency coefficient, n is the flow behaviour index, and $\dot{\gamma}$ (s^{-1}) is the shear rate.

Densities of the liquids were measured with a pycnometer at room temperature. Density and viscosity measurements were made at 25°C. Properties of the test liquids are shown in Table 3.

Table 3. Physical properties of the test liquids.

Solution (w/w)	Density, kg/m^3	m, $Pa\ s^n$	n	shear rate range , s^{-1}	number of data	r^2
2% CMC-L	1008	0.022	0.99	18.5 to 461	23	0.99
2% CMC-M	1056	0.179	0.87	11.6 to 581	26	0.99
1.5% CMC-H	1190	1.105	0.73	11.6 to 146	23	0.99
0.15% Xanthan polymer	1056	0.427	0.38	5.81 to 921	25	0.99
0.25% Xanthan polymer	1088	0.944	0.27	0.58 to 921	28	0.99
80% Glycerol	1197	0.05384[1]	1	na[2]	8	na
50% Glycerol	1116	0.00562[1]	1	na	8	na
25% Glycerol	1044	0.01890[1]	1	na	8	na

[1] absolute viscosity

[2] na: not applicable

3.4. Equipment

3.4.1. Test Cylinder

The test cylinder was made of a Plexiglass™ material having internal length of 9.88 cm and inside diameter of 7.44 cm. The flat front surface was constructed of Plexiglass™ (Cadillac Plastic, Dartmouth, NS) while the back end was made of aluminum which was connected to a variable speed drive (Figure 5). The flat back end wall was painted black to reduce the reflections from the incident laser light which may increase the noise. The axis of the cylinder was aligned with the axis of the shaft of the variable speed drive system which provided rotational speeds ranging from 200 to 350 rpm. A pneumatic-clutch was used to produce sudden starts and stops to simulate the Sterilmatic™ retort operation.

The experimental setup was placed on a three dimensional traverse table (Figure 6) which provided for positioning of the test cylinder with respect to the LDV setup. Horizontal traversing was achieved using one dimensional cross sliding tables (Busy Bee Machine Tool, Model B339, Halifax, NS). These two tables were mounted on a scissor lift table (HTS Handling Speciality Manufacturer Ltd., Model D 30-10M, Halifax, NS), which provided the movement in the vertical direction.

. The rotational speed of the cylinder was measured with a Cole-Palmer electronic tachometer (H-08200-50, Cole-Palmer, Niles, IL). The static-height of the container contents was measured with a micrometer.

3.4.2. Preliminary Experiments

Preliminary experiments were conducted to check the alignment of the LDV system by using a rotating disk. A 15.3 cm diameter aluminium disc was covered using fine sand paper to simulate the motion of moving particles through the measurement volume. The linear velocity (v, m/s) at a given radial position on the rotating disc can be calculated as;

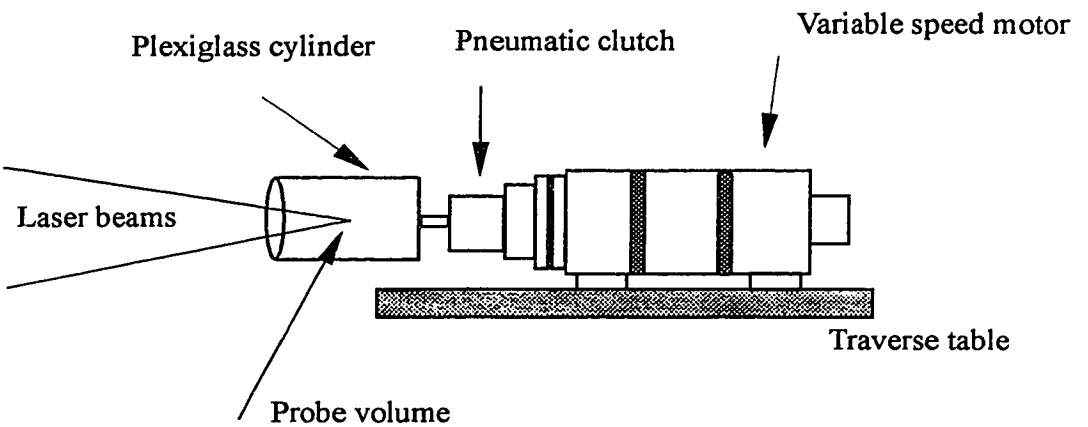

Figure 5. Experimental setup to obtain continuous and intermittent rotation of the horizontal cylinder.

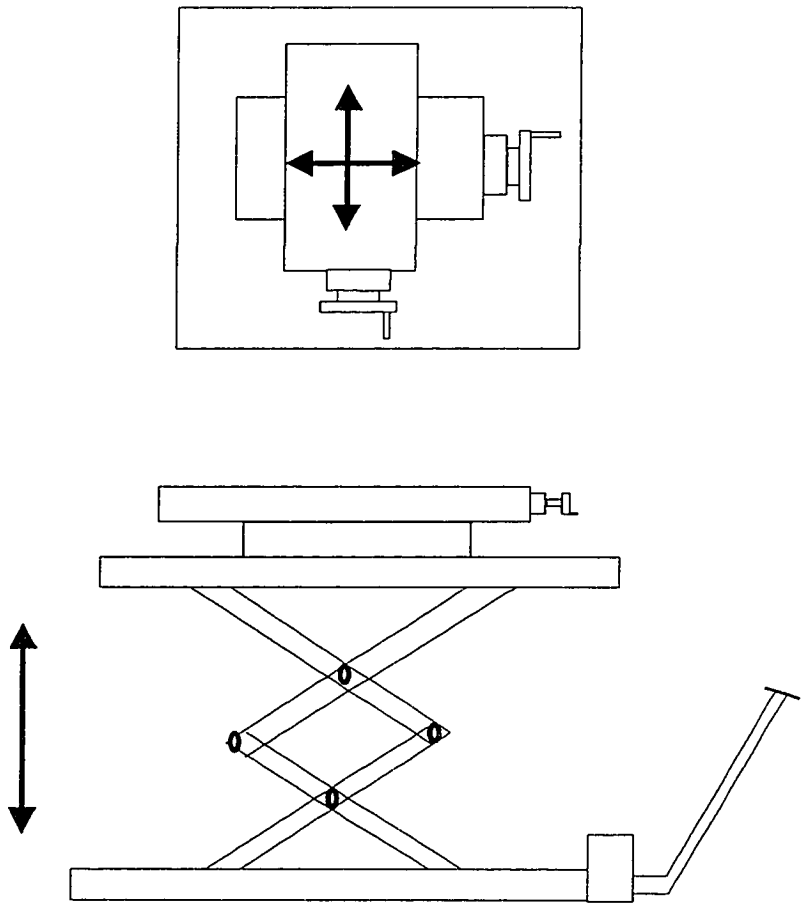

Figure 6. Three dimensional traversing table for positioning the rotating test cylinder in relation to the LDV system.

$$v = \frac{2\pi Nr}{60} \tag{62}$$

where N (rpm) is the rotational speed measured by using the electronic tachometer (H-08200-50, Cole-Palmer, Niles, IL), r is radius (m). Excellent agreement was obtained between experimental and calculated velocity values confirming that the LDV system was properly aligned.

3.5. Rotational Velocity

It has been reported that speed of can rotation is a major factor that would affect the heat transfer. To investigate its effect, three different can rotational speeds were used: 200, 300 and 350 rpm. Commercial retorts have reel speeds between 8 to 10 rpm. However, the rationale behind the selection of rotational velocity of the containers was as follows:

a) Consider a container (of diameter D_c) rotating at N_r rpm on a reel having diameter D_r (See Figure 7). Assuming no slip conditions, the linear velocity of the liquid surface in the container equals the linear velocity of the reel;

$$\pi N_r D_r = \pi N_c D_c \tag{63}$$

and

$$N_c = \frac{N_r D_r}{D_c} \tag{64}$$

Assuming that N_r = 10 rpm, D_r = 200 cm, and D_c = 8 cm, N_c is found to be 250 rpm.

b) Rotation of the can takes place for a short duration of time in order to simulate the Sterilmatic™ operation. The rotation time can be calculated as follows. The rotation takes place in an arc as shown in Figure 6. The reciprocal of the reel rotation gives us the time for

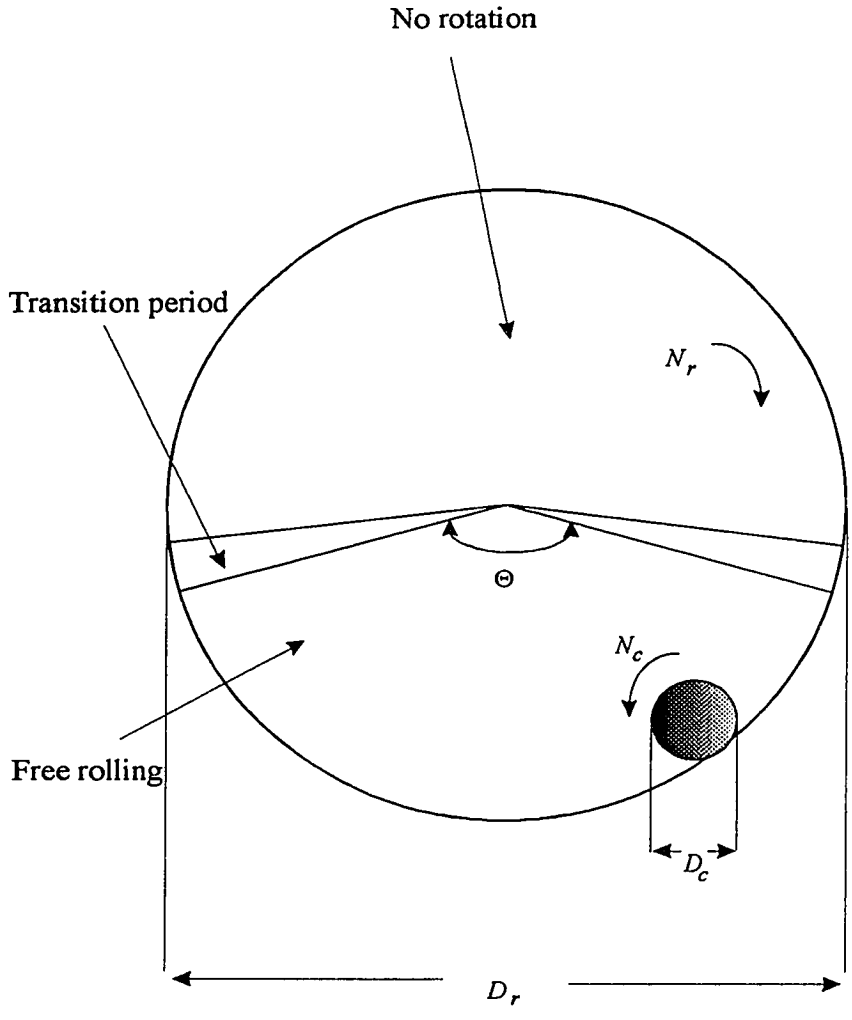

Figure 7. Schematic diagram of rotary cooker.

a reel rotation, designated as t_{rl}. The angle Θ_c characterizes the length of reel arc over which the can will rotate, θ. The time for every reel rotation can be found from the following relationship;

$$t_{rr} = t_{rl}\left(\frac{\theta}{360}\right) \tag{65}$$

and the length of time during which the can does not rotate, t_s is

$$t_s = t_{rl} - t_{rr} \tag{66}$$

Zaman et al. (1991) introduced a factor considering non-ideal can rotation because of slip between the can and reel. Otherwise the factor should be multiplied by instantaneous can rpm. In the present study, this was not considered. In the Sterilmatic™ simulation study, the test cylinder was stationary for 5.53 s and then rotated for 2.37 s with the help of the pneumatically controlled clutch system.

3.6. Seeding

LDV measurements require scattering of light from particles suspended in the flow (already present or seeded). The seed particles whose motion is assumed to represent the fluid motion, must be small enough to follow the flow faithfully, be chemically inactive and have good light scattering characteristics. Seed particles may affect the fluid motion due to their size, shape, density and body forces. For example, the shape of the particle may affect the drag force acting upon it, thus causing slip. Seeding of water flows is normally unnecessary because they usually contain naturally present small particles, depending on the range of velocity and turbulence intensity investigated. Polystyrene latex particles were satisfactorily used by Goldstein and Adrian (1971), and Menon and Lai (1991). Flocculation and coagulation of seed particles can be prevented by the presence of emulsifiers in the suspension.

In practice, however, there are only a few situations where particles naturally present in the flow are sufficient to provide good signal quality and follow the flow.

Therefore, very small particles in varying amounts are usually added to obtain an adequate number of scattering surfaces. Menon and Lai (1991) discussed the factors involving particle requirements for LDV, and indicated that they;

a) must be small enough to faithfully follow the flow,

b) must scatter sufficient light to produce measurable signals,

c) must be present in desirable concentration, and

d) must be inexpensive, non-toxic, non-abrasive and chemically inactive.

Geometric and physical parameters of the particles such as refractive index, particle size and density, shape, etc., affect the quality of signals. Silicon carbide, alumina, polystyrene, microballoons, and TiO_2 are commonly encountered seed particles used in most liquid flow measurements.

It has been shown that seed particles with large relative refractive indices would be a good choice for water flows in backscatter applications. However, particles should be able to follow rapid changes in velocity, and a very slow settling velocity of the particles is important for low velocity flows. Drag force on the particle is also an important factor; it has been shown that drag on the particle creates a velocity lag which can seriously affect fluid flow measurements (Jones et al., 1980). In liquid flows the velocities are usually so small that the primary limitation on the particle size comes from the settling velocity rather than the ability to follow flow. Generally, one particle per measuring volume is satisfactory for particle concentration. In this study, silicon carbide (diameter = 1 μm, $\mu_r = n_p/n_w = 1.95$, $\rho = 3.3$ g/cm^3, $v_s = 1.20$ μm/s), alpha alumina (diameter = 1 μm $\mu_r = n_p/n_w = 1.32$, $\rho = 3.8$ g/cm^3, $v_s = 1.40$ μm/s) and polystyrene latex particles (diameter = 1 μm, $\mu_r = n_p/n_w = 1.95$, $\rho = 1.60$ g/cm^3, $v_s =$ 0.007 μm/s) were tested initially, where μ_r = relative refractive index, n_p= refractive index of particle, n_w = refractive index of water, ρ = density, v_s = settling velocity. Several tests were conducted in water and glycerol using all three seeding particles. Signal qualities at different concentration and velocity ranges were monitored and compared for each group of particles. Polystyrene latex particles of 1 μm diameter were then selected as seeding particles at a concentration of 1 part in 5 x 10^5, since they

provided the best signal to noise ratios that was checked by an oscilloscope.

3.7. Velocity Measurement

3.7.1. Determination of the Location of Measurement Points

Initial tests indicated that measurements of fluid velocity in the immediate vicinity of a bubble were not possible because of the error introduced by the bubble movement during rotation. Furthermore, measurements at very large distances from the front flat surface and near the back end wall were not possible due to the interference of the light scattered from the end wall. Two types of measurements, therefore, were conducted.

a) Measurements taken at z = 25 mm behind the front flat surface (z is the axial direction, see Figure 8). To minimize the effect of front wall (boundary layer effects) and bubble movement that may block the laser beams and change the probe volume placement, 25 mm behind the front flat surface was found to be the best location for this purpose (see Figure 4). All measurements except axial direction studies were taken at 25 mm behind the front flat surface.

The test cylinder was divided into four quadrants in order to easily reference the measurement point (Figure 9). The measurements in the axial direction at the cylinder were conducted in quadrant IV. Since the bubble never reached this quadrant during its rotation in the rotational speeds used, therefore, the limitations imposed by the bubble for velocity measurement were avoided.

b) Axial direction measurements were done in quadrant IV (Figure 9) and (y = -15 mm and x = -15 mm). This eliminated the effect of bubble movement and provided comparisons on the axial direction.

The effect of side walls was also checked by measuring the velocities at different locations parallel to the axis of the cylinder while holding y and x constant (x = -15 mm, y = -15 mm).

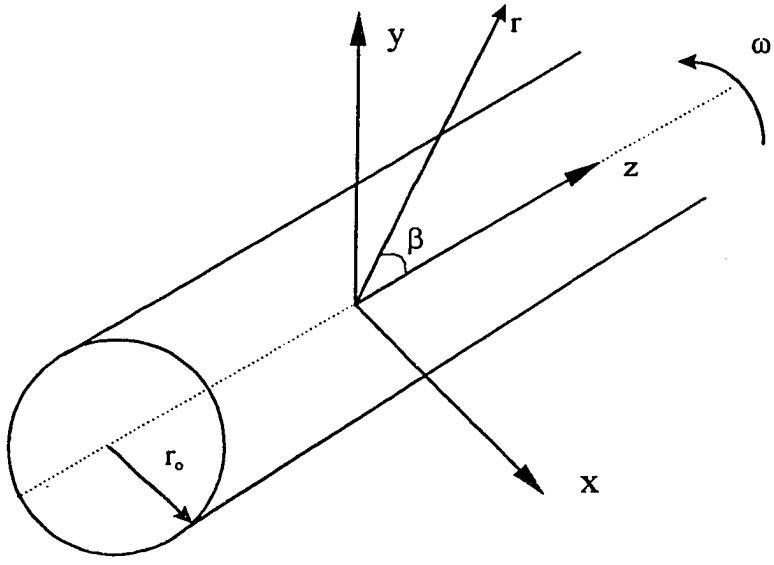

Figure 8. Schematic of coordinate systems for velocity measurement and conversion in the horizontal rotating test cylinder.

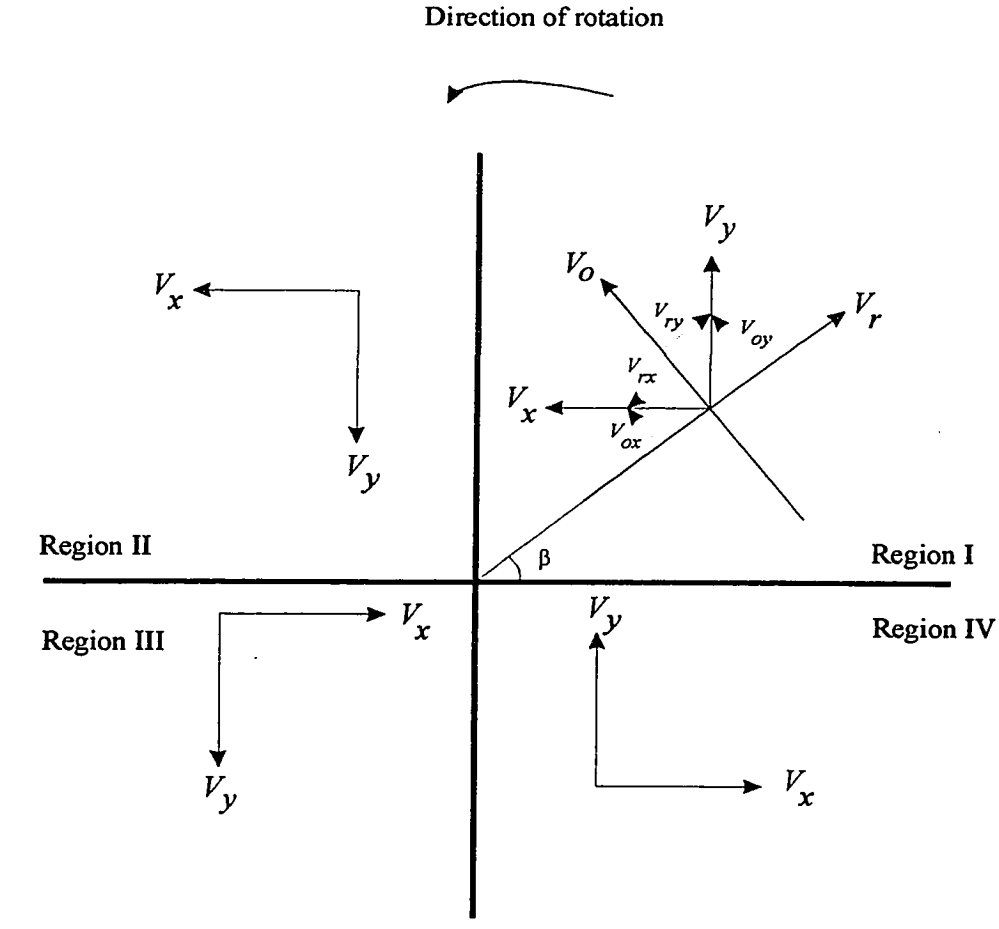

V_x Horizontal component

V_o Tangential component

V_y Vertical component

V_r Radial component

Figure 9. Diagram showing velocity components.

Throughout the experiments for all the measurement locations listed, two types of rotation were used for each experimental point:

a) continuous rotation at various speeds, and

b) Sterilmatic™ simulation of intermittent rotation in which the cylindrical container was initially at rest at time t = 0, then the cylinder was impulsively started rotating around the third axis at a constant speed for 2.37 s and stopped for 5.53 s. Measurements were taken continuously to see the time-velocity profiles.

3.7.2. Velocity Conversion

The traversing mechanism used to conduct the measurement was limited to three linear movements in the x, y and z direction with respect to the fixed measurement volume. In the experimental phase, laser beams were set up to measure the vertical and horizontal velocity components in a partially filled rotating cylinder. Therefore, the experimental data obtained using the LDV system were defined in the Cartesian coordinate system. However, for proper treatment of data and to compare with literature values, conversions of the velocity components into radial and tangential components were required. Therefore, radial and tangential components were calculated from horizontal and vertical components using the following equations (see Figure 9). The equations used for the conversion are as follows:

For quadrant I,

$$V_o = V_x \sin\beta + V_y \cos\beta \tag{67}$$

$$V_r = -V_x \cos\beta + V_y \sin\beta \tag{68}$$

For quadrant II,

$$V_o = V_x \cos\beta + V_y \sin\beta \tag{69}$$

$$V_r = V_x \sin\beta - V_y \cos\beta \tag{70}$$

For quadrant III,

$$V_o = V_x \sin \beta + V_y \cos \beta \quad (71)$$

$$V_r = -V_x \cos \beta + V_y \sin \beta \quad (72)$$

For quadrant IV,

$$V_o = V_x \cos \beta + V_y \sin \beta \quad (73)$$

$$V_r = V_x \sin \beta - V_y \cos \beta \quad (74)$$

CHAPTER 4

RESULTS AND DISCUSSION

4.1. Introduction

The effects of experimental factors; namely, the rotational speed, headspace and apparent viscosity on the overall hydrodynamic behavior of a cylindrical container were investigated for Newtonian (water and glycerol) and non-Newtonian (CMC and xanthan) liquids. Two cartesian velocity components, in the vertical and radial directions were measured by changing the rotational speed, headspace and the consistency. From these measurements, horizontal and tangential velocities, turbulence intensities, and Reynolds stresses were generated.

This chapter begins with explaining the general features of the hydrodynamics of axially rotating cylinders and visual observations carried out during the experiments. Then, the effect of each factor was investigated separately. The power spectrum and the velocity-time histogram analyses which reveal some interesting points about the turbulence structure inside the cylinder were followed by a section which proposes two generalized mixing correlations for axially rotating cylinders containing either Newtonian or non-Newtonian liquids.

4.2. General Features And Visual Observations

With the presence of headspace inside a rotating cylinder, the hydrodynamics of axially rotating cylinders showed complex flow behavior. Before presenting the detailed quantitative data, an explanation of the flow phenomena visualized during the experiments would be useful to highlight some basic features of the axially rotating cylinders. Also, the results obtained by taking photographs can give the overall pattern of fluid motion and qualitatively illustrate the flow (Figures 10 and 11).

Some preliminary experiments were conducted to visualize the flow field, the bubble shape and position of different rotational velocities, headspace and viscosities.

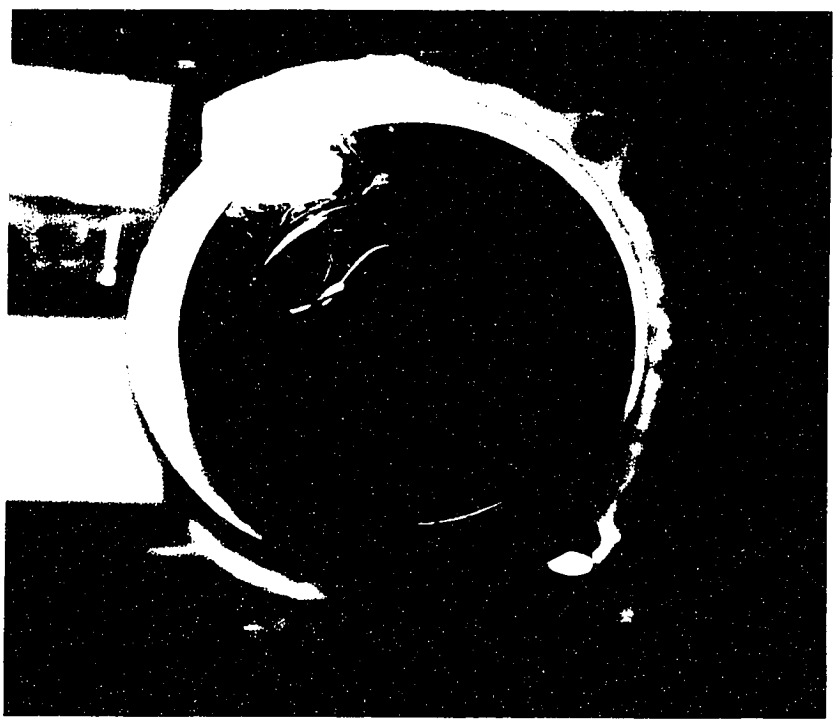

Figure 10. End view of the rotating cylinder partially filled with water showing the cross-sectional shape of the air bubble.

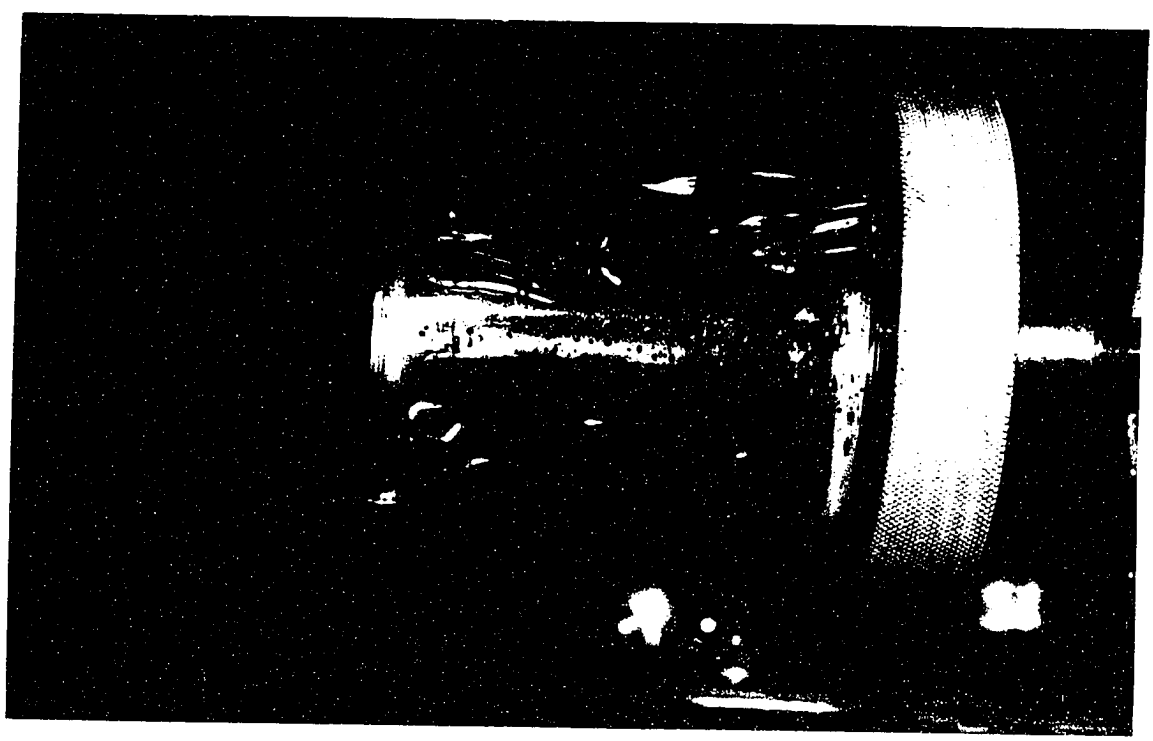

Figure 11. Side view of a typical bubble during rotation of the rotating cylinder at 300 rpm, partially filled with 80% glycerol showing the shape and location of typical air bubble.

The presence of the bubble inside the cylinder caused the turbulence-induced mixing. If the cylinder was completely filled with a liquid, the whole system rotated as a solid body without any mixing taking place. However, when a small portion of the cylinder was left unfilled as a headspace, the headspace bubble maintained its position at the top of the cylinder and acted as a barrier to the rotation of the fluid, thereby causing turbulent flow inside the cylinder (Figure 10).

The cross-sectional shape of the bubble appeared to be similar to an air-foil as can be seen in Figure 10. The bubble movement inside the container showed different behavior with increasing rotational speed, depending on viscosity. For liquids having a low viscosity, the bubble stayed at the top of the cylinder and did not change its shape and position with increasing rotational speed. For higher viscosity fluids, the increase of rotational speed caused the bubble to break into numerous smaller elongated bubbles (Figure 11). These elongated bubbles also caused the diversion of the fluid flow towards the center of the cylinder (Figure 12).

It should be noted that the flow inside the axially rotating cylinder showed chaotic behavior due to this bubble-induced turbulent motion. Depending on the parameters such as rotation rate, headspace and viscosity, an interplay between the gravitational, viscous, and inertial (centrifugal) forces caused an oscillatory flow due to the wavy structure of the internal free surface, which resulted in highly turbulent and vortical flow. The collapse of the headspace bubble into smaller bubbles and their unpredictable motion added more complexity to the problem.

To provide a two-dimensional view of flow structure of the working fluid, velocity, turbulence intensity and Reynolds stream contours were generated under various experimental conditions. These contour plots drawn for both Newtonian and non-Newtonian liquids used in the experiments are shown in Figures 13 to 23. Contours of the mean tangential velocity for 50% glycerol are illustrated in Figure 13. This figure shows that two distinct flow regions developed in the cylinder during its rotation. The first region is the "near wall region" where the fluid gained a strong tangential velocity due to the rotation of the cylinder in which the viscous and inertial (centrifugal) forces

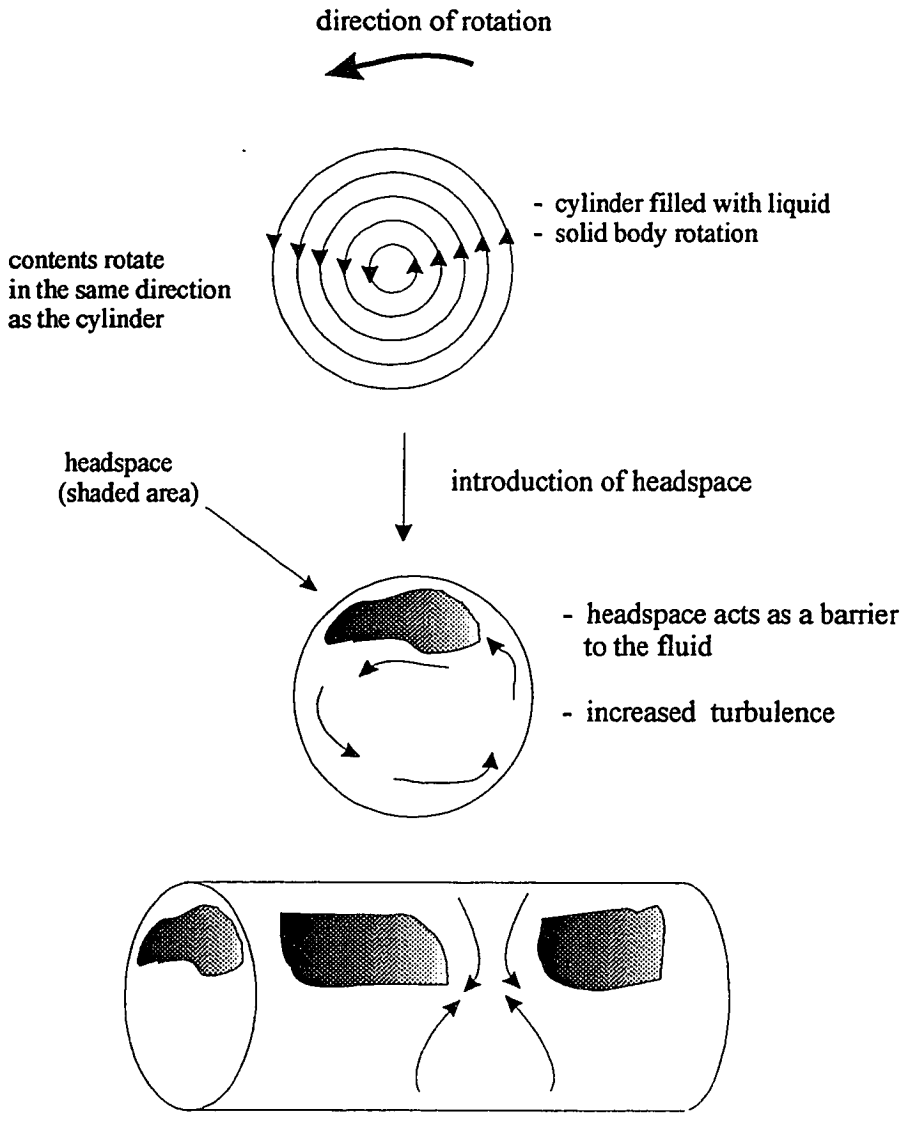

Figure 12. Flow patterns observed before and after introducing headspace into cylinder during rotation.

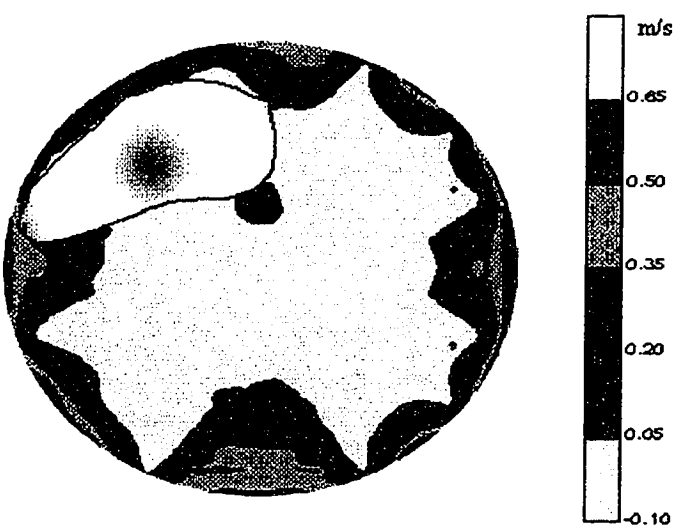

Figure 13. Contours of tangential velocity shown as end view of a horizontal rotating cylinder containing 50% glycerol; 200 rpm, 0.5 cm headspace

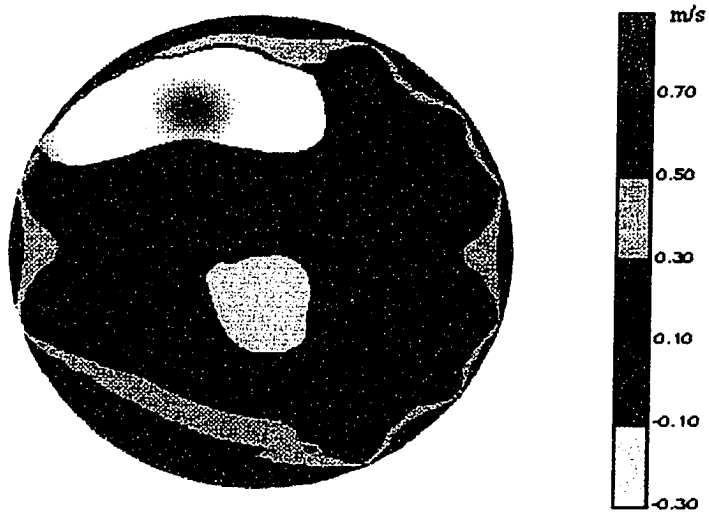

Figure 14. Contours of tangential velocity shown as end view of a horizontal rotating cylinder containing water; 200 rpm, 0.25 cm headspace

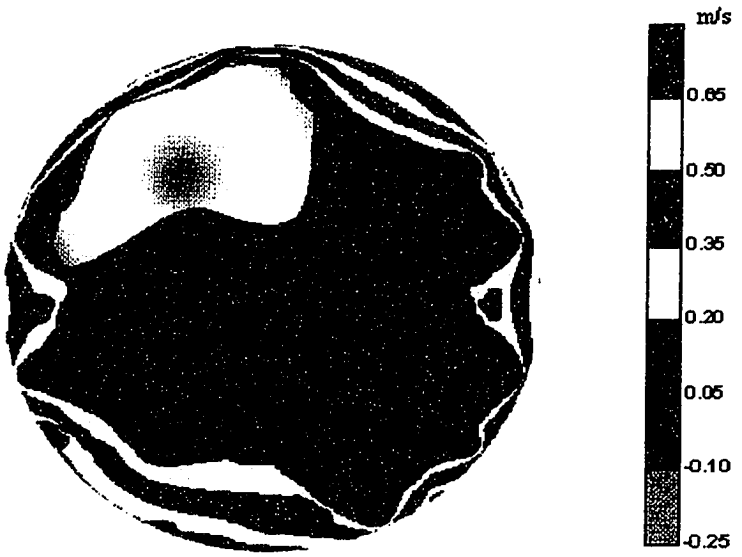

Figure 15. Contours of tangential velocity shown as end view of a horizontal rotating cylinder containing 1.5% CMC-H; 200 rpm, 1.0 cm headspace

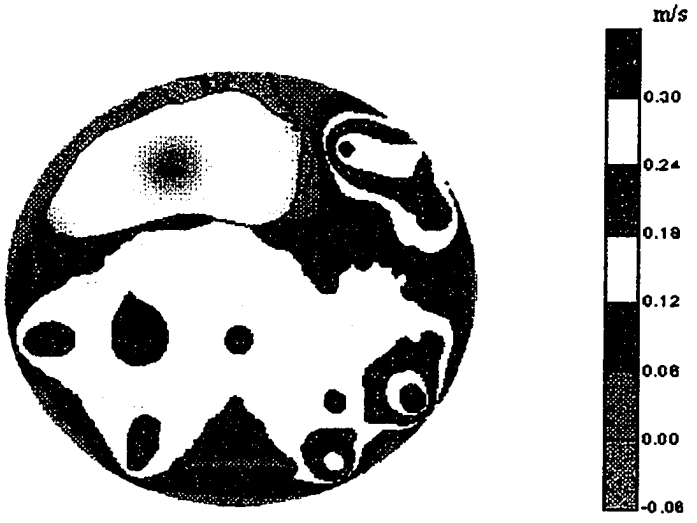

Figure 16. Contours of radial velocity shown as end view of a horizontal rotating cylinder containing 25% glycerol; 300 rpm, 1.0 cm headspace

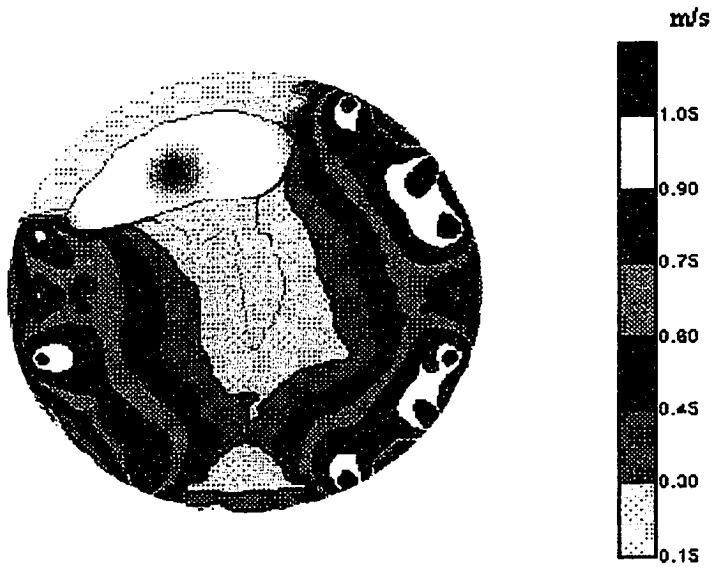

Figure 17. Contours of radial velocity shown as end view of a horizontal rotating cylinder containing 2% CMC-L; 350 rpm, 0.25 cm headspace

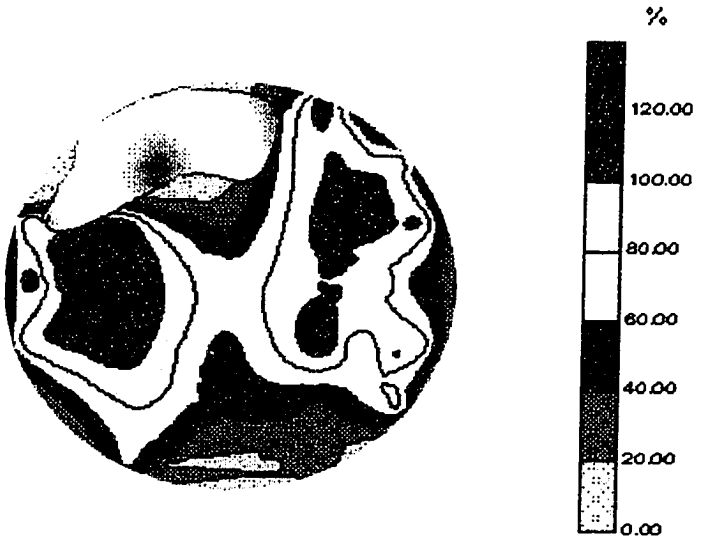

Figure 18. Contours of tangential turbulence intensity shown as end view of a horizontal rotating cylinder containing 50% glycerol; 200 rpm, 0.5 cm headspace

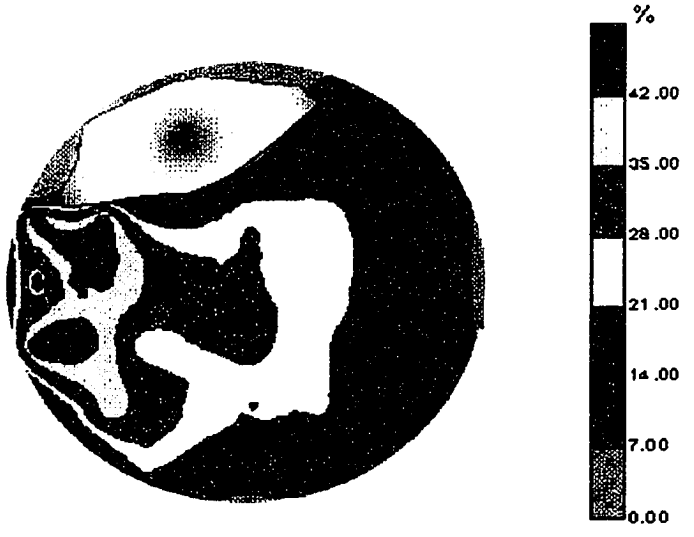

Figure 19. Contours of radial turbulence intensity shown as end view of a horizontal rotating cylinder containing 50% glycerol; 200 rpm, 0.5 cm headspace

Figure 20. Contours of tangential turbulence intensity shown as end view of a horizontal rotating cylinder containing 1.5% CMC-H; 200 rpm, 1.0 cm headspace

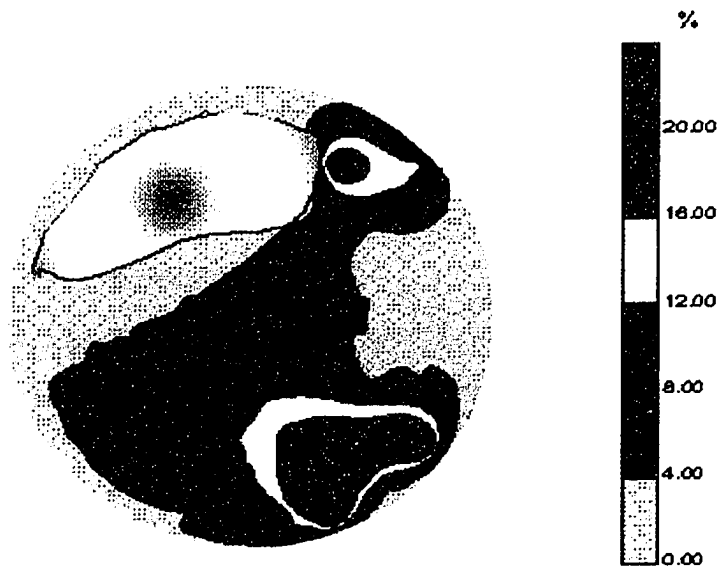

Figure 21. Contours of radial turbulence intensity shown as end view of a horizontal rotating cylinder containing 1.5% CMC-H; 200 rpm, 1.0 cm headspace

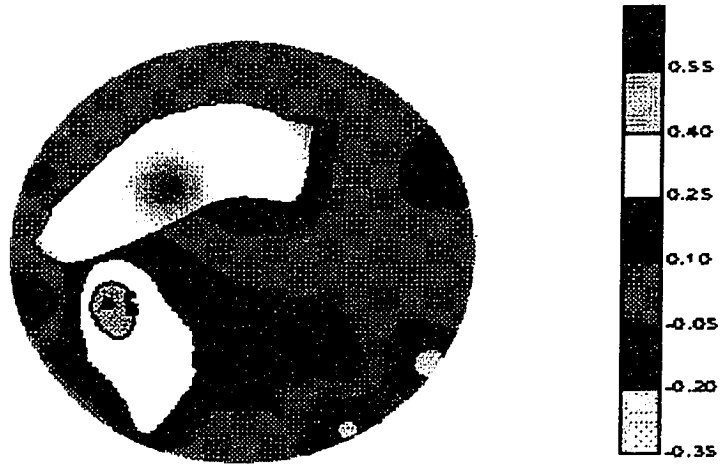

Figure 22. Contours of Reynolds stress shown as end view of a horizontal rotating cylinder containing 50% glycerol; 200 rpm, 0.5 cm headspace

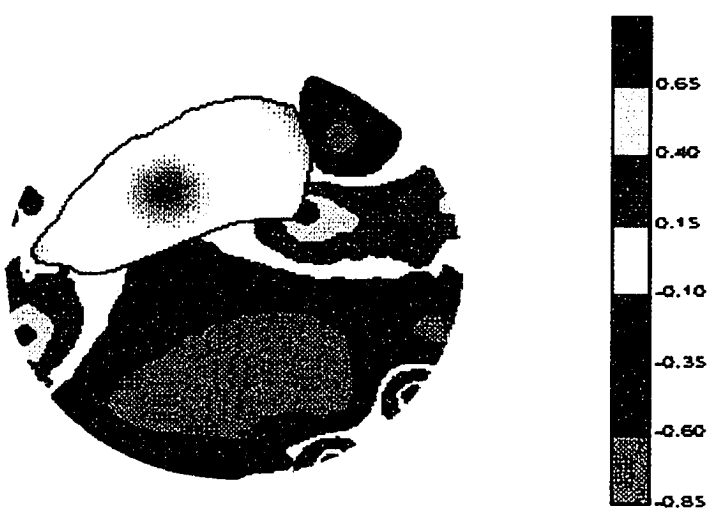

Figure 23. Contours of Reynolds stress shown as end view of a horizontal rotating cylinder containing 1.5% CMC-H; 200 rpm, 1.0 cm headspace

were dominant when compared to gravitational forces. The "no slip" condition on the can wall should manifest itself with the magnitude of the mean tangential velocity on the wall being equal to the can velocity (for instance, the tangential velocity of 50% glycerol on the wall at 200 rpm was found to be 77.5 cm/s). The momentum transferred to the liquid by the container was directly proportional to the viscosity and the rotational speed and diffused towards the center of the cylinder.

Apart from the near wall region, gravitational and inertial forces dominated in the rest of the cylinder, the magnitude of the latter depending on rotational speed. Figures 14 and 15, which show the mean tangential velocity contours for water and CMC-H at 200 rpm, exhibited the same patterns explained above.

Figures 16 and 17 show the distribution of radial velocity in the cylinder for glycerol and CMC-L. As a general pattern, the radial velocity magnitude increased towards the wall. This was due to the increase in centrifugal force as the radius increased. In both figures, one can see the local high velocity regions occurring near the wall. It should be also noted that Figure 17 shows a smoother velocity distribution than that in Figure 16, since the apparent viscosity of the CMC-L was higher than that of 25% glycerol.

Turbulence intensity values and the Reynolds stresses which can present useful information about turbulent motion in the cylinder were also measured in the experiments.

One of the most striking aspects of the system studied is the quantitative difference of magnitudes of the tangential and radial turbulence intensities as can be seen through Figures 18 to 21. For all of the liquids used in the experiment, the tangential component of the turbulent intensity was measured to be one order of magnitude larger than the radial component. This information clearly indicates that the total turbulent kinetic energy transferred from the mean motion to the large eddies by the action of turbulent stresses (Reynolds stresses) was dissipated mostly by the tangential component rather than the radial component due to viscous forces. The local maximum values of both the tangential and radial turbulence intensities corresponded

approximately to the same regions in the cylinder as seen in those figures.

The turbulence production was directly proportional to the Reynolds stress and the mean velocity gradient. Figures 22-23 show the Reynolds stress distribution for glycerol and CMC-H. The maximal values of Reynolds stresses were measured at distances away from the center for both cases. As the overall velocity gradient increased towards the wall, it can be stated that these local regions with maximal values of Reynolds stress corresponded to regions of maximal turbulence generation inside the cylinder.

In light of the contour plots and the observations made during the experiments, it was concluded that viscous, gravitational and inertial forces (centrifugal) determine the structure of flow inside the cylinder. It is very interesting that even at the smallest rotational speeds, the flow inside the cylinder was turbulent due to the agitative motion of the bubble. The viscous forces became more predominant on the small scale motion with increasing viscosity. Conversely, the centrifugal force depended on the rotational speed and the distance from the center. The ratio of the centrifugal forces to the gravitational force is known as the Froude number, written as:

$$Fr = \frac{r\omega^2}{g} \tag{75}$$

where r is the distance from the center, ω is the rotational velocity and g is the gravitational acceleration. The larger the Froude number, the greater the effect of inertial (centrifugal) forces on the overall flow structure. Figure 24 shows the variation of the Froude number with cylinder radius used in the study.

As can be seen from this figure, the magnitude of centrifugal force was comparable to gravitational force in the speed ranges used in this study and cannot be neglected. It should also be pointed out that Figure 24 does not represent the actual physical comparison inside the cylinder since the tangential velocity of the fluid will be only equal to the rotational speed of the cylinder on the wall as the fluid is not in a solid

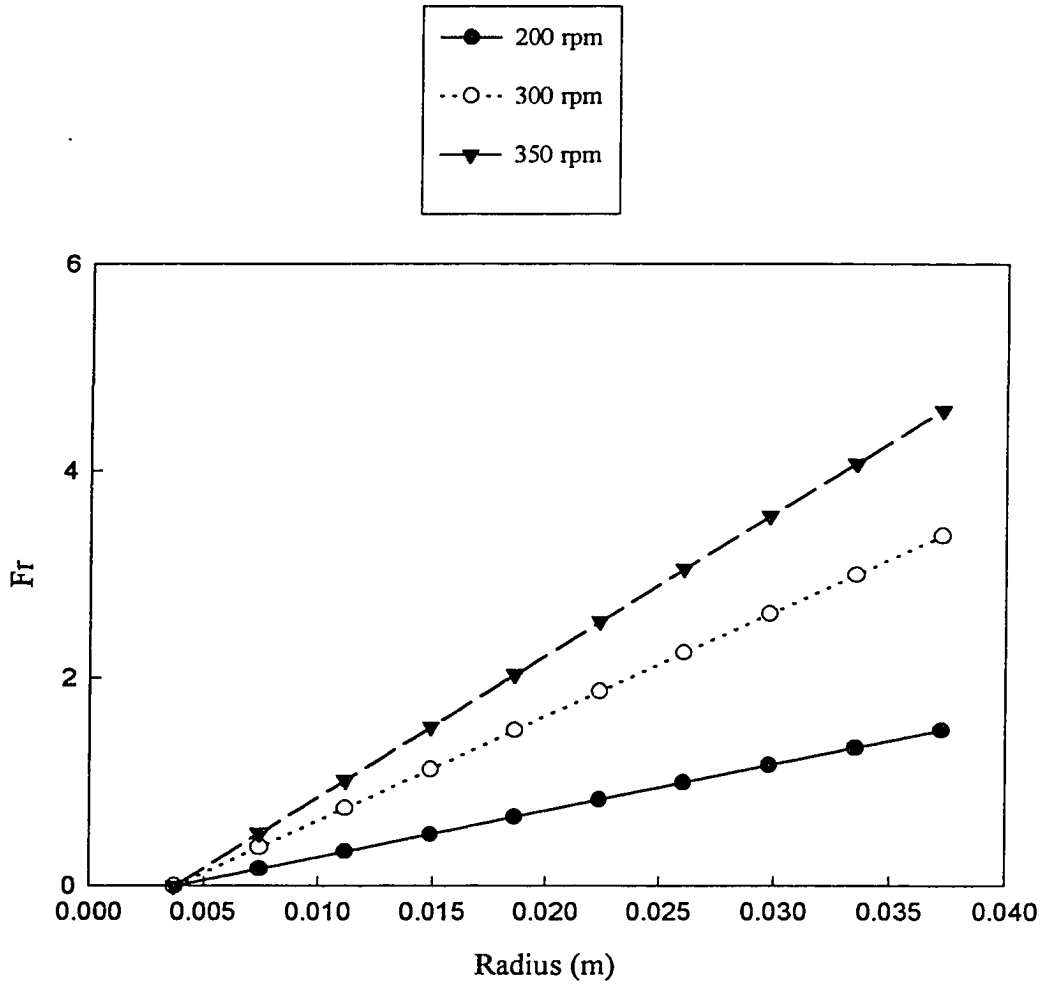

Figure 24. Froude number (Fr) versus radius as a function of rotational speed.

body rotation. However, it gives an indication of the ratio of the magnitudes of the two important forces in the cylinder.

4.3. Effect of Rotational Speed

Rotational speed is one of the three controlling parameters which affect the flow characteristics inside the axially rotating cylinders. In this section, the effects of rotational speed on the mean axial and radial velocity distributions, turbulence intensities, and Reynolds stresses are analyzed for Newtonian and non-Newtonian liquids used in the experiments.

4.3.1. Tangential and Radial Velocity Distributions

4.3.1.1. Newtonian Liquids

Figures 25a and 25b show for water the mean tangential and radial velocities along the radial direction for 0.25 cm headspace at different rotational speeds. Both figures suggest that it is very difficult to propose a pattern for velocity distribution of water in the radial direction especially for the tangential velocity. Water had the lowest viscosity of the fluids used in the experiments. Hence, the flow inside the cylinder depended more on the gravitational and centrifugal forces rather than viscous forces except for a very thin region near the solid boundary. This gravity dominant, bubble induced turbulent motion caused a chaotic flow structure. Nevertheless, some interesting points exist which are worth mentioning. First of all, the radial velocity increased towards the wall with increasing rotational speed. An average increase of 92% in the radial velocity took place when the rotational speed was increased from 200 rpm to 350 rpm at a radius of 30 mm (Figure 25a). A clear trend could not be found in Figure 25b which shows the tangential velocity distribution along the radial direction. However, the largest tangential velocities were still measured at 350 rpm, at the highest rotational speed used in the experiments. Showing the effect of centrifugal force is another interesting point which depicts the drastic difference in the magnitude of the

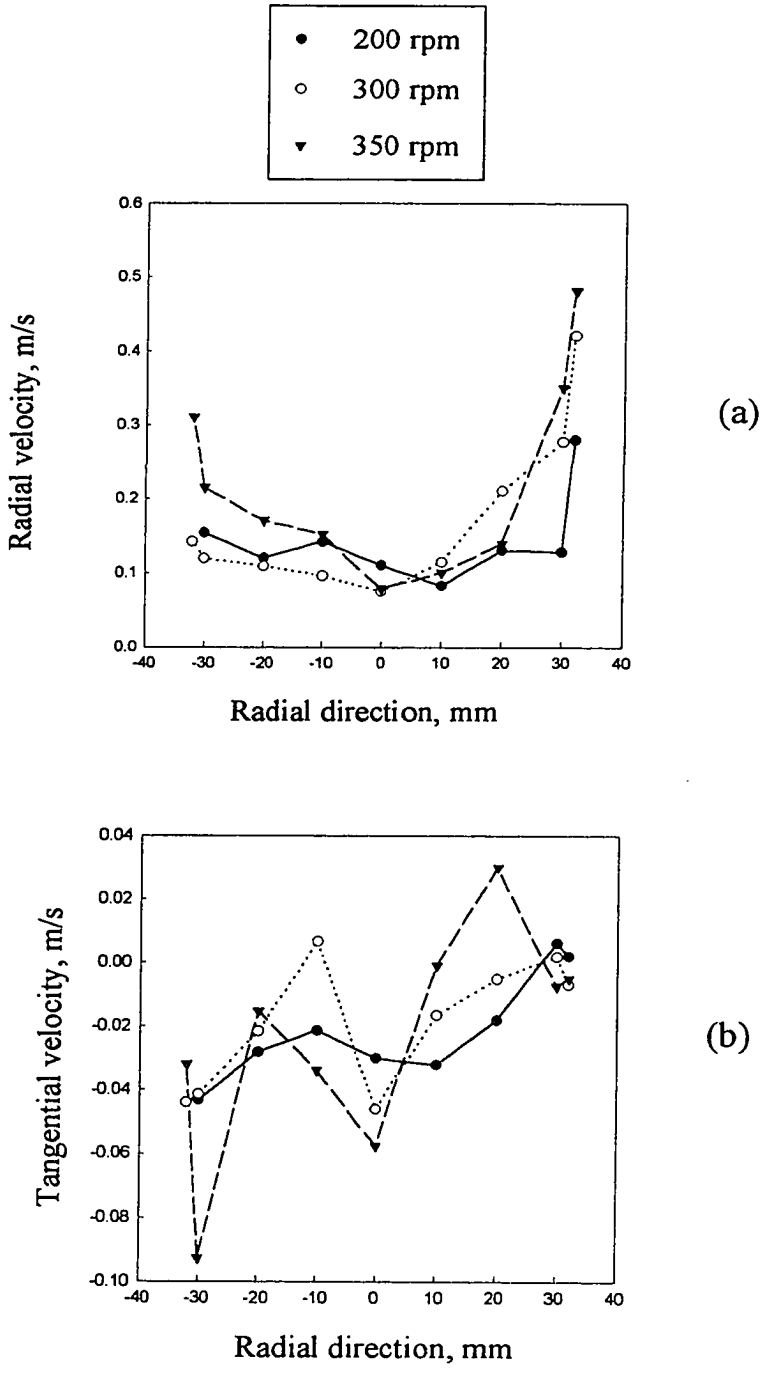

Figure 25. Distribution of radial and tangential velocities for water in continuous rotation, taken along the radial direction; 0.25 cm headspace, y = -10 mm

tangential and radial velocities. When Figures 25a and 25b are compared, it is seen that the magnitude of the average radial velocity was about one order of magnitude larger than that of the tangential velocity, indicating that the mean flow was essentially in the radial direction rather than tangential.

Figures 26 to 28 present the radial and tangential velocity distributions for 25, 50, and 80% glycerol solutions. The trends observed for water were also observed in those figures. In Figures 26a, 27a, and 28a the increase in the mean radial velocity with increasing speed can be seen clearly. The tangential velocity distribution again did not show any conclusive trend (Figures 26b, 27b and 28b). Comparison of the magnitudes of tangential and radial velocities reveals that the mean flow was in the radial direction.

4.3.1.2. Non-Newtonian Fluids

Figures 29 to 31 show the mean radial and tangential velocity distributions along the radial direction for 0.15% xanthan polymer, 0.15% CMC-H and 2% CMC-M at different rotational velocities. Both the radial and tangential mean velocity profiles showed smoother trends as compared to Newtonian liquids. Radial velocity patterns for each of the non-Newtonian liquids, show an increase in the radial velocity with increasing rotational speed, very clearly due to increasing centrifugal forces in the radial direction (Figures 29a, 30a and 31a). The difference in velocities at different speeds increased towards the wall. The magnitude of radial velocities was found to be larger than those of Newtonian fluids.

The tangential velocity profiles for 1.5% xanthan polymer, 1.5% CMC-H and 2% CMC-L, like water and glycerol, revealed a distinct pattern (Figures 29b, 30b and 31b). Although Figure 29b shows that the tangential velocity increased with increasing speed, the same trend was not evident in Figures 30b and 31b. The mean flow was again in the radial direction. The possible cause of the scattered mean tangential velocity data for all the liquids is thought to be the oscillatory motion of the bubble.

For the velocity distribution analysis in the radial direction, the following conclusions can be stated:

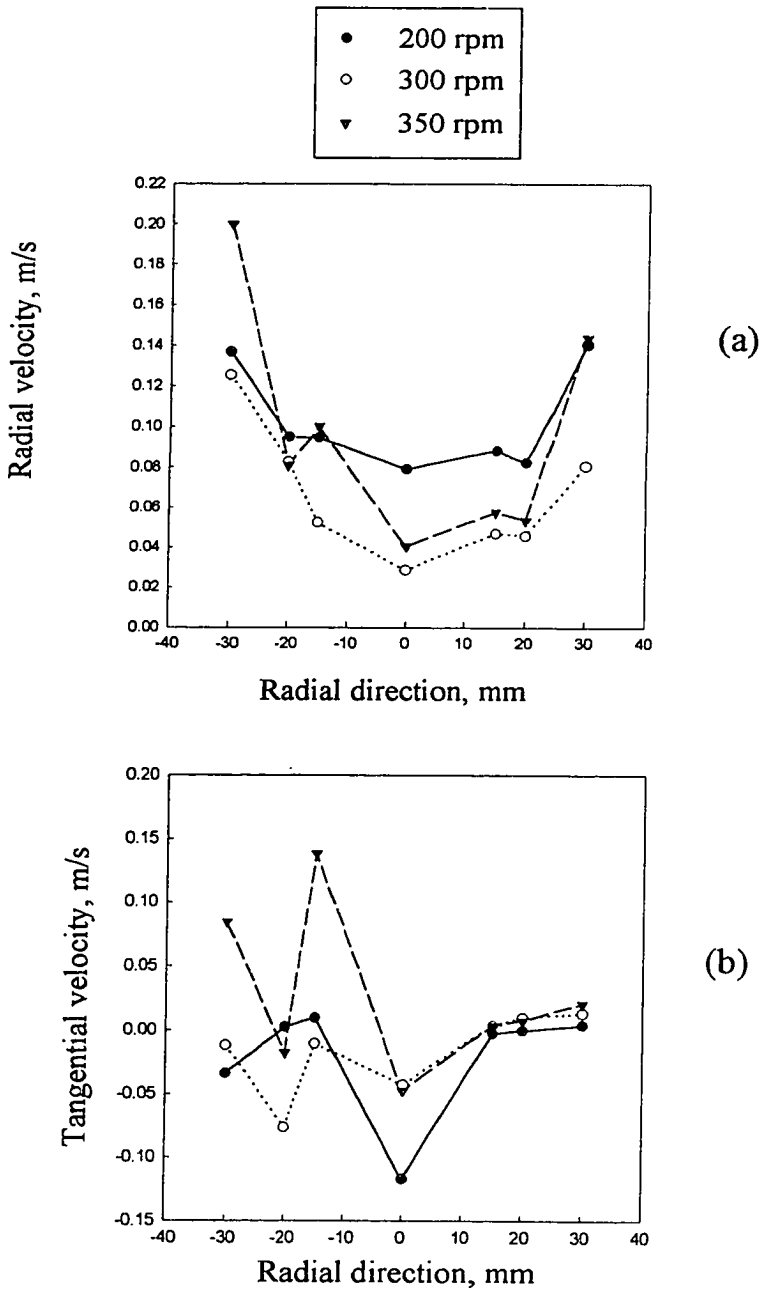

Figure 26. Distribution of radial and tangential velocities for 25% glycerol in continuous rotation, taken along the radial direction; 0.25 cm headspace, y = -10 mm

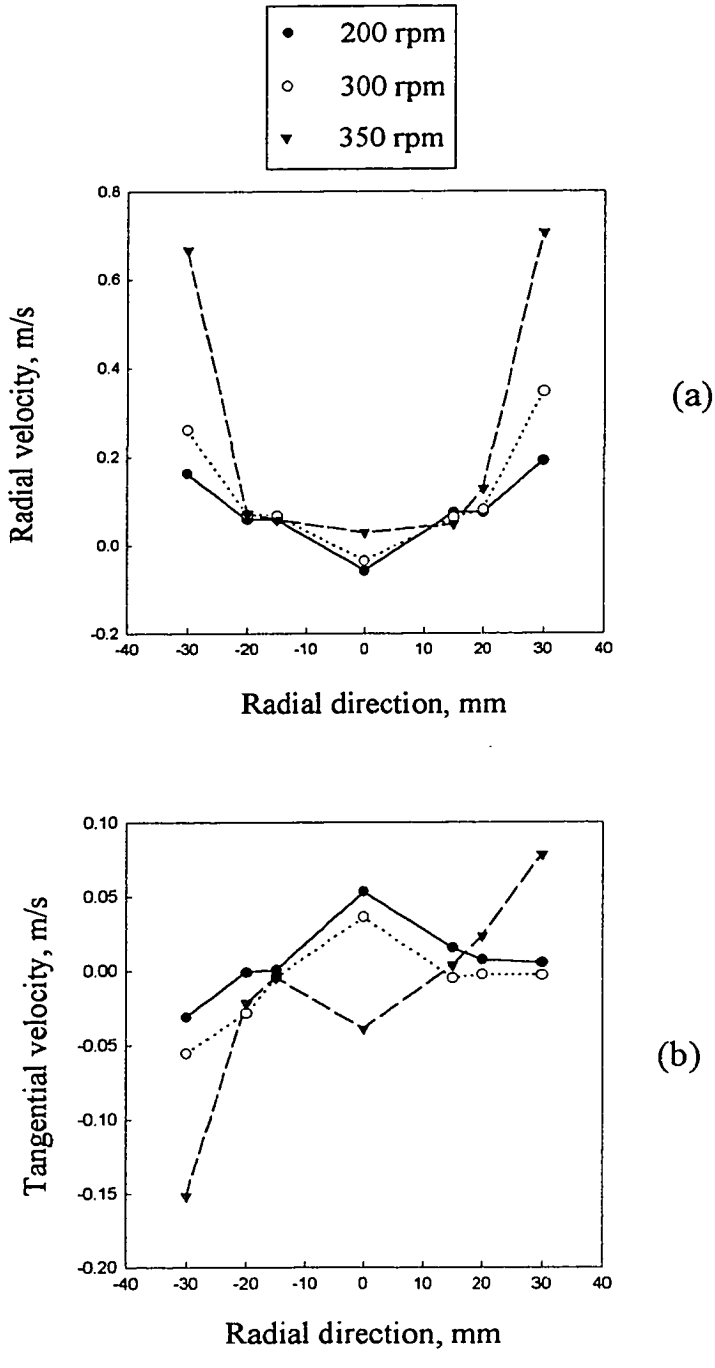

Figure 27. Distribution of radial and tangential velocities for 50% glycerol in continuous rotation taken along the radial direction; 0.25 cm headspace, y = -10 mm

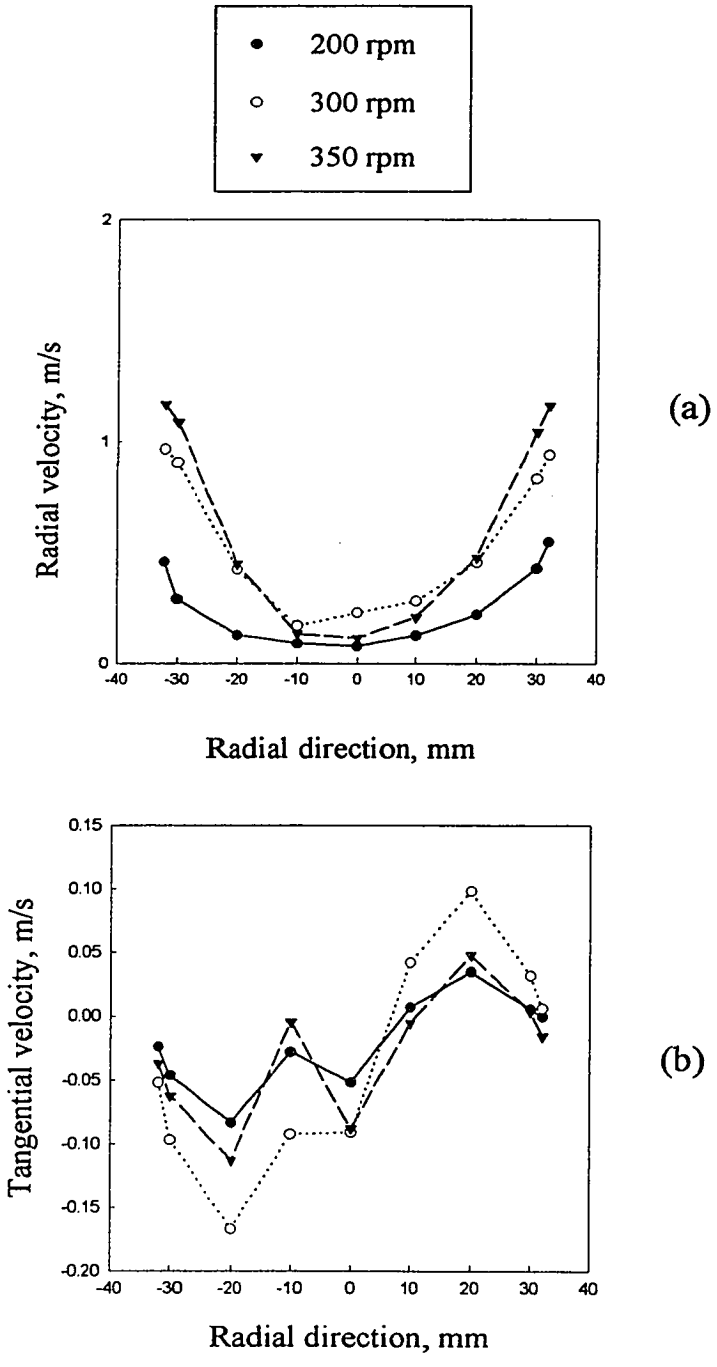

Figure 28. Distribution of radial and tangential velocities for 80% glycerol in continuous rotation, taken along the radial direction; 0.25 cm headspace, y = -10 mm

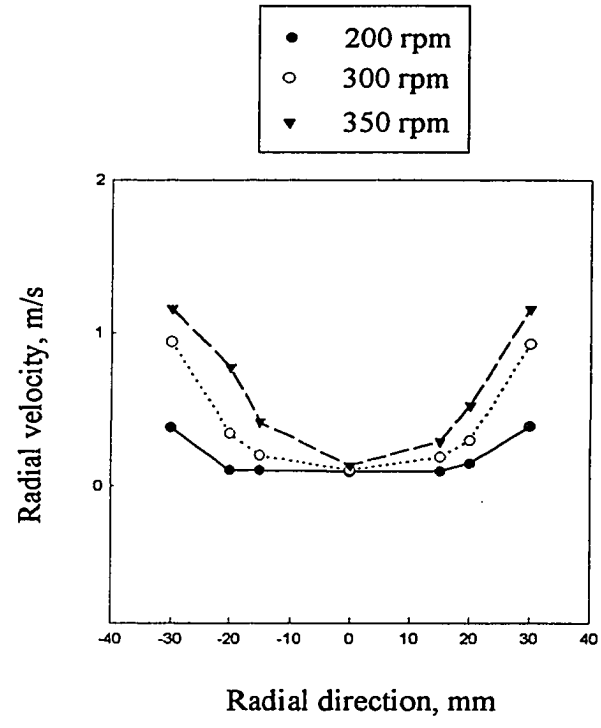

(a)

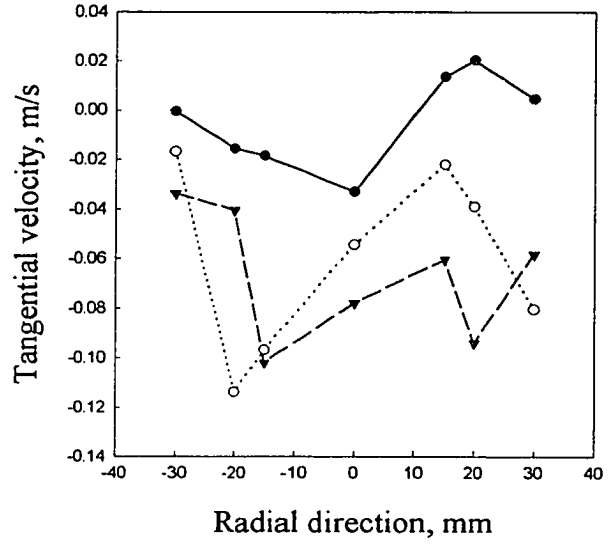

(b)

Figure 29. Distribution of radial and tangential velocities for 0.15% xanthan polymer in continuous rotation, taken along the radial direction; 0.25 cm headspace, y = -10 mm

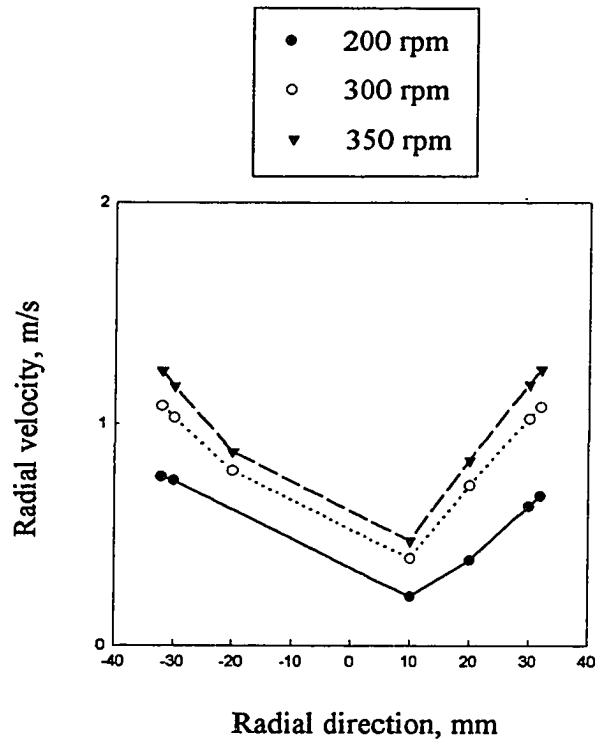

(a)

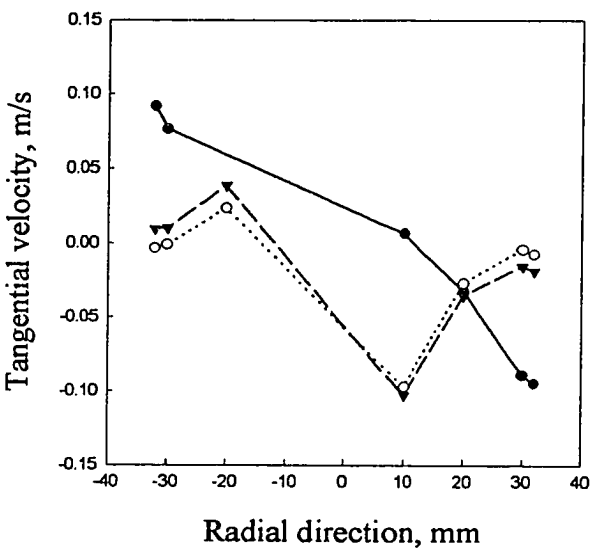

(b)

Figure 30. Distribution of radial and tangential velocities for 1.5% CMC-H in continuous rotation, taken along the radial direction; 1.0 cm headspace, y = -10 mm

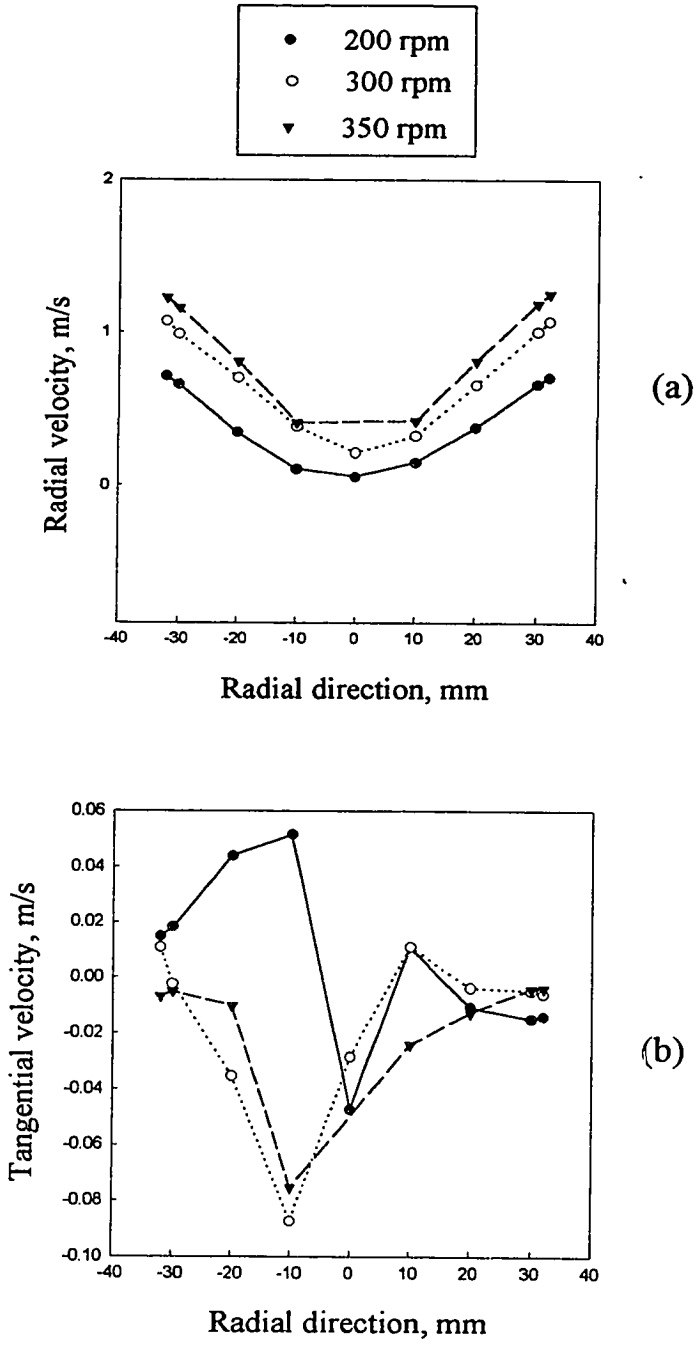

Figure 31. Distribution of radial and tangential velocities for 2% CMC-M in continuous rotation, taken along the radial direction; 0.25 cm headspace, y = -10 mm

(a) For both non-Newtonian and Newtonian liquids, the mean radial velocity along the radial direction generally increased with increasing rotational speed.

(b) For both Newtonian and non-Newtonian liquids, a general trend was not evident for the radial variation of the mean tangential velocity.

(c) The mean flow direction was the radial direction for all of the liquids used in these experiments.

4.3.2. Turbulence Intensities and Reynolds Stresses

LDV measurements include three sources of fluctuations: random fluctuations caused by turbulence in the flow, random measurement error and non-random fluctuations such as periodic changes caused by the oscillatory motion of the bubble. All three fluctuations are normally included in the measurement of the turbulence intensity (TI) defined as:

$$TI = \frac{\sqrt{\overline{V'^2}}}{\overline{V}} \tag{76}$$

where and V' and V are the fluctuating and mean components of the fluid velocity.

A wide range of turbulence intensity values ranging from 1% to several hundred percent were measured for the experimental conditions studied suggesting that the flow was turbulent inside the cylinder.

4.3.2.1. Newtonian Liquids

Figures 32 and 33 show the variation of radial turbulence intensity along the radial direction for water and 50% glycerol at different rotational speeds. Both of the figures revealed that as the rotational speed was increased, the radial turbulent intensity also increased due to augmentation of the agitation caused by the bubble. The up and down oscillatory motion of the bubble was probably the primary source of fluctuations as observed during the experiments.

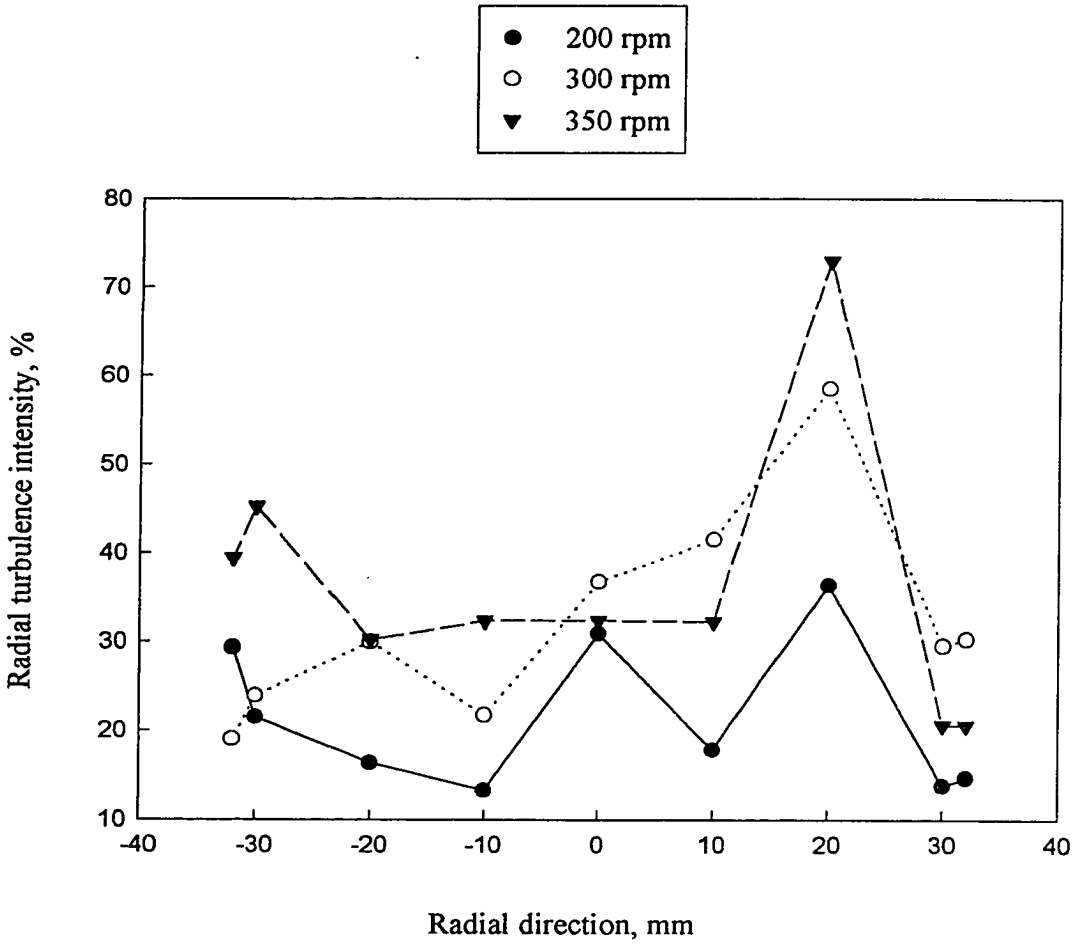

Figure 32. Radial turbulence intensity for water in continuous rotation; 0.50 cm headspace, y = -10 mm

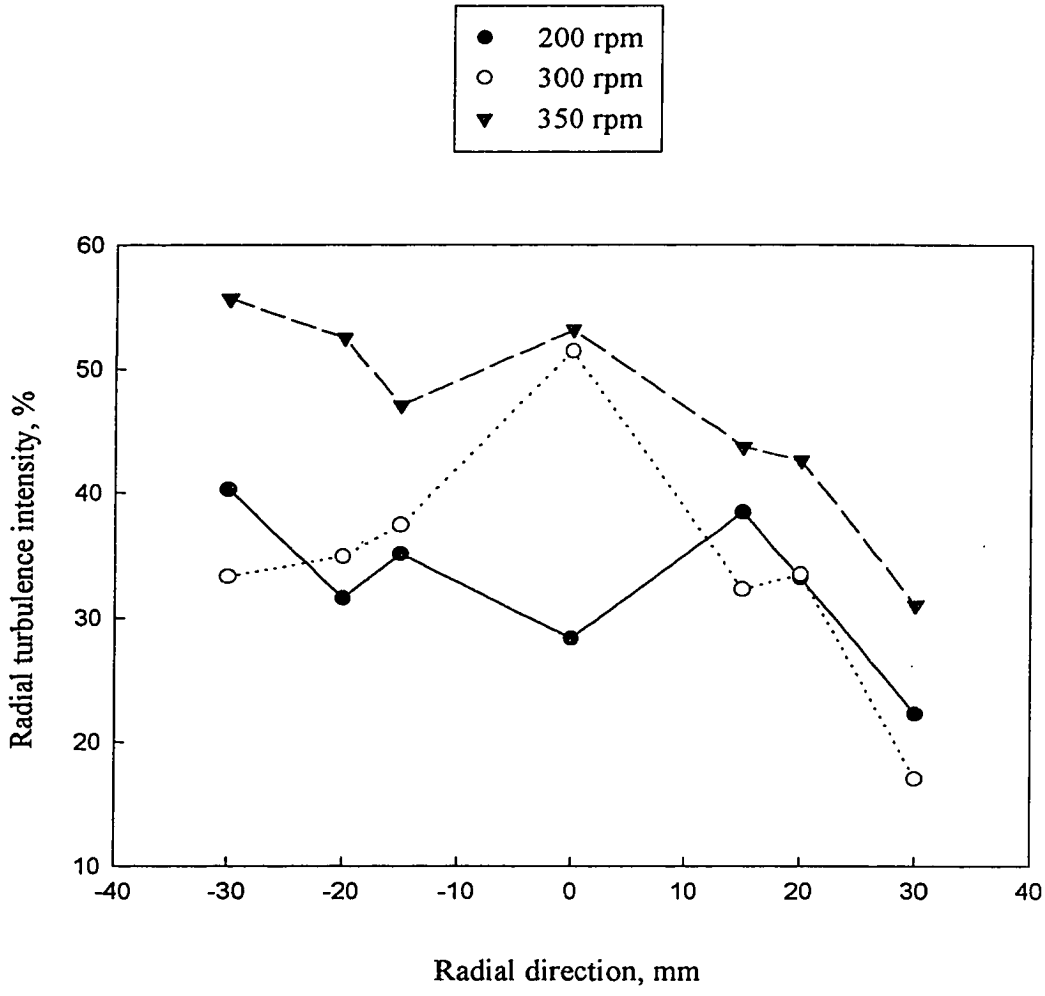

Figure 33. Radial turbulence intensity for 50% glycerol in continuous rotation; 1.0 cm headspace, y = -10 mm

The variation of tangential turbulence intensities with rotational speed is shown in Figures 34 and 35 for water and 80% glycerol, respectively. As can be seen in Figure 34, the tangential turbulent intensity distribution was more scattered (point-to-point variability at a single speed) than the radial turbulent intensity distribution (Figure 32) along the radial direction. In most cases, it was very difficult to predict a pattern in the range of rotational speeds used in the experiments. For higher speeds (N > 1000 rpm), visualization experiments similar to those of Cannon and Kays (1969) showed a strong suppression of the turbulent velocity fluctuations near the rotating tube wall because of the radially growing centrifugal forces. However, such suppression effect was not quantitatively measured in the experiments done in this study.

Figure 35, which presents the tangential turbulent intensity variation along the radial direction for 80% glycerol shows an overall increase in the tangential turbulent intensity with increasing rotational speed although the data were somewhat scattered. For all of the cases measured, the tangential turbulent intensity either increased or remained constant with increasing rotational speed for Newtonian liquids.

The radial variation of the tangential turbulent intensity also showed that intensity values decreased around the centerline region (Figures 34 and 35).

Figure 36 presents the variation of the Reynolds stress along the radial direction for water. This figure clearly indicates that Reynolds stress increases with increasing rotational speed towards the wall due to the increase in the bubble movement (oscillation) and agitation. Reynolds stresses were probably responsible for transferring the energy from the mean motion to the large scale eddies and assumed to be directly related to the turbulence production. The highly anisotropic nature of the flow was seen with high gradients of the Reynolds stress along the radial direction with increasing rotational speed as illustrated in Figure 36.

A general pattern for Reynolds stresses could not be found for the results of the experiments carried out with 25% glycerol as seen in Figure 37.

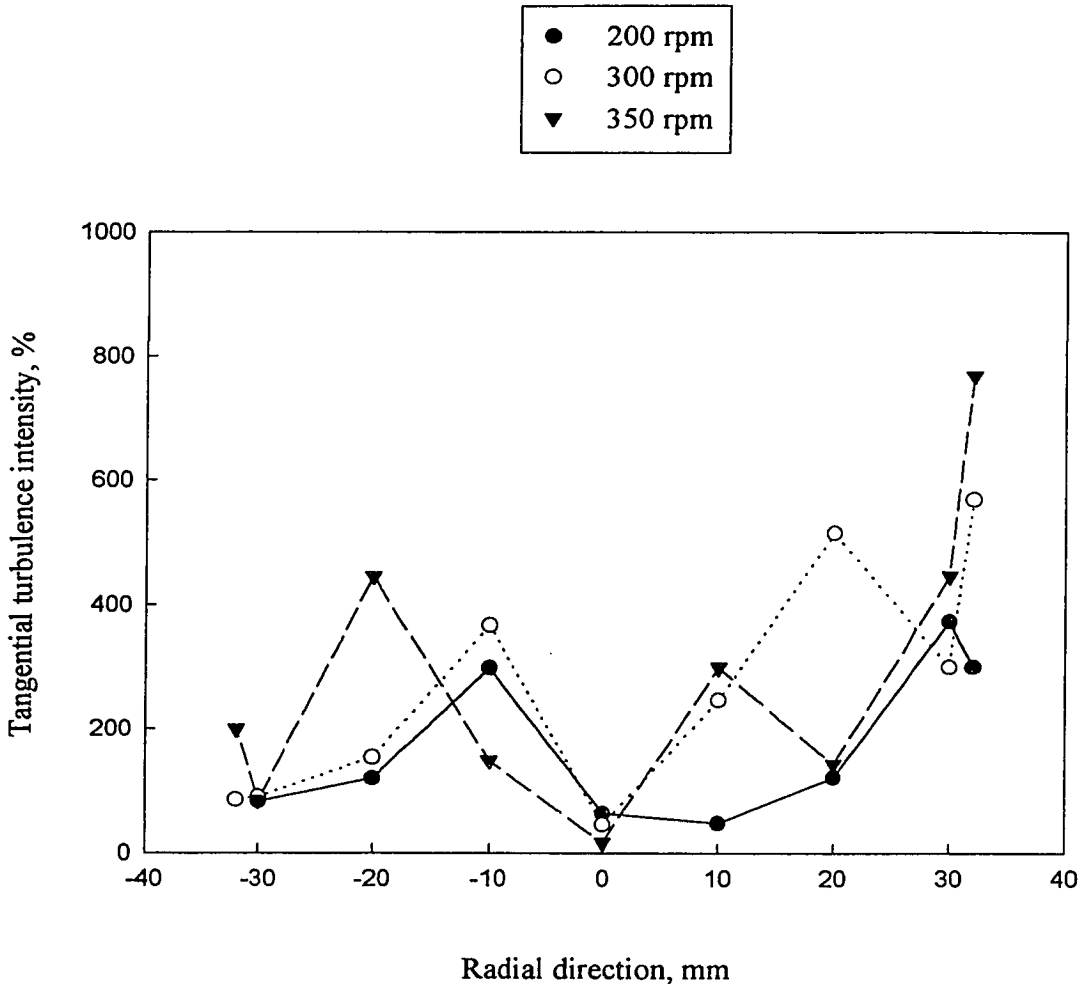

Figure 34. Tangential turbulence intensity for water in continuous rotation; 0.25 cm headspace, y = -10 mm

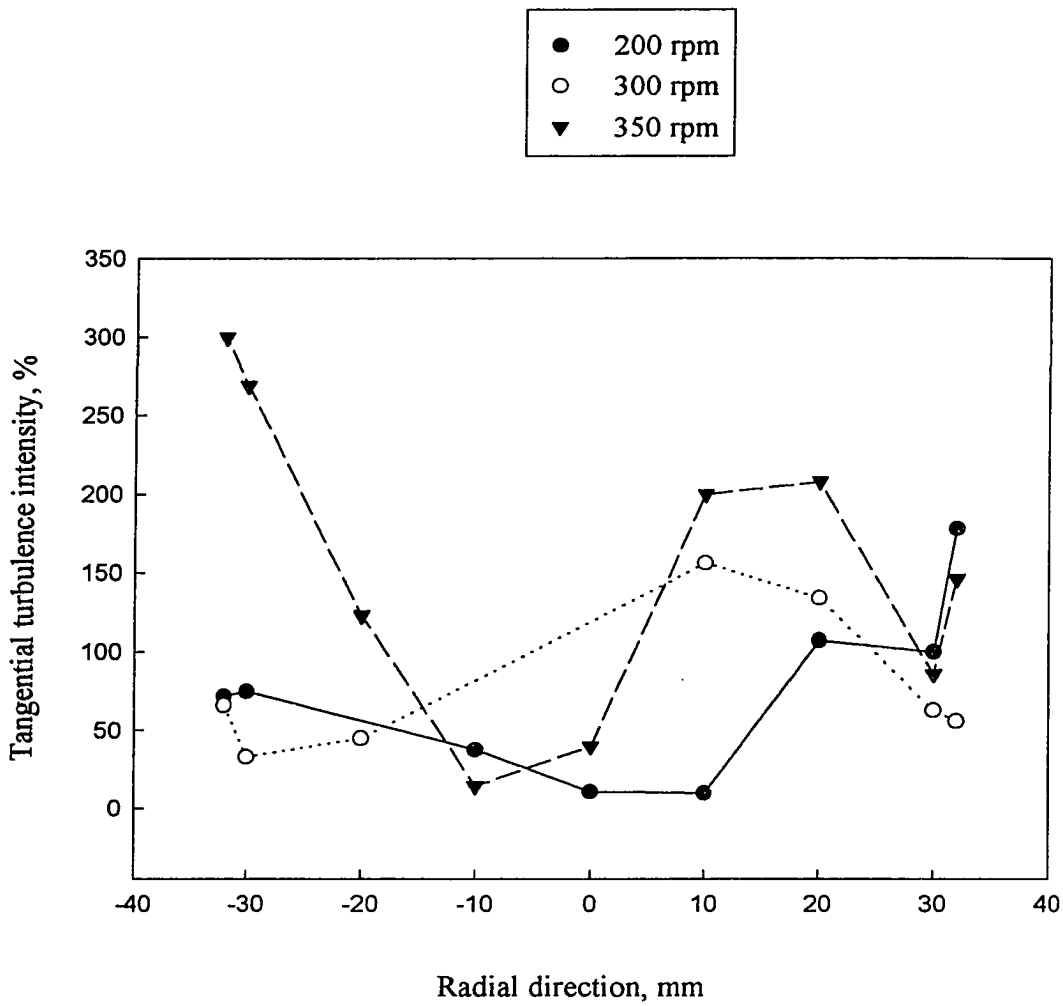

Figure 35. Tangential turbulence intensity for 80% glycerol in continuous rotation; 0.25 cm headspace, y = -10 mm

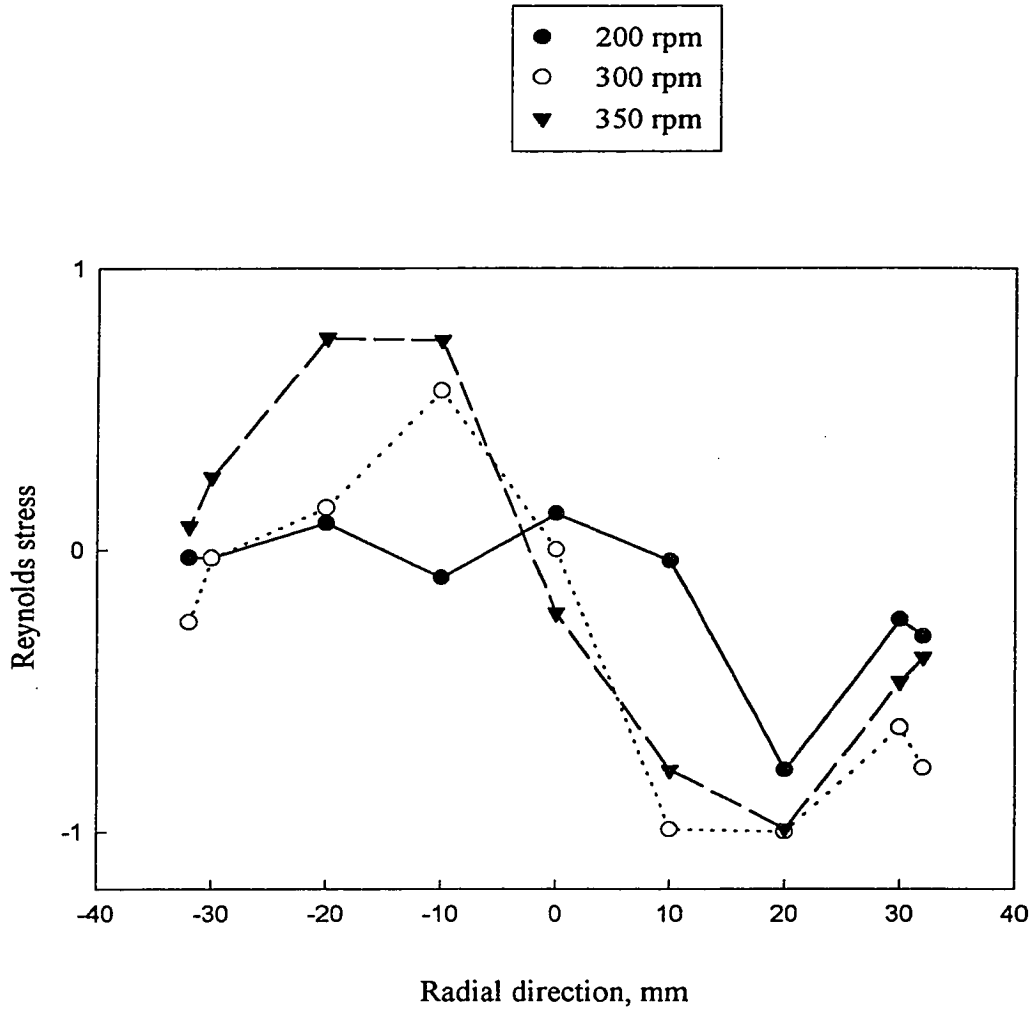

Figure 36. Reynolds stress distribution for water in continuous rotation; 0.50 cm headspace, y = -10 mm

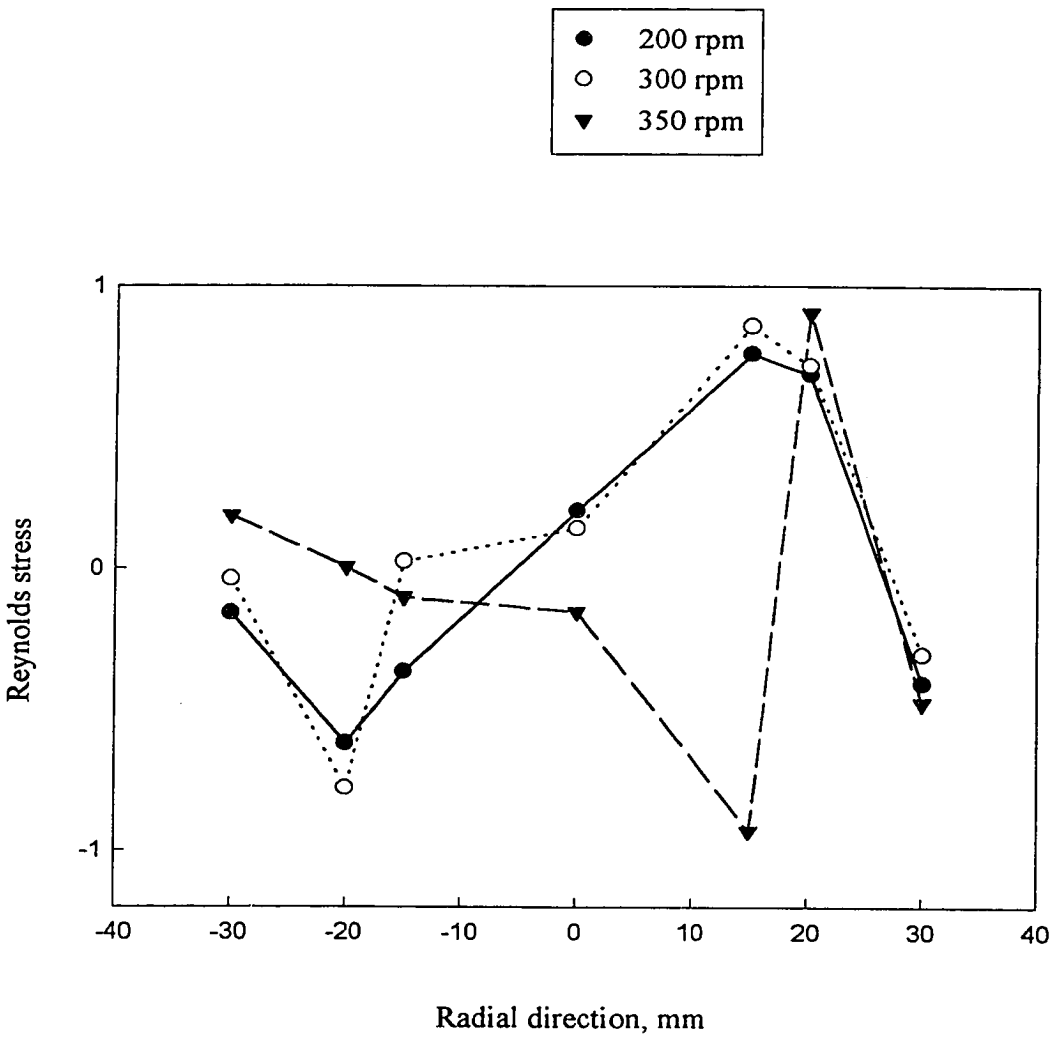

Figure 37. Reynolds stress distribution for 25% glycerol in continuous rotation; 1.0 cm headspace, y = -10 mm

4.3.2.2. Non-Newtonian Liquids

The same patterns identified for Newtonian fluids were also found for the non-Newtonian liquids used in the experiments. Figure 38 shows the variation of the radial turbulence intensity along the radial direction for 2% CMC-M solutions with a 1.0 cm headspace. The increase in turbulence intensity with increasing rotational speed was remarkable. The tangential variation of the turbulent intensity also showed an increasing pattern with the rotational speed for this solution as well as 1.5% CMC-H with 0.5 cm headspace (Figures 39 and 40). As in the case of Newtonian liquids, the magnitude of the tangential turbulence intensity was larger than the radial turbulence intensity indicating that the turbulent kinetic energy dissipation was due mainly to the tangential component for non-Newtonian liquids in axially-rotating cylinders. Figure 41 shows the variation of Reynolds stress for 2% CMC-M. The rotational speed had an increasing effect on the Reynolds stresses as the radial direction increased. The experiments conducted to investigate the effect of rotational speed on the turbulence intensity and the Reynolds stresses showed similar patterns for Newtonian and non-Newtonian liquids. The increase in the rotational speed augments the agitation in the system and the oscillatory motion of the bubble. Thus, increasing the speed had a favorable effect on the mixing phenomena inside the cylinder. However, one still has to note that the speed in this study was not high enough for the inertial forces to be effective at such a level to suppress the turbulence inside the cylinder, as stated by Cannon and Kays (1969).

4.4. Effect of Headspace

When filling metal cans with food prior to thermal processing, it is not desirable to fill the entire can volume with the food material. This is mainly because water-based foods have a greater volumetric expansion upon heating in comparison with the steel of which most food cans are constructed. Failure to leave adequate headspace could result in damaged can seams and loss of hermetic integrity of the can if filled completely with food prior to thermal processing. Accordingly, a certain amount of space containing air at a low pressure is usually left between the free liquid surface and the inside of the can

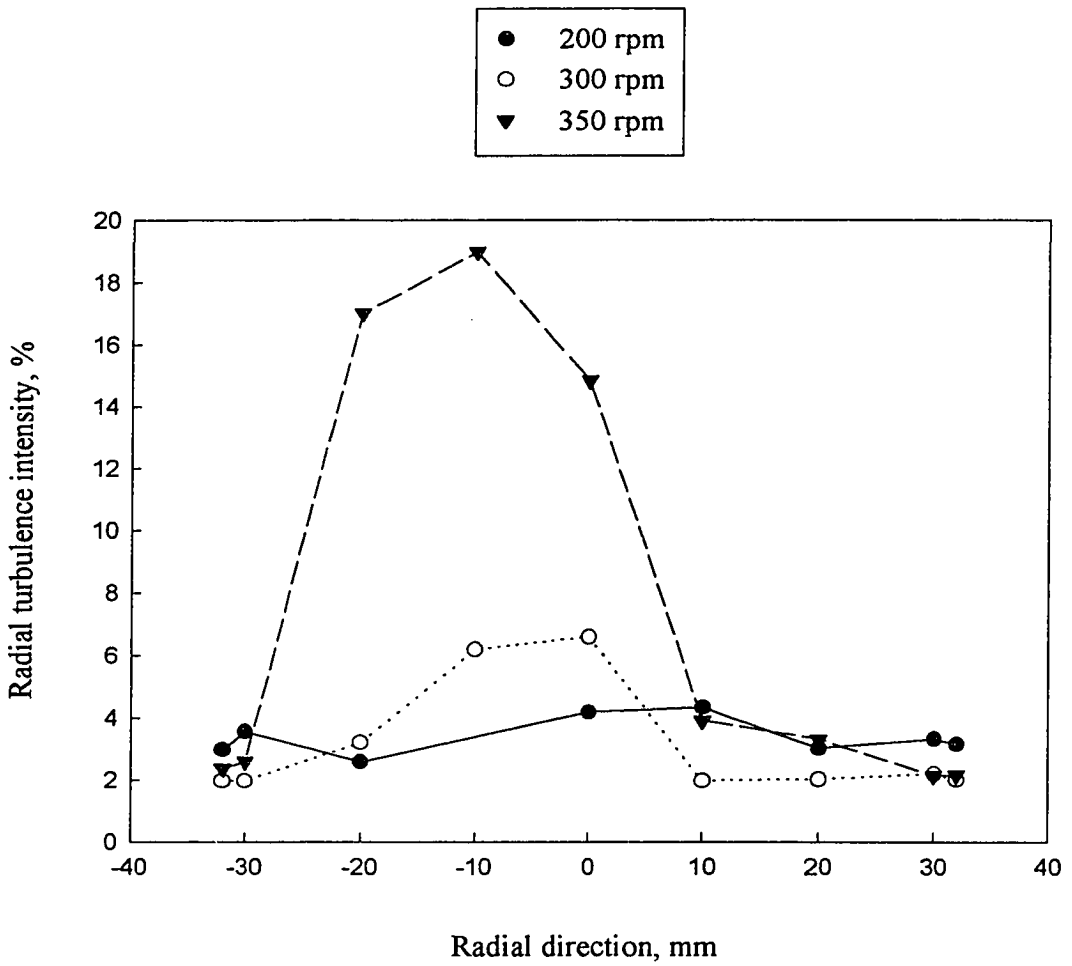

Figure 38. Radial turbulence intensity for 2% CMC-M in continuous rotation; 1.0 cm headspace, y = -10 mm

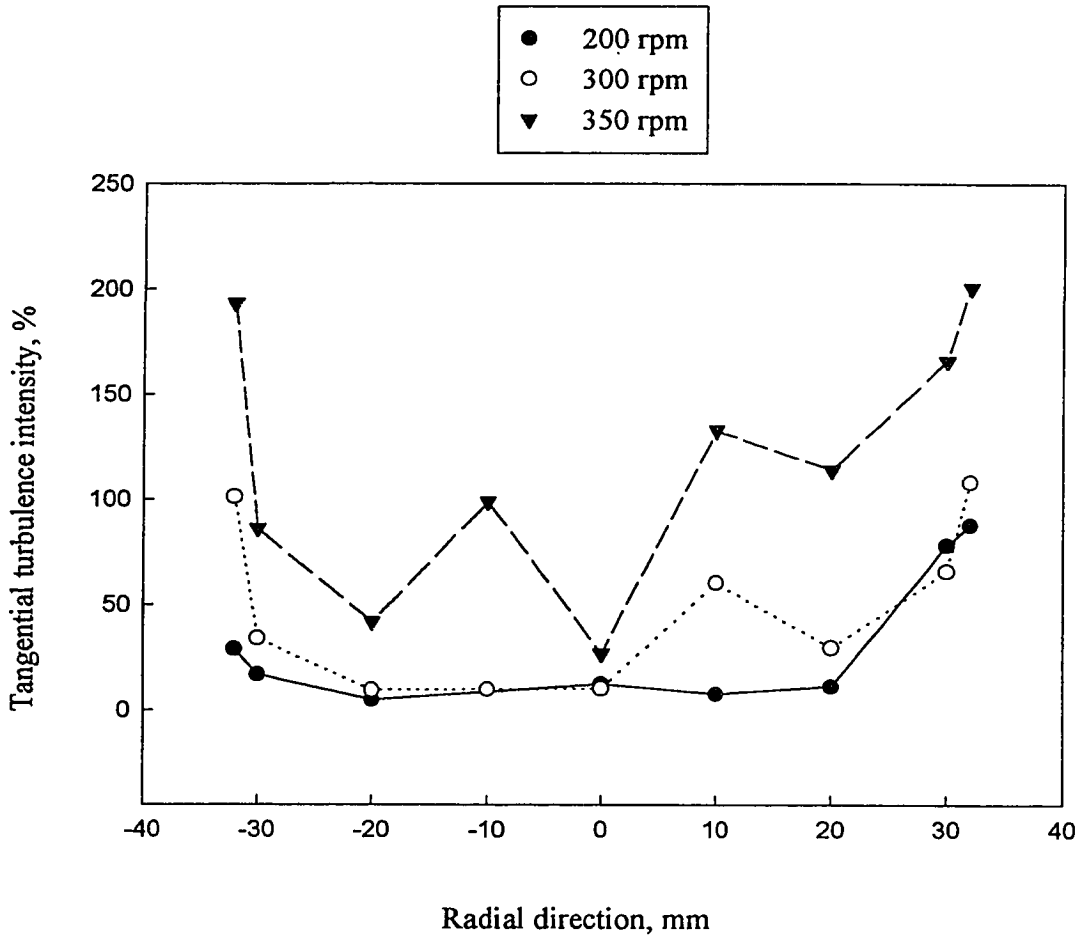

Figure 39. Tangential turbulence intensity for 2% CMC-M in continuous rotation; 1.0 cm headspace, y = -10 mm

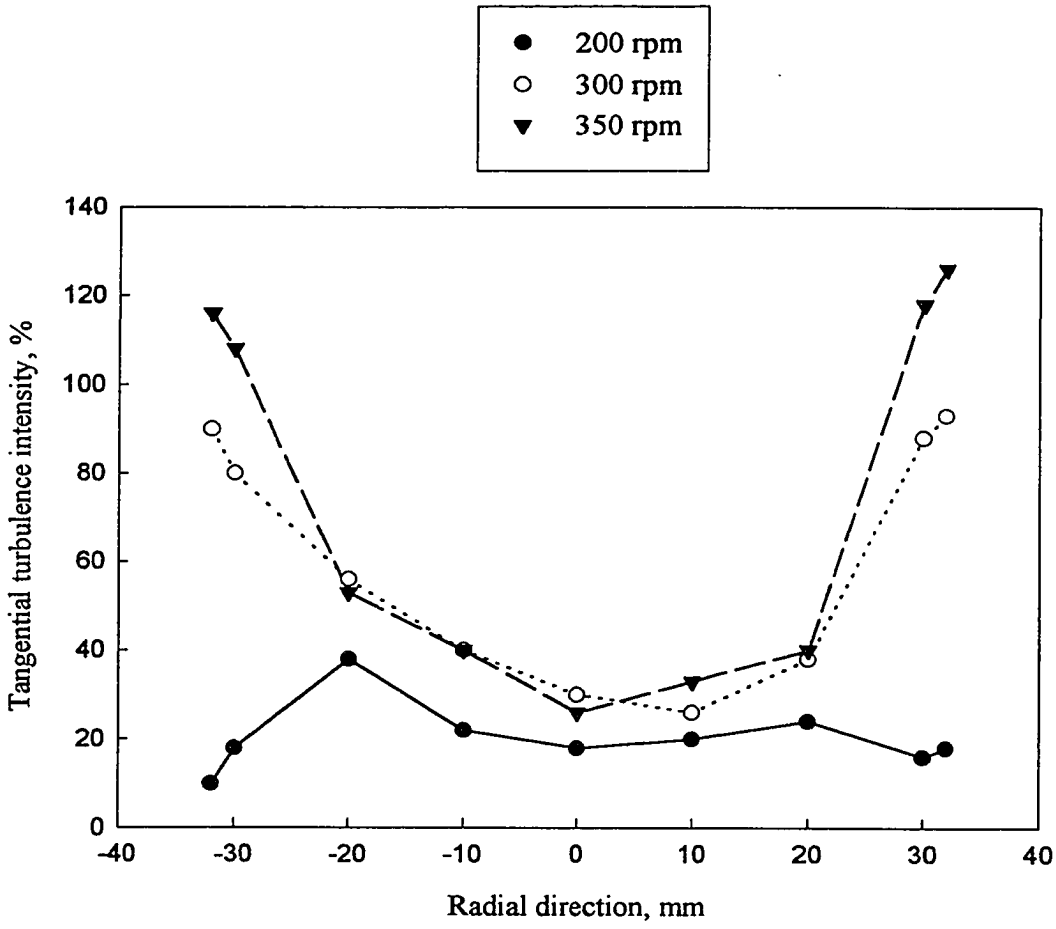

Figure 40. Tangential turbulence intensity for 1.5% CMC-H in continuous rotation; 0.5 cm headspace, y = -10 mm

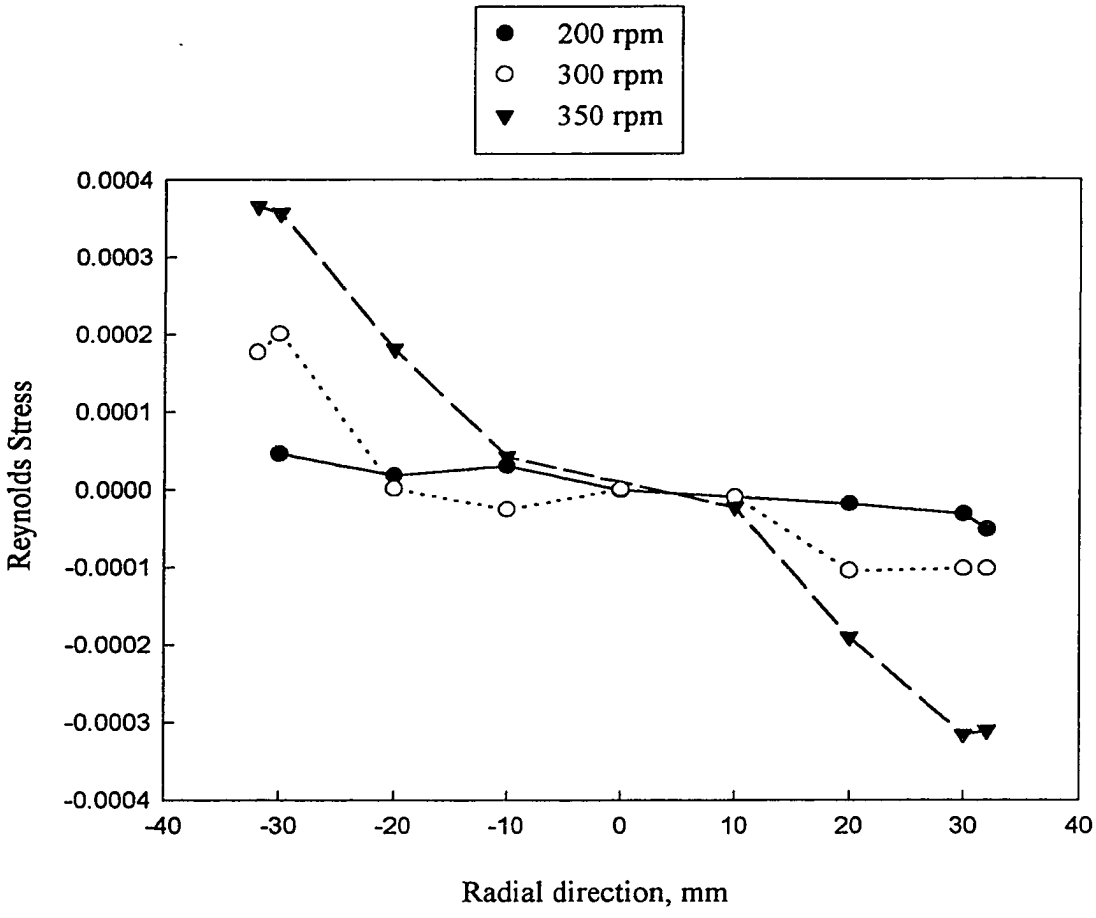

Figure 41. Reynolds stress distribution for 2% CMC-M in continuous rotation; 0.50 cm headspace, y = -10 mm

lid. During rotation, the headspace transforms into an air bubble and becomes a critical element in promoting or inhibiting the degree of mixing within the can. This, of course, can directly influence the heat transfer rate and thus the optimal time required for sterilization.

As explained at the beginning of this chapter, the motion of the headspace bubble depends on the fluid viscosity and the rotational speed. In the present experiments, three different headspace levels were used, 0.25 cm, 0.50 cm and 1.0 cm which corresponded to 2.53%, 5.06% and 10.12% of the total can volume, respectively. The aim of this section is to present the effect of the headspace on the velocity profiles, turbulence intensities and Reynolds stress of Newtonian and non-Newtonian liquids used in the experiments.

Figures 42 to 45 show the variation of radial and tangential velocities along the radial direction for glycerol and CMC. As can be inferred from these figures, the headspace volume appeared to have little or no effect on the mean fluid motion in the cylinder. A general trend for the mean velocity distribution could not be found for any of the fluids used in the experiments.

The turbulence intensity values in the fluids, on the other hand, were affected considerably by changes in headspace. Figure 46 shows the variation of the radial turbulence intensity along the radial direction for 80% glycerol at 200 rpm. As can be inferred from the figure, the increase in the headspace to 1 cm augments the radial turbulence intensity by up to 168% and 472% in comparison to 0.5 cm and 0.25 cm headspace values, respectively. Figure 47 shows a similar behavior for the radial distribution of the radial turbulent intensity of CMC-M. It is interesting to note that the augmentation of the radial intensity was more pronounced around the centerline, whereas approaching towards the wall, the effect of headspace diminished possibly due to increasing viscous and inertial effects.

Figures 48 and 49 show the effect of headspace on the tangential turbulence intensity for CMC-M and CMC-H at 200 rpm and 300 rpm, respectively. These figures show very clearly that the tangential turbulence intensity was suppressed with

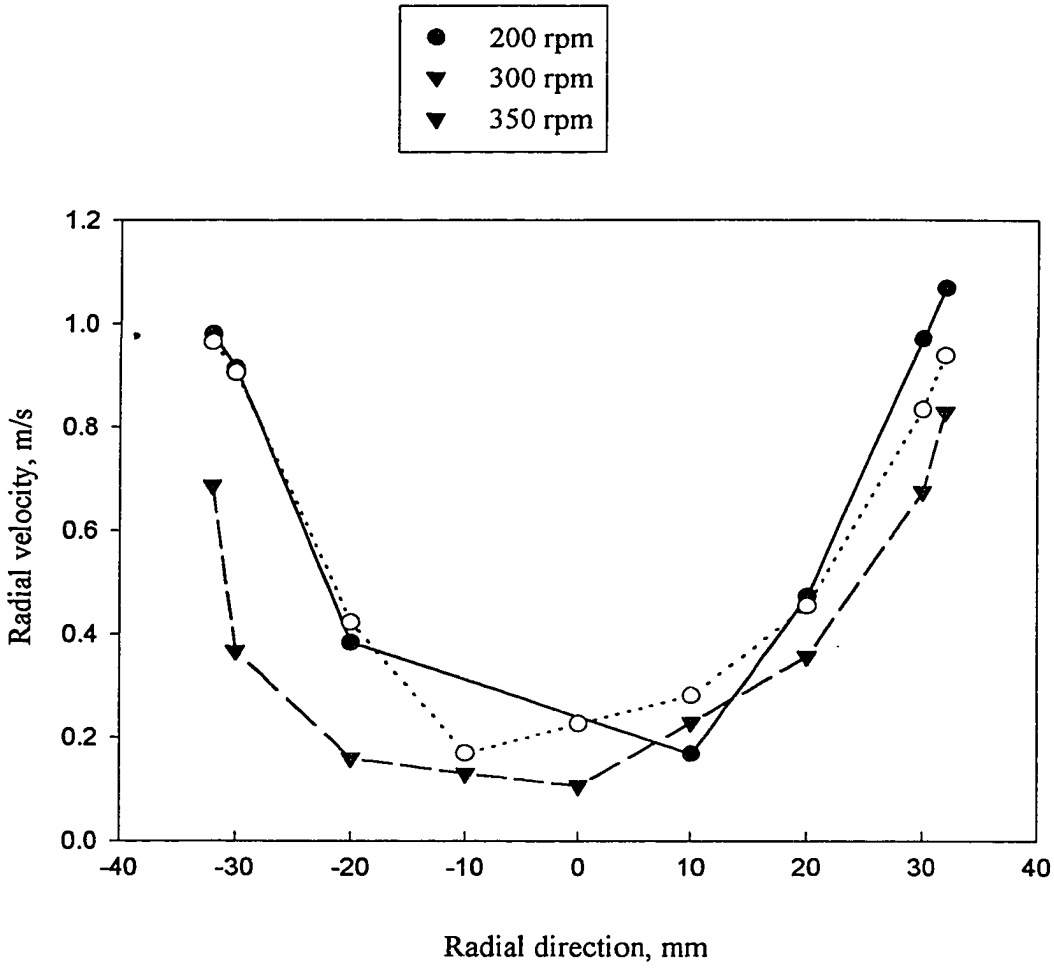

Figure 42. Radial velocity distribution for 80% glycerol in continuous rotation; 300 rpm, y = -10 mm

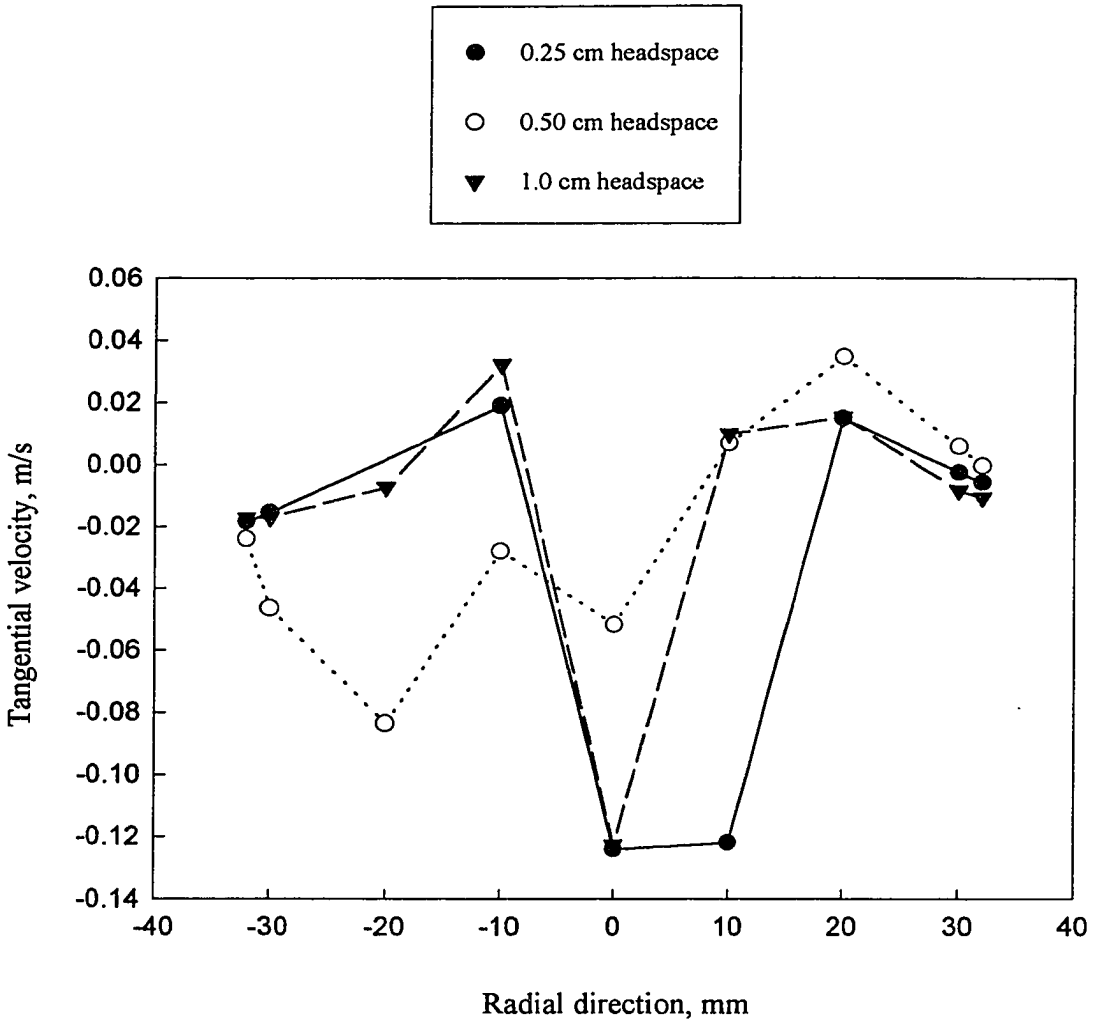

Figure 43. Tangential velocity distribution for 80% glycerol in continuous rotation; 200 rpm, y = -10 mm

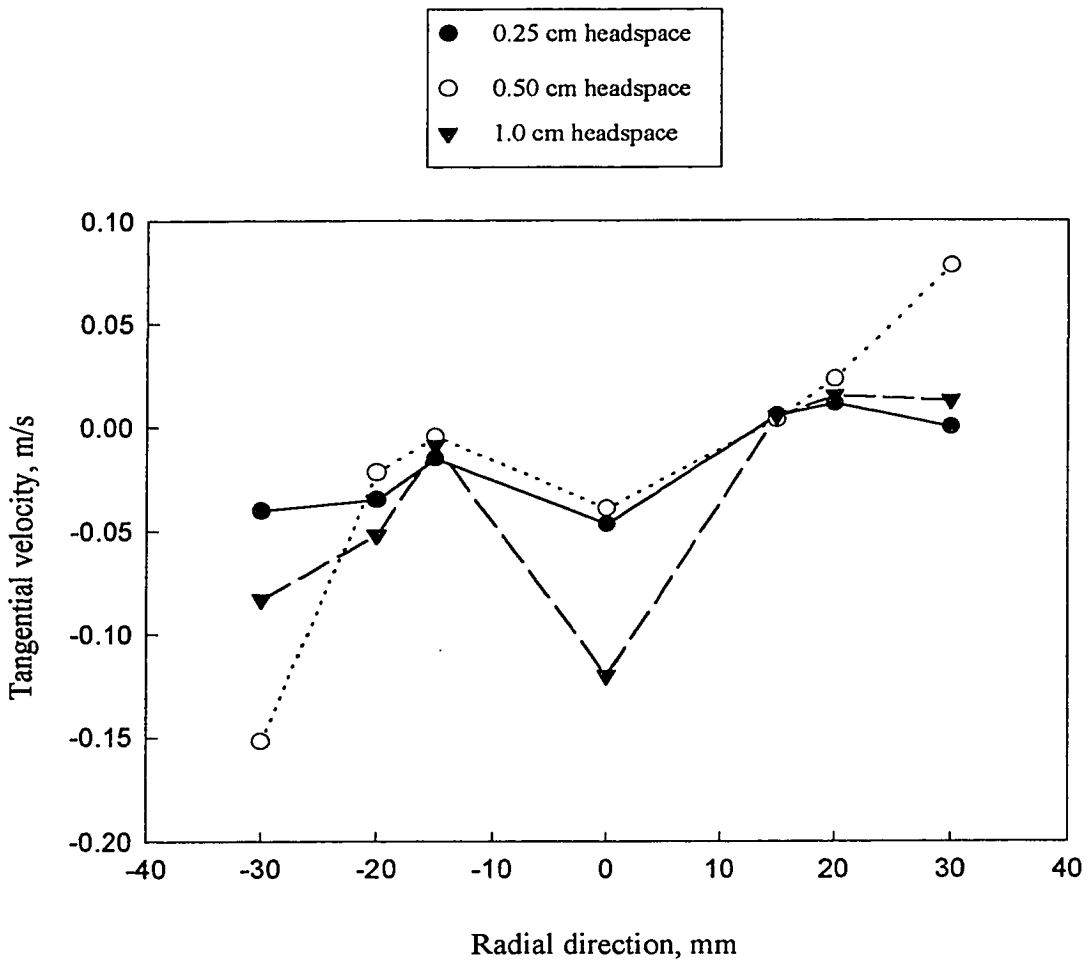

Figure 44. Tangential velocity distribution for 50% glycerol in continuous rotation; 350 rpm, y = -10 mm

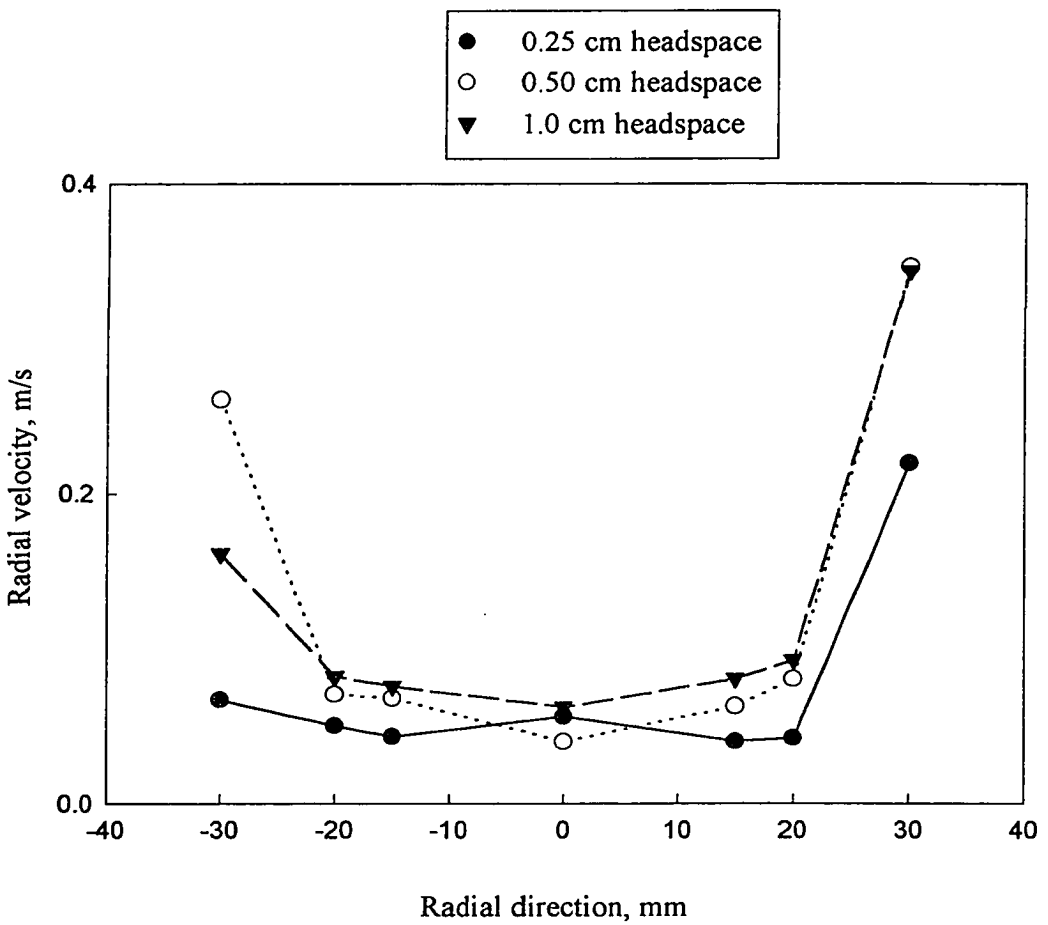

Figure 45. Radial velocity distribution for 50% glycerol in continuous rotation; 300 rpm, y = -10 mm

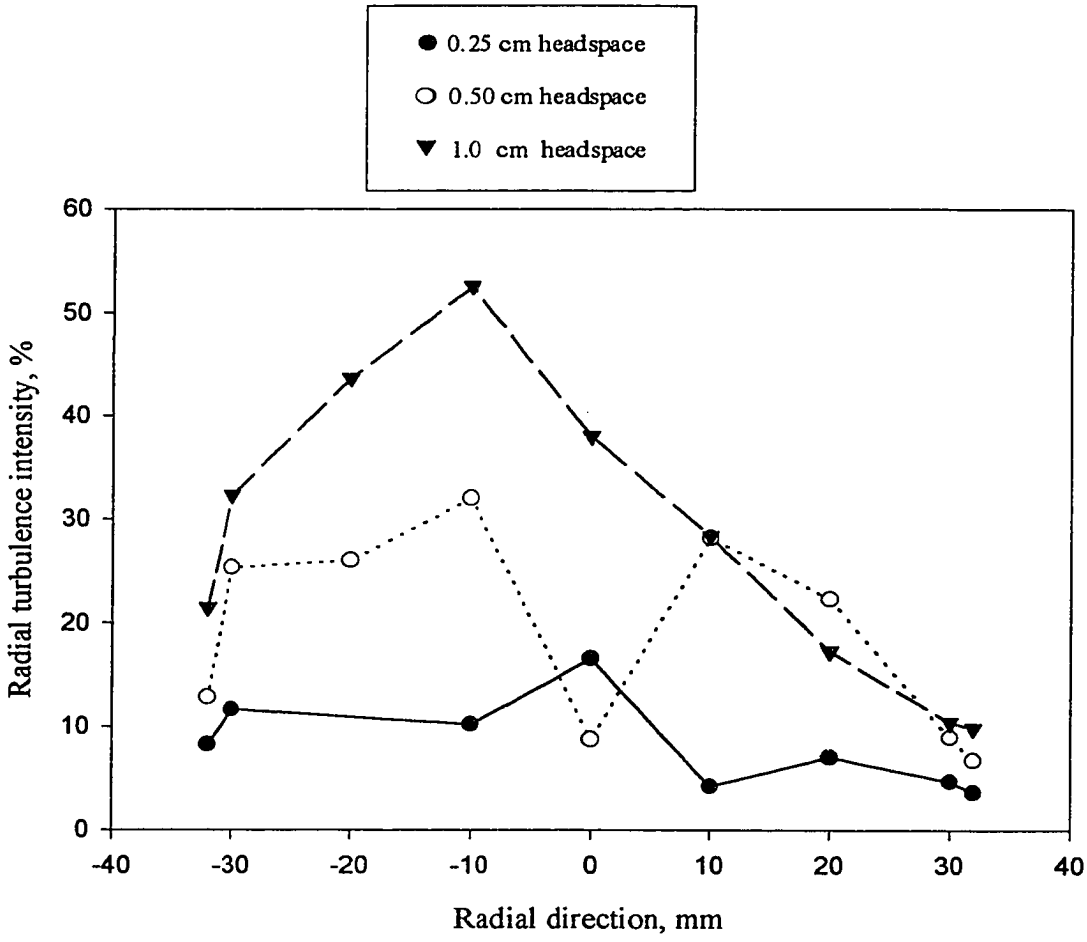

Figure 46. Effect of headspace on radial turbulence intensity for 80% glycerol in continuous rotation; 200 rpm, y = -10 mm

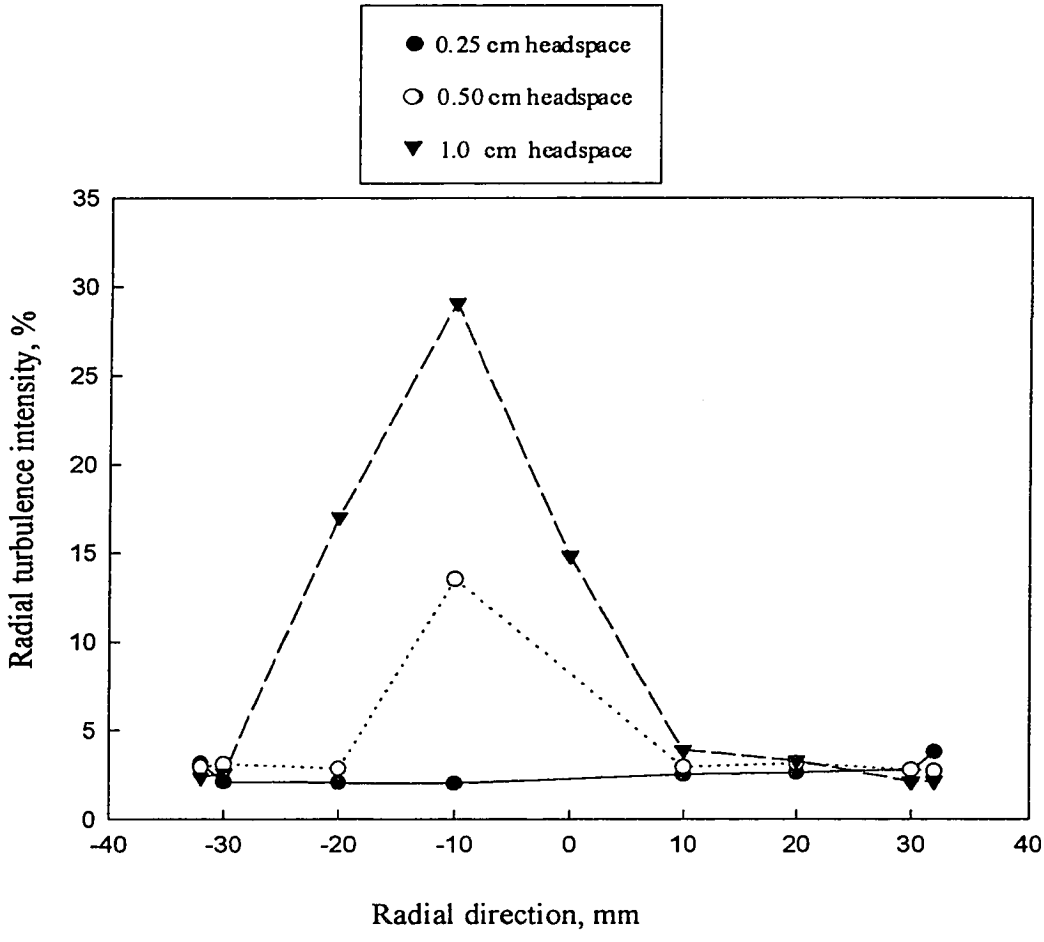

Figure 47. Effect of headspace on radial turbulence intensity for 2% CMC-M in continuous rotation; 350 rpm, y = -10 mm

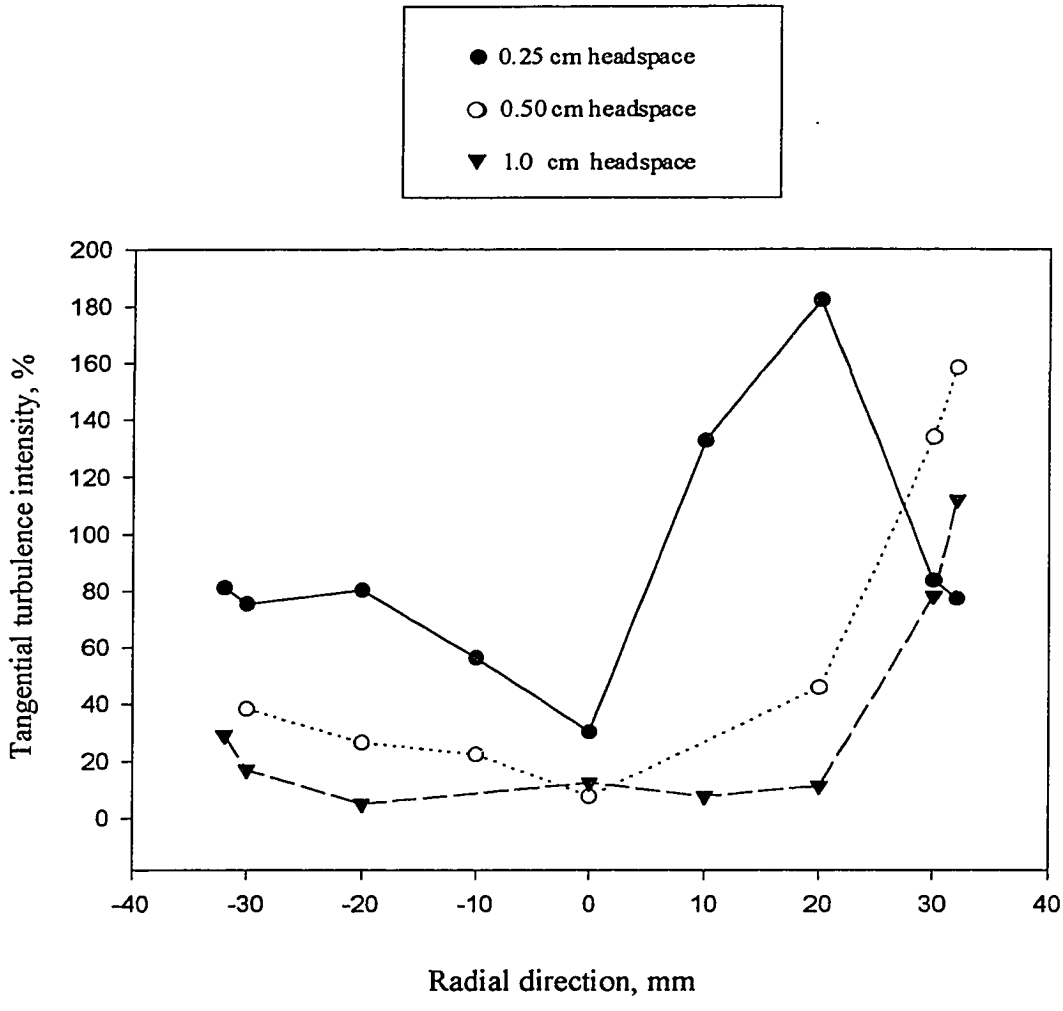

Figure 48. Effect of headspace on tangential turbulence intensity for 2% CMC-M in continuous rotation; 200 rpm, y = -10 mm

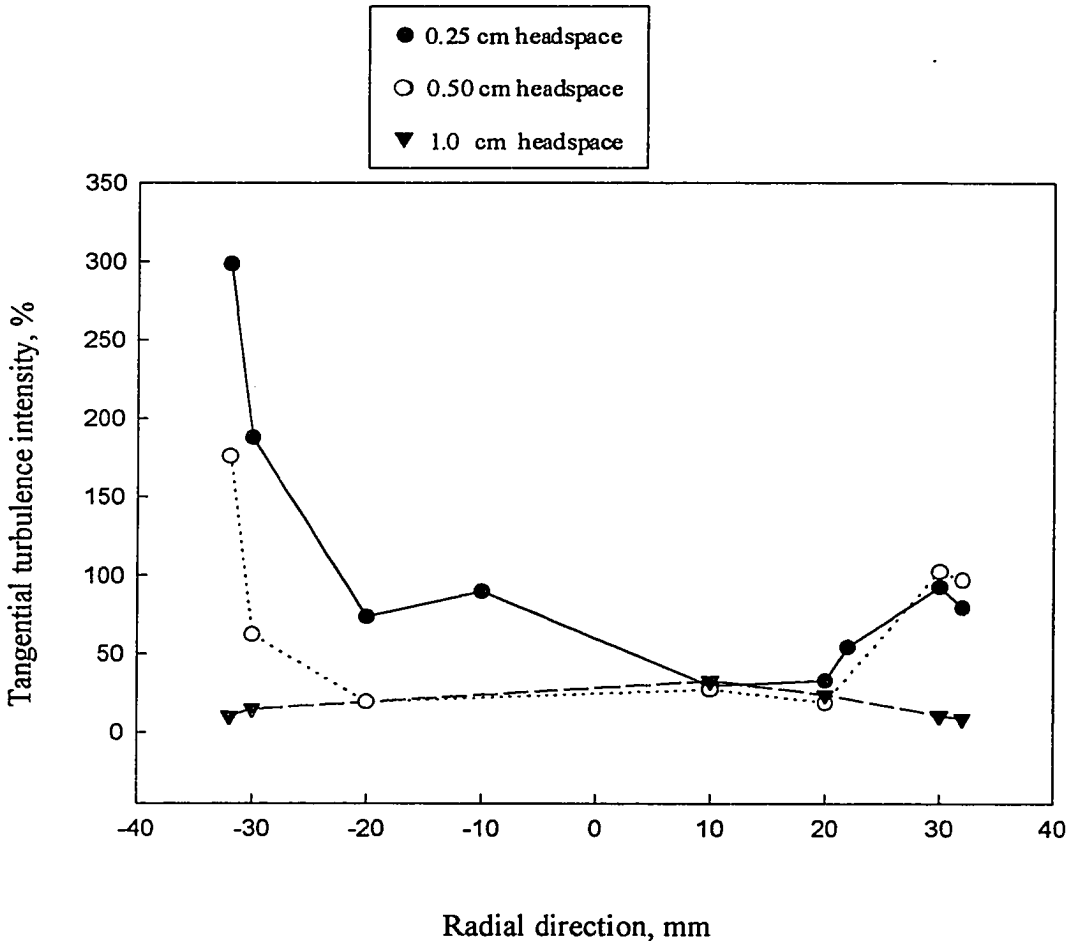

Figure 49. Effect of headspace on tangential turbulence intensity for 1.5% CMC-H in continuous rotation; 300 rpm, y = -10 mm

increasing headspace for CMC solutions except near the container wall. This may be due to the motion of the bubble towards the center for high viscosity fluids, which may have a stabilizing effect on the tangential velocity fluctuations. Figures 50 and 51 also suggest a decrease in the tangential turbulence intensity with increasing headspace for glycerol. However, this effect was not as clear as in the case of CMC-M and CMC-H solutions which were appreciably more viscous than 25% glycerol.

4.5. Effect of Viscosity

Viscosity of the fluid plays an important role on the hydrodynamics of the fluids in axially rotating cylinders. In this section, the effect of viscosity on the mean axial and radial velocity distributions, turbulence intensities, and Reynolds stresses were investigated in detail.

4.5.1. Tangential and Radial Velocity Distributions

Figure 52 shows the variation of the mean radial velocity along the radial direction for three different glycerol solutions. Results clearly show that increasing the viscosity increased the radial velocity towards the outside of the cylinder. As can be seen in Figure 52, for 300 rpm and 0.5 cm headspace, the effect of viscosity on the radial velocity distribution becomes more predominant near the wall region where the viscous forces were large when compared to gravitational forces. Near the center, the effect of viscosity diminished. For instance, a a distance 3 cm away from the center, the magnitude of the radial velocity of 80% glycerol was 2 and 6 times larger than the magnitude of the radial velocities of 50% and 25% glycerol, respectively. This increase in the radial velocity, especially towards the wall, can be explained by the combined effect of the viscous and inertial (centrifugal) forces. It is known that the total momentum that is transferred to the liquid inside the cylinder is directly proportional to the liquid viscosity (Schlichting, 1987). For the same rotational speed and can radius, increasing the apparent viscosity of the liquid increased the torque transmitted to the liquid, hence the tangential force per unit area (i.e., the shear stresses increased). This

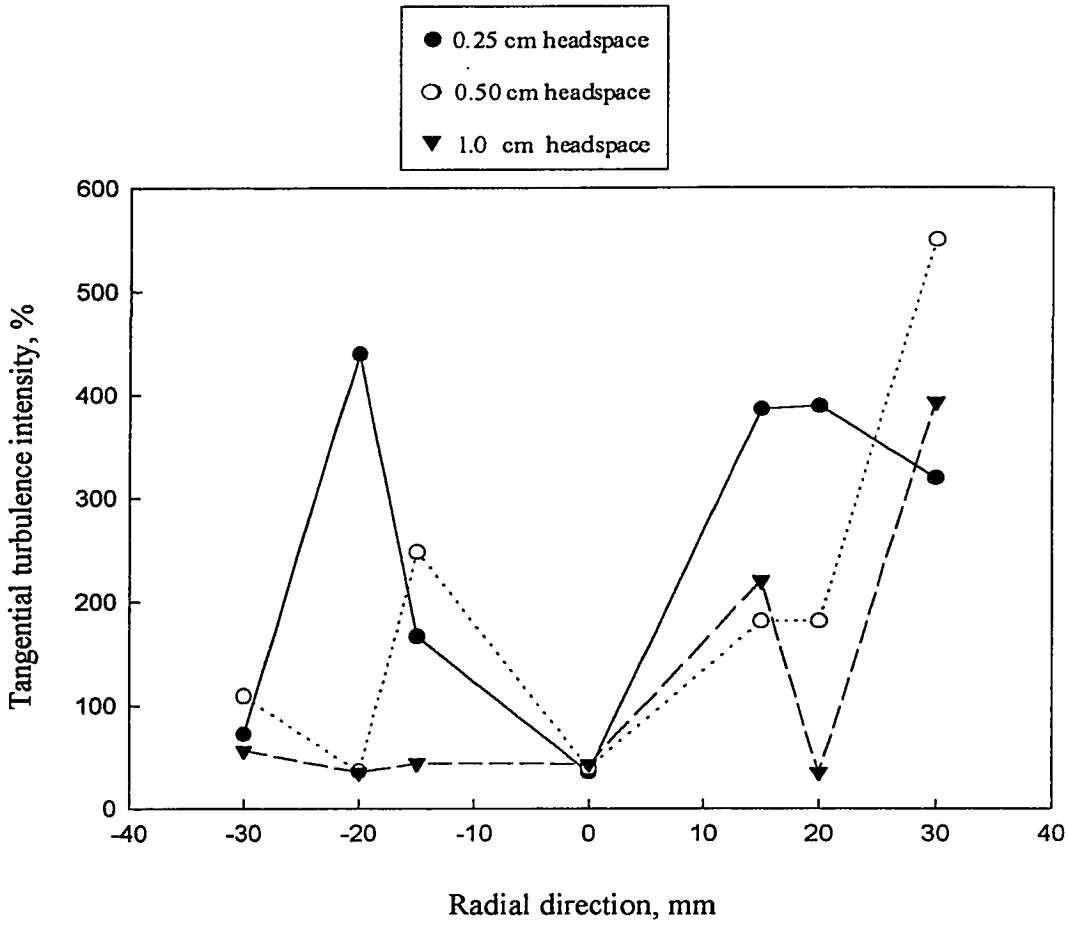

Figure 50. Effect of headspace on tangential turbulence intensity for 25% glycerol in continuous rotation; 200 rpm, y = -10 mm

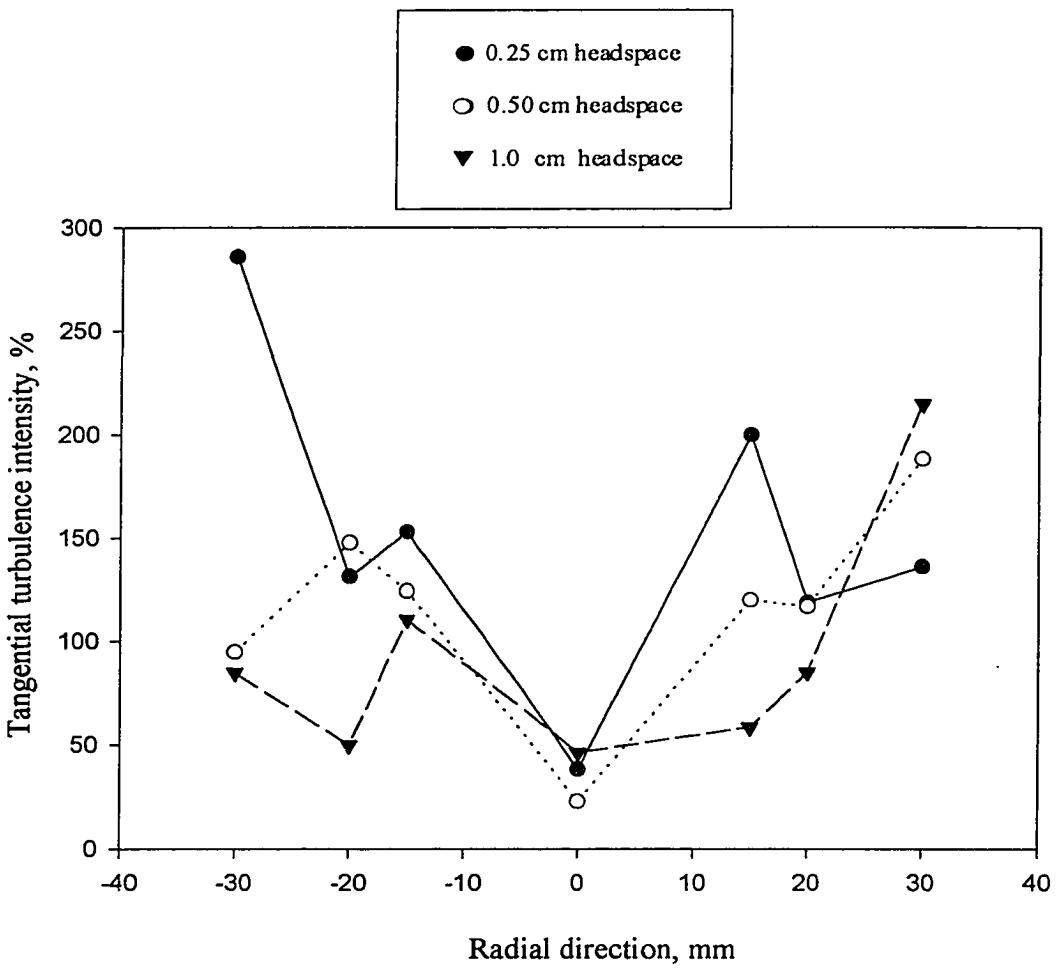

Figure 51. Effect of headspace on tangential turbulence intensity for 25% glycerol in continuous rotation; 300 rpm, y = -10 mm

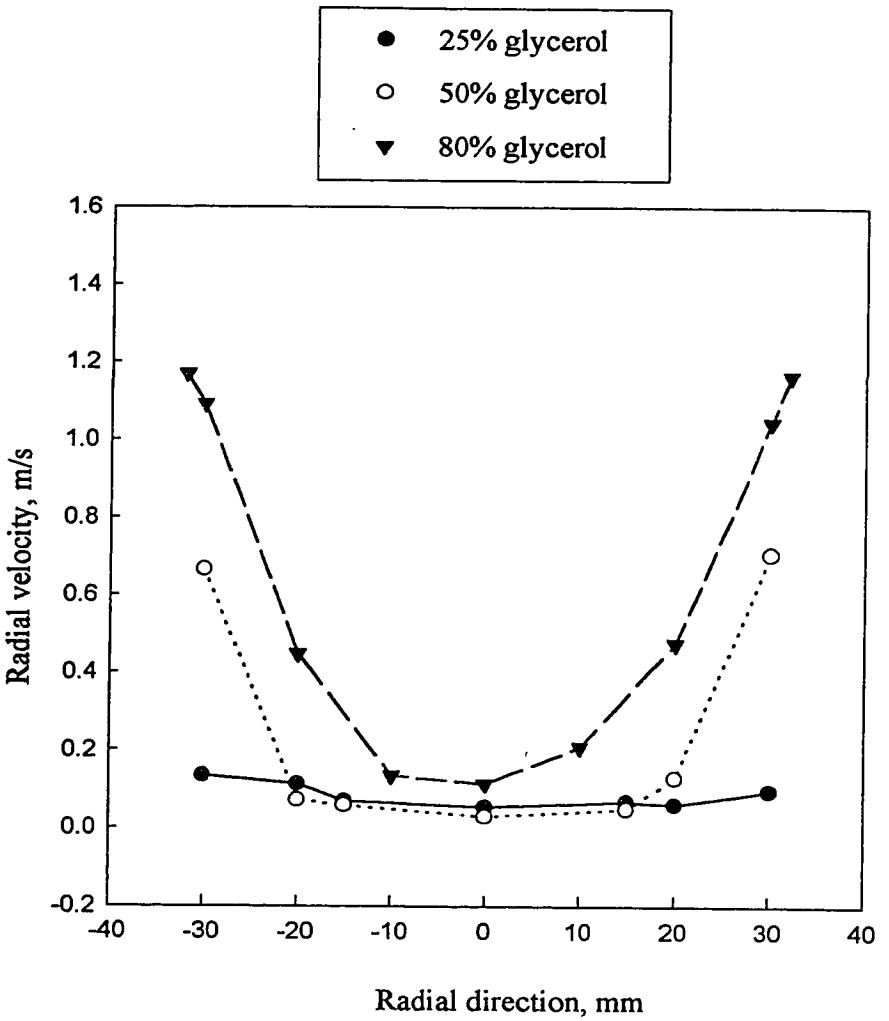

Figure 52. Radial velocity distribution for aqueous glycerol solutions in continuous rotation; 350 rpm, 0.50 cm headspace, y = -10 mm

increase in shear stress resulted in higher values of radial acceleration, leading to higher centrifugal forces whose values increased towards the wall.

Non-Newtonian liquids also showed the same pattern for the radial velocity distribution with liquids of increasing viscosity as seen in Figure 53. This apparent increase in the radial velocity can also be explained by the proposition presented above for Newtonian liquids.

The tangential velocity distribution along the radial direction for glycerol and CMC is shown in Figures 54 and 55. The effect of viscosity on the mean tangential velocity was not clear-cut, as was the case for radial velocity as seen in these figures for both glycerol and CMC. Figures 54 and 55 reflect the typical features of the data obtained for the other cases, as well. No definite pattern could be found for the effect of viscosity on the mean tangential velocity for either Newtonian or non-Newtonian liquids.

The effect of viscosity shows itself perhaps mostly in the case of turbulence intensity measurements along the radial direction for glycerol and CMC solutions at different apparent viscosities. As can be inferred from Figures 56 to 59, the radial turbulence intensity was attenuated by increasing viscosity for both glycerol and CMC solutions. This was an expected result, typical of turbulent flow. The overall energy cascade of the system can be explained as follows: the mean motion takes its energy from the rotation of the cylinder. The energy of the mean motion is transferred to the large eddies by the Reynolds stresses generated by turbulence. The visual observations during the experiments showed two large eddies beneath the headspace bubble, each occupying approximately half the size of the cylinder. The motion of these large eddies were independent of the apparent viscosity of the fluid. These large "most energetic" eddies broke up into smaller "less energetic" high frequency eddies with mechanisms such as vortex stretching, bursting, etc., until a certain length scale was reached at which viscous forces started to become effective and dissipated the energy of the smallest scale eddies (dissipative scale) into heat. When a more viscous fluid is used, the size of the large scale eddies do not change but the energy of Kolmogorov scale

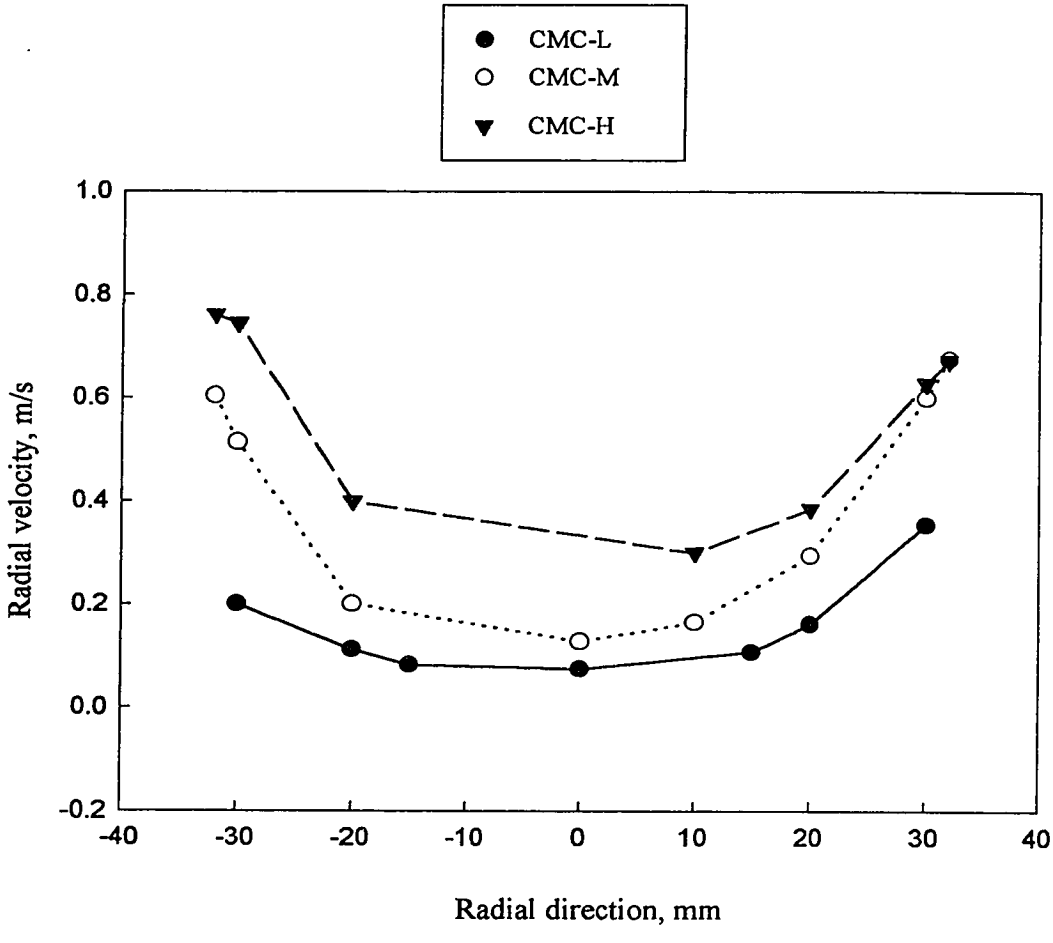

Figure 53. Radial velocity distribution for CMC in continuous rotation; 200 rpm, 1 cm headspace, y = -10 mm

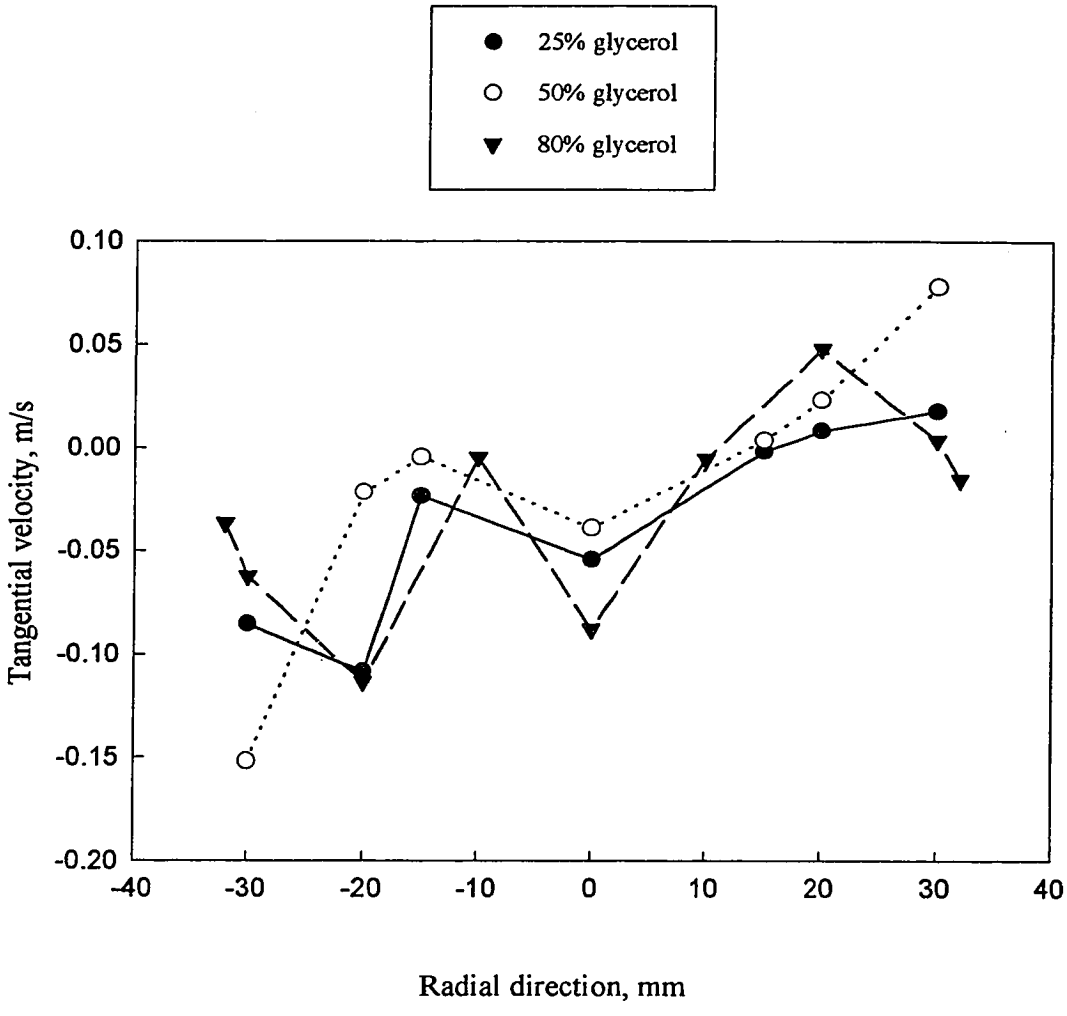

Figure 54. Tangential velocity distribution for glycerol in continuous rotation; 350 rpm, 0.50 cm headspace, y = -10 mm

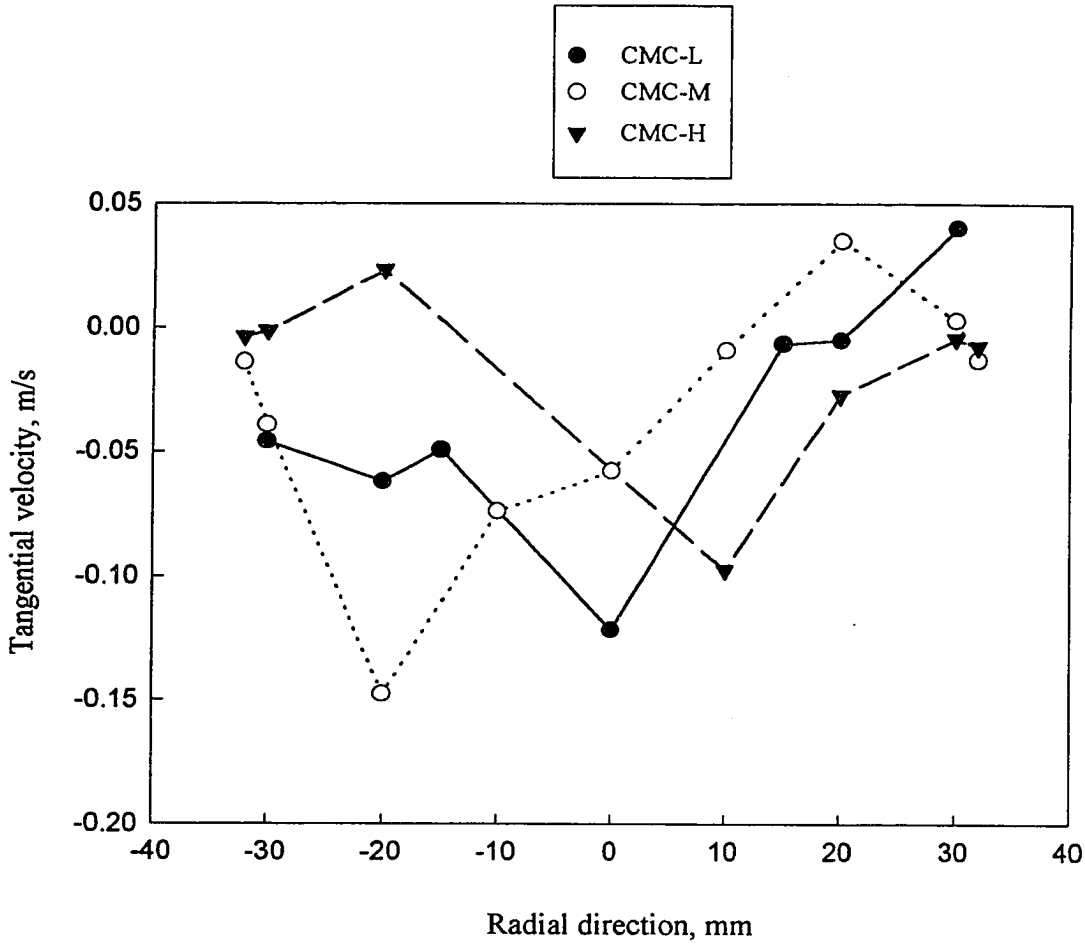

Figure 55. Tangential velocity distribution for CMC in continuous rotation 300 rpm, 1.0 cm headspace, y = -10 mm

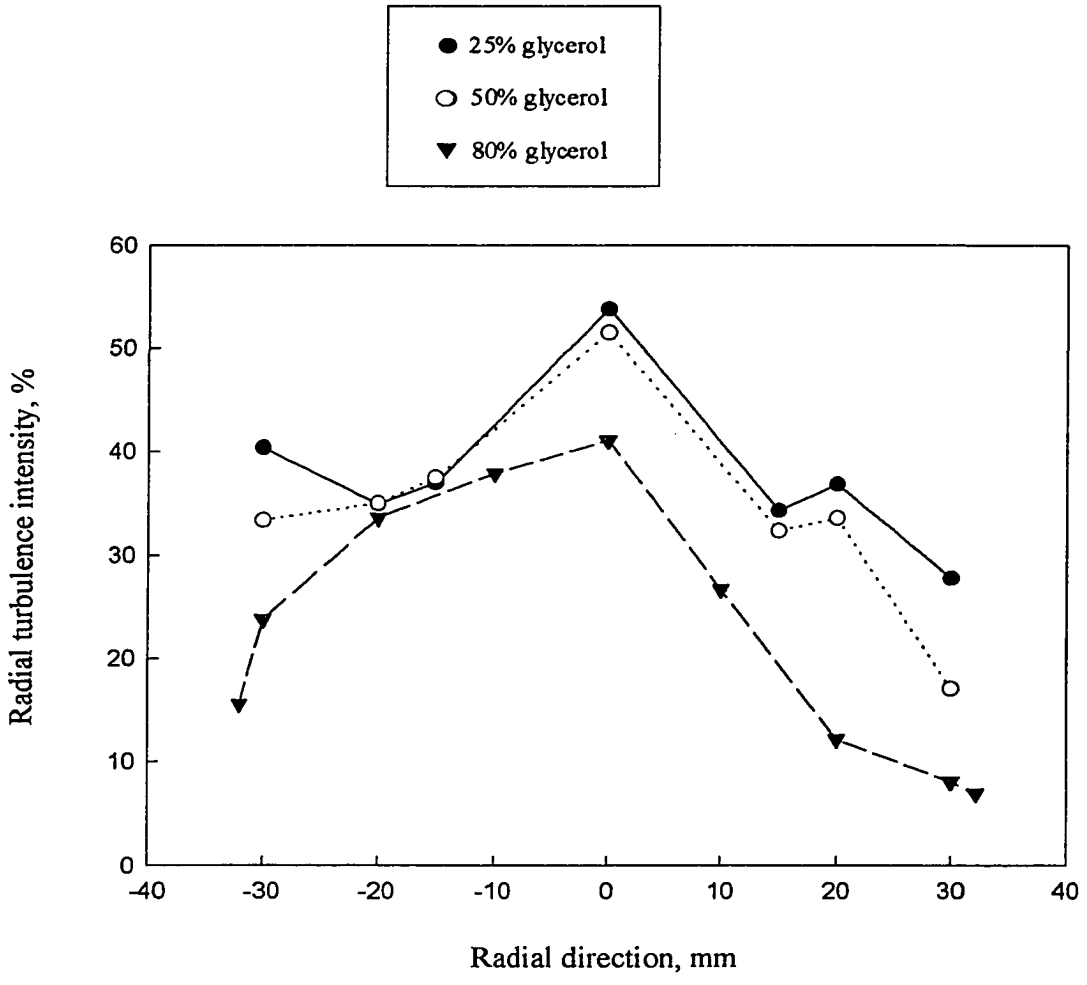

Figure 56. Radial turbulence intensity for glycerol in continuous rotation; 300 rpm, 1.0 cm headspace, y = -10 mm

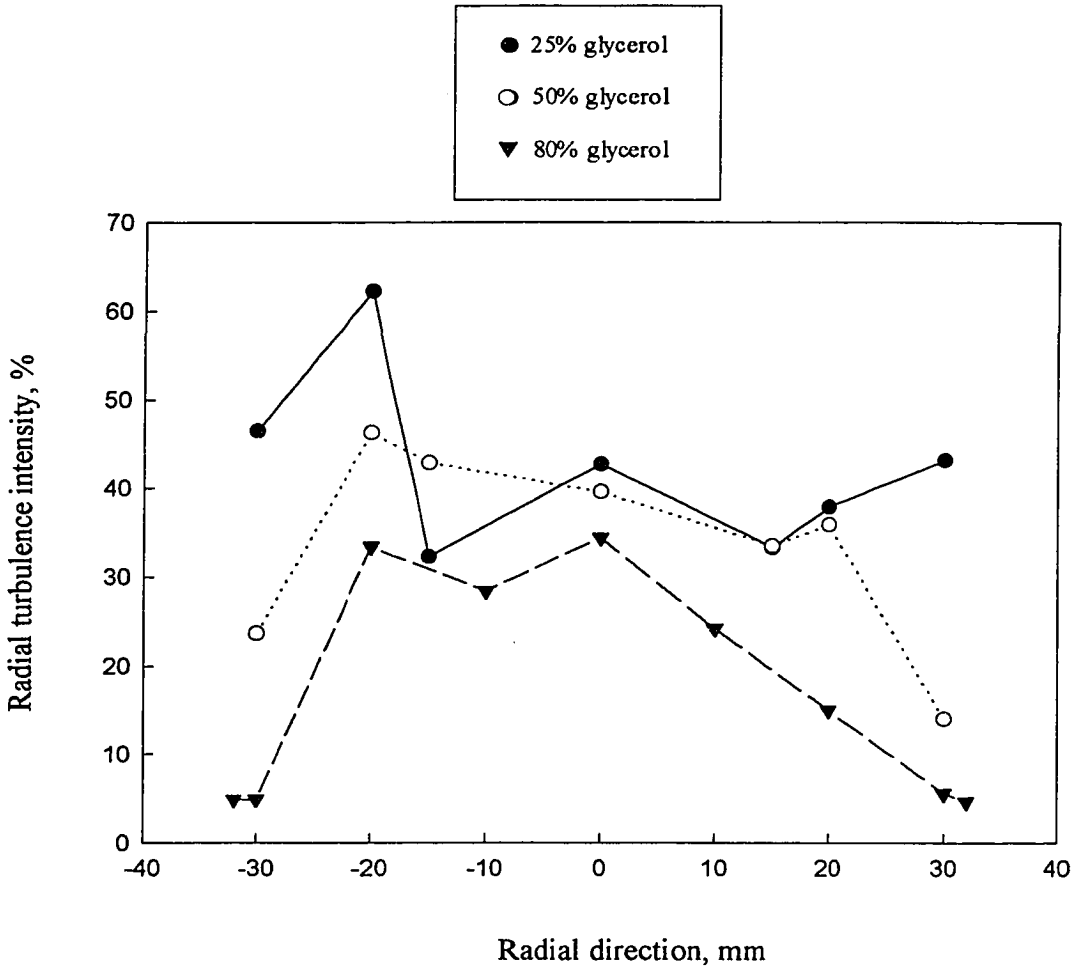

Figure 57. Radial turbulence intensity for glycerol in continuous rotation; 350 rpm, 0.50 cm headspace, y = -10 mm

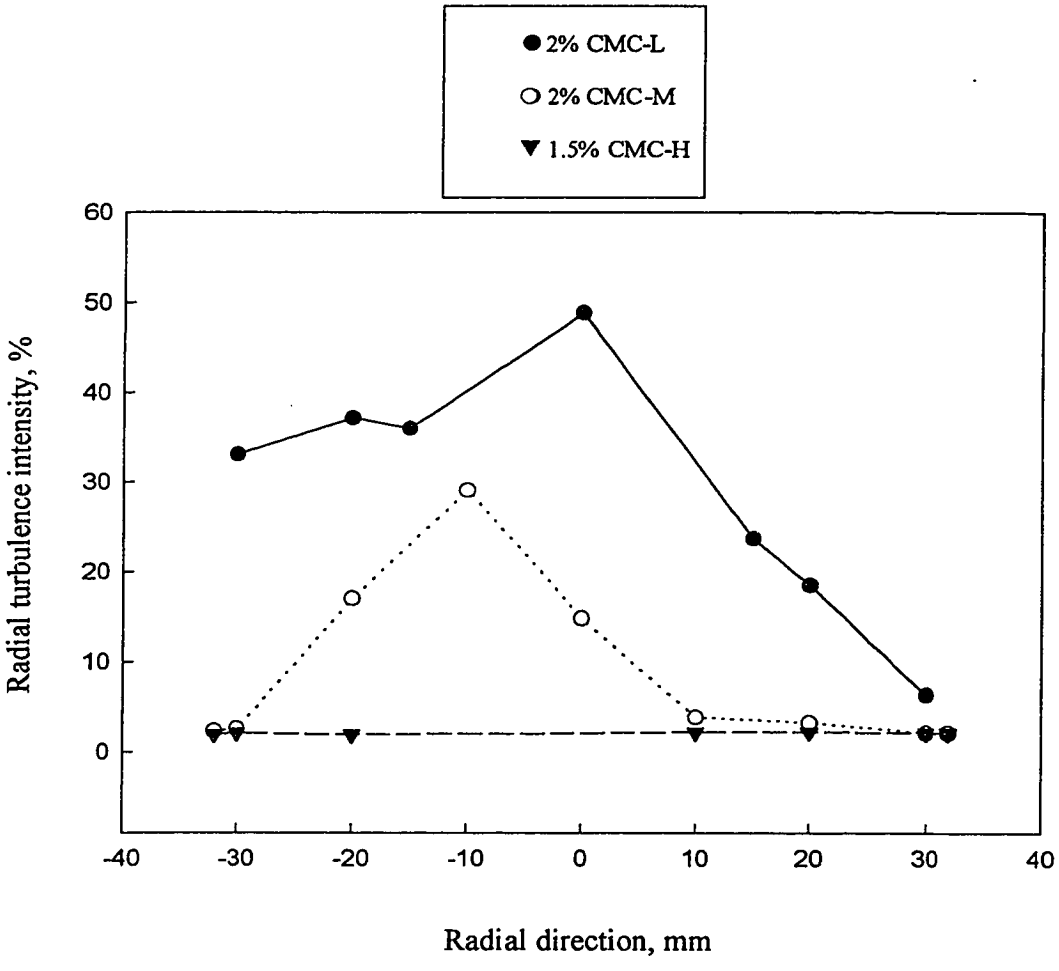

Figure 58. Radial turbulence intensity for CMC in continuous rotation 350 rpm, 1.0 cm headspace, y = -10 mm

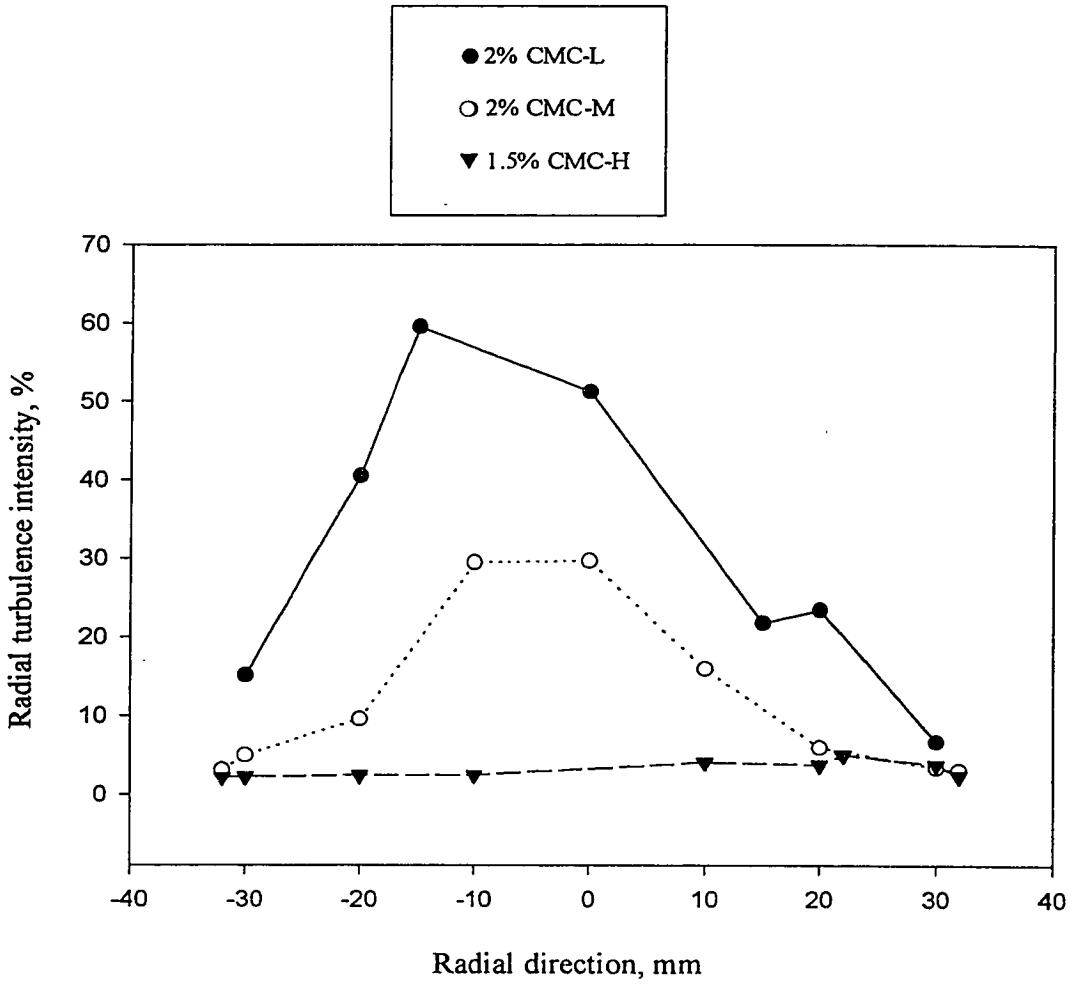

Figure 59. Radial turbulence intensity for CMC in continuous rotation; 200 rpm, 0.25 cm headspace, y = -10 mm

eddies of high viscosity fluids are dissipated at larger size and lower frequency when compared that of lower viscosity fluid.

Figures 60 and 61 show the typical behavior of the tangential turbulence intensities with increasing viscosity. For Newtonian liquids, a conclusive trend could not be found in the experiments, as can be seen in Figure 60. However, for non-Newtonian liquids, the tangential turbulent intensity was suppressed with increasing apparent viscosity as seen in Figure 61.

The following results can be suggested for the effect of viscosity on the flow hydrodynamics in axially rotating cylinders:

a) The mean radial velocity increased with increasing viscosity due to a combined effect of inertial and viscous forces,
b) The mean tangential velocity seems to remain unchanged with increasing viscosity,
c) The radial turbulent intensity was substantially decreased with increasing viscosity for both Newtonian and non-Newtonian liquids, and
d) The tangential turbulent intensity did not show any conclusive pattern for Newtonian liquids, whereas it decreased in non-Newtonian liquids with increasing viscosity.

4.6 Velocity-time Histories

Figures 62 and 63 show the velocity-time histories at different radial locations for the vertical (v) component for continuous rotation as a function of radial direction for water and 50% glycerol. These figures display the fluctuations which may be attributed to inherent features of the liquid motion.

For simulation of a typical Sterilmatic™ thermal processing system, several experiments were conducted. The amplitude of the time-velocity curves (Figures 64 and 65) tended to grow when rotation started, reaching an almost constant value then decreased again. During the initial acceleration process, both vertical and horizontal components of the velocity increased linearly. The velocity fluctuations increased towards the center of the cylinder due to the decrease in viscous forces for both water

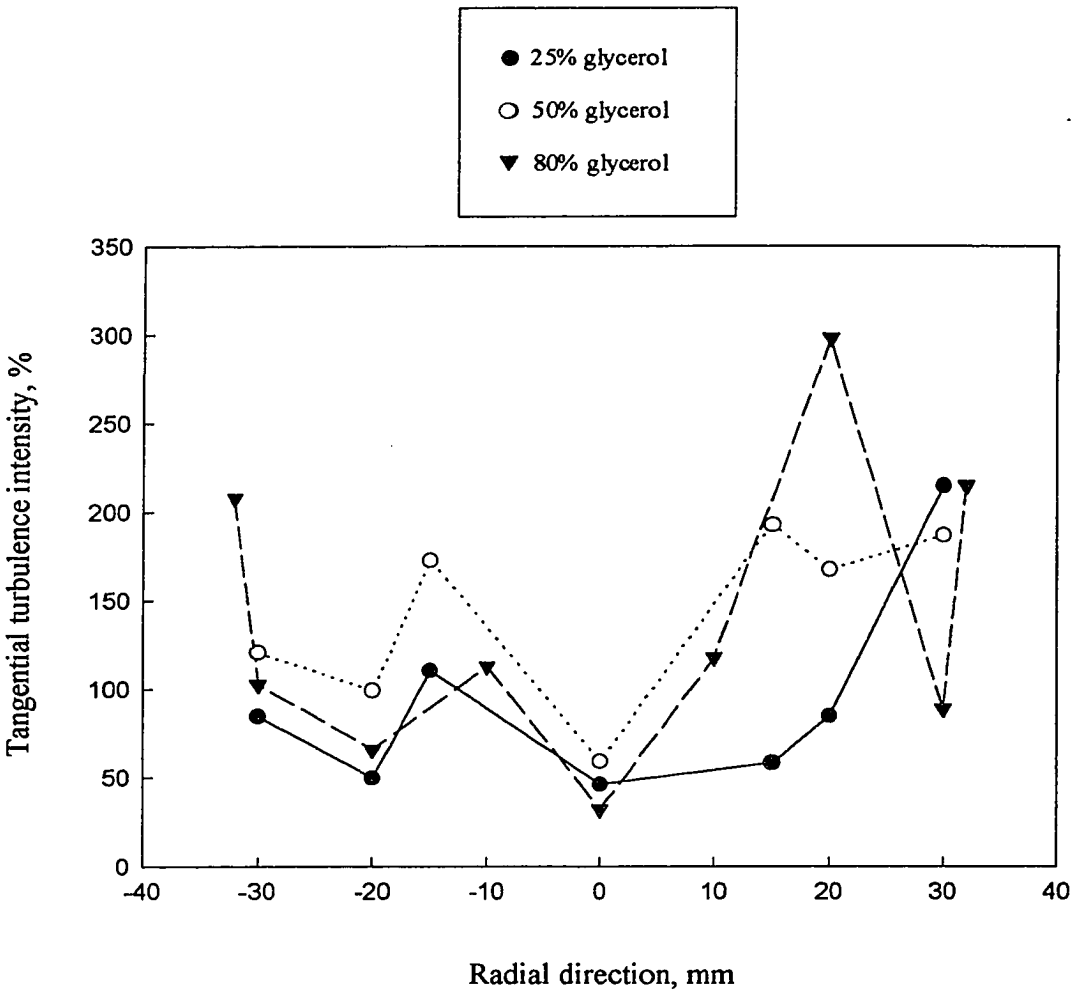

Figure 60. Tangential turbulence intensity for glycerol in continuous rotation; 300 rpm, 1.0 cm headspace, y = -10 mm

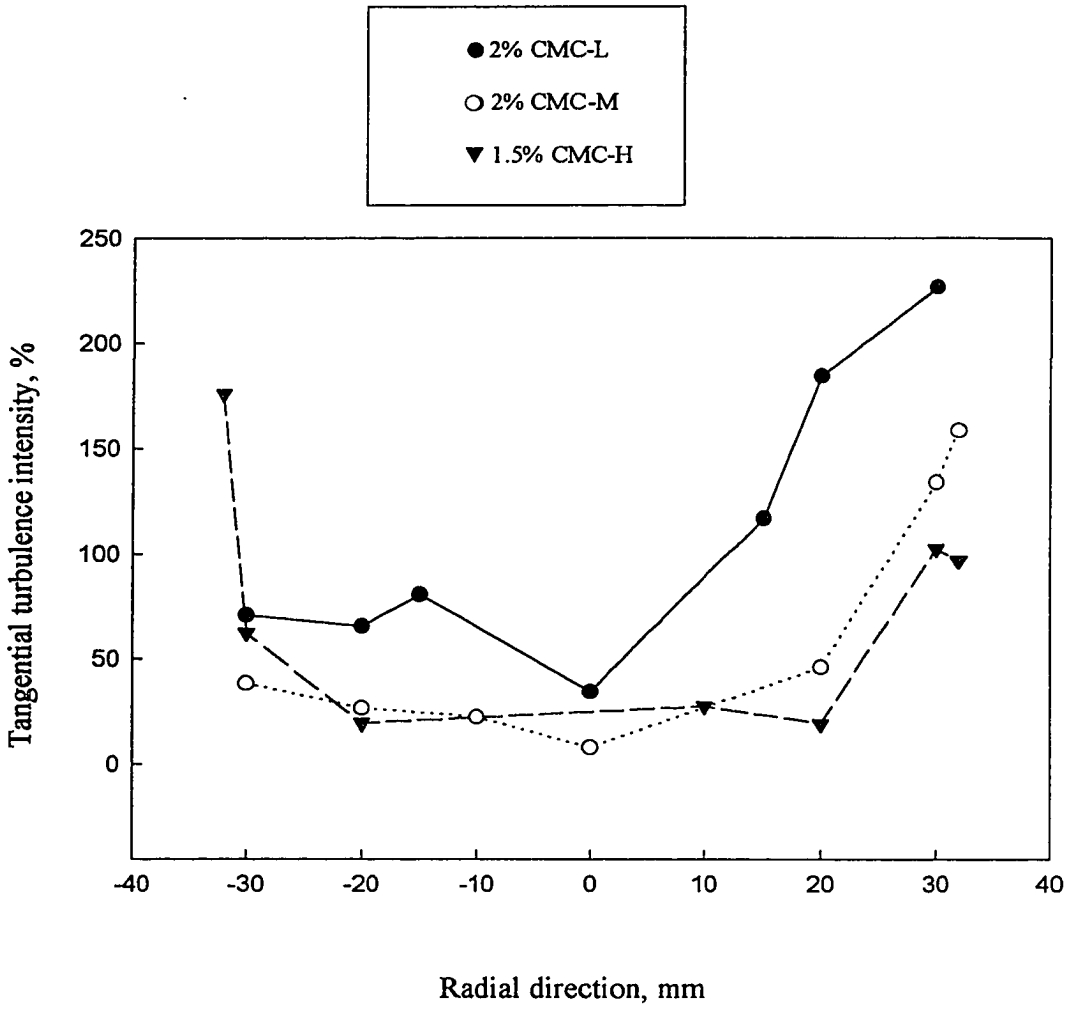

Figure 61. Tangential turbulence intensity for CMC in continuous rotation; 200 rpm, 0.25 cm headspace, y = -10 mm

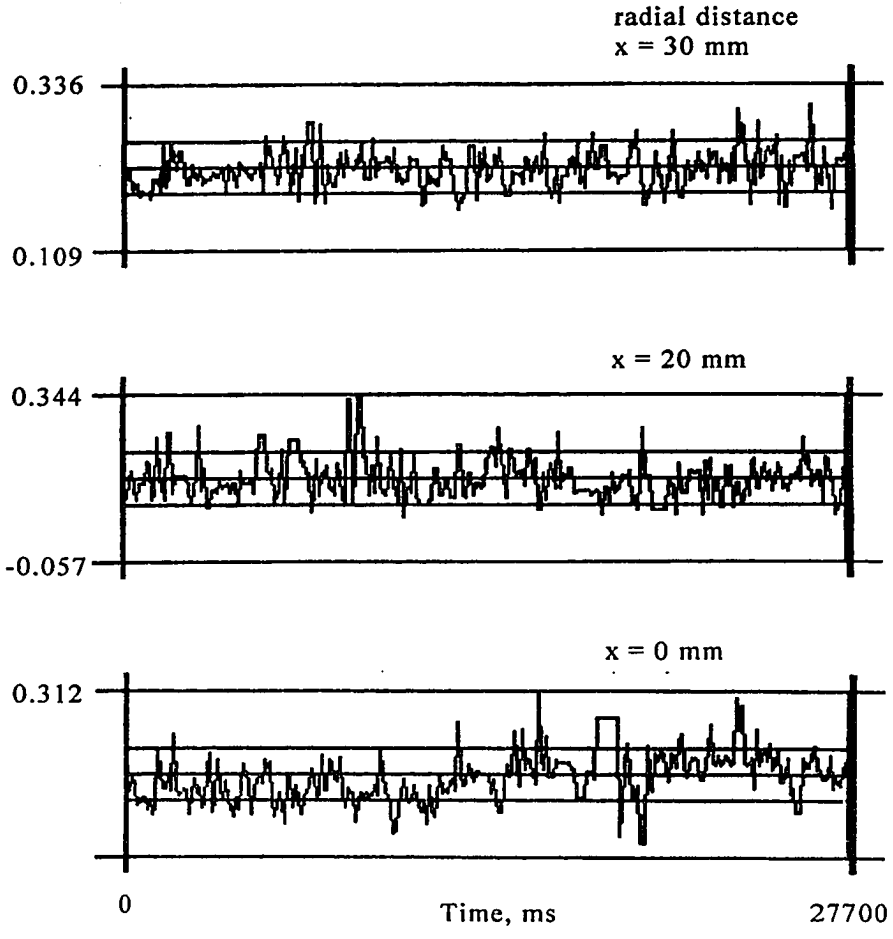

Figure 62. Time-velocity (vertical component) histogram for water in a continuous system, as a function of radial position; 300 rpm, 0.5 cm headspace, y = - 15 mm

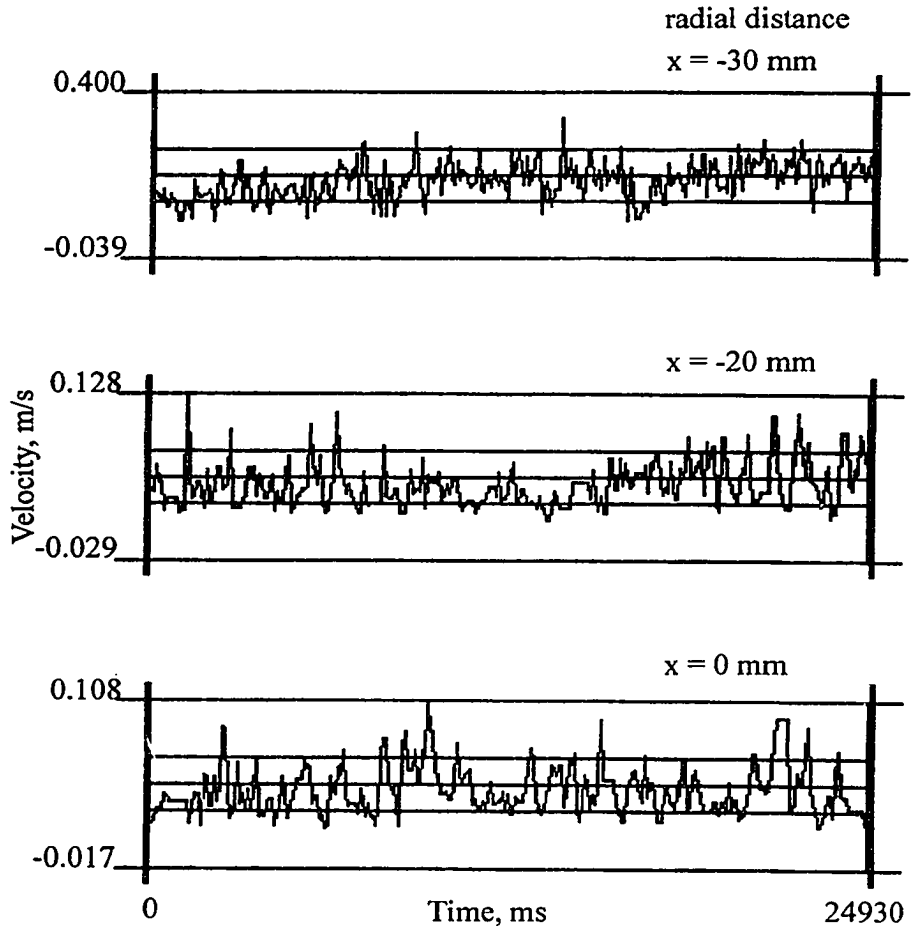

Figure 63. Time-velocity (vertical component) histogram for 50% glycerol in a continuous system, shown as a function of radial position; 350 rpm, 0.5 cm headspace, y = - 15 mm

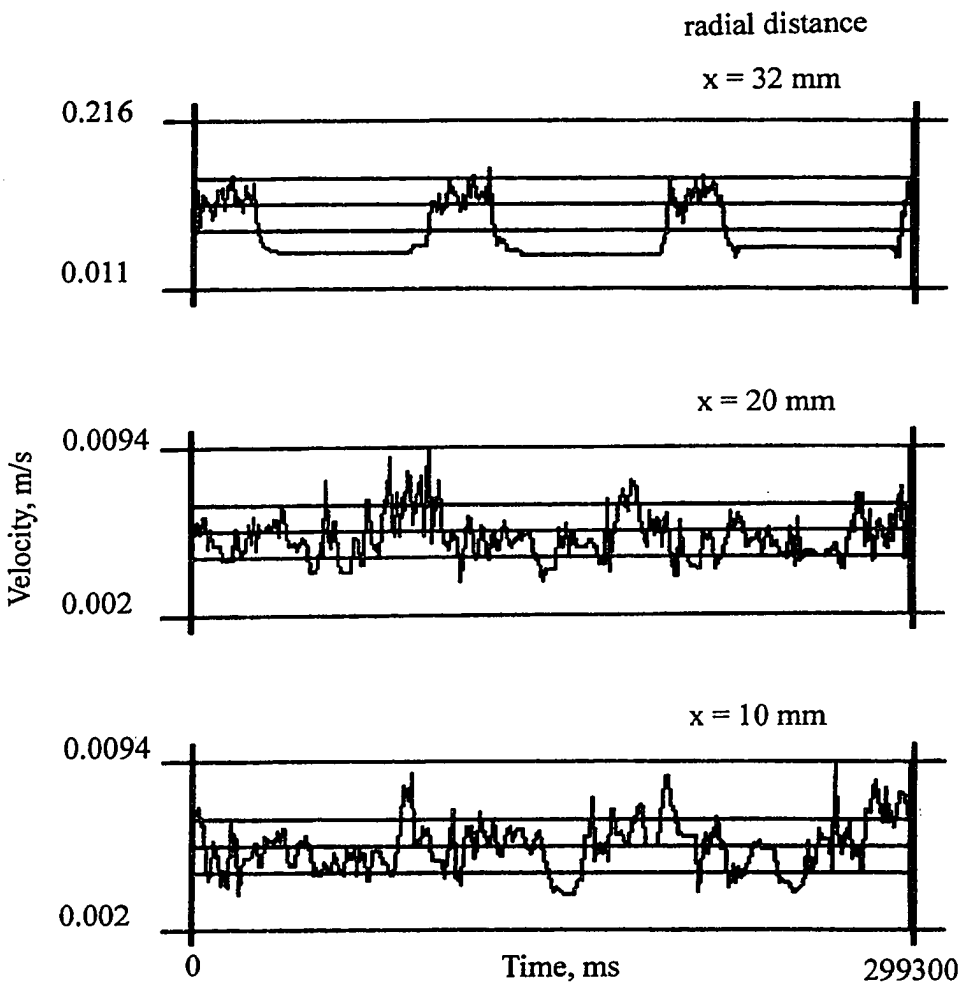

Figure 64. Time-velocity (vertical component) histogram for water in an intermittently rotating horizontal cylinder simulating a Sterilmatic™ retort simulation system, shown as a function of radial position; 300 rpm, 0.5 cm headspace, y = - 15 mm

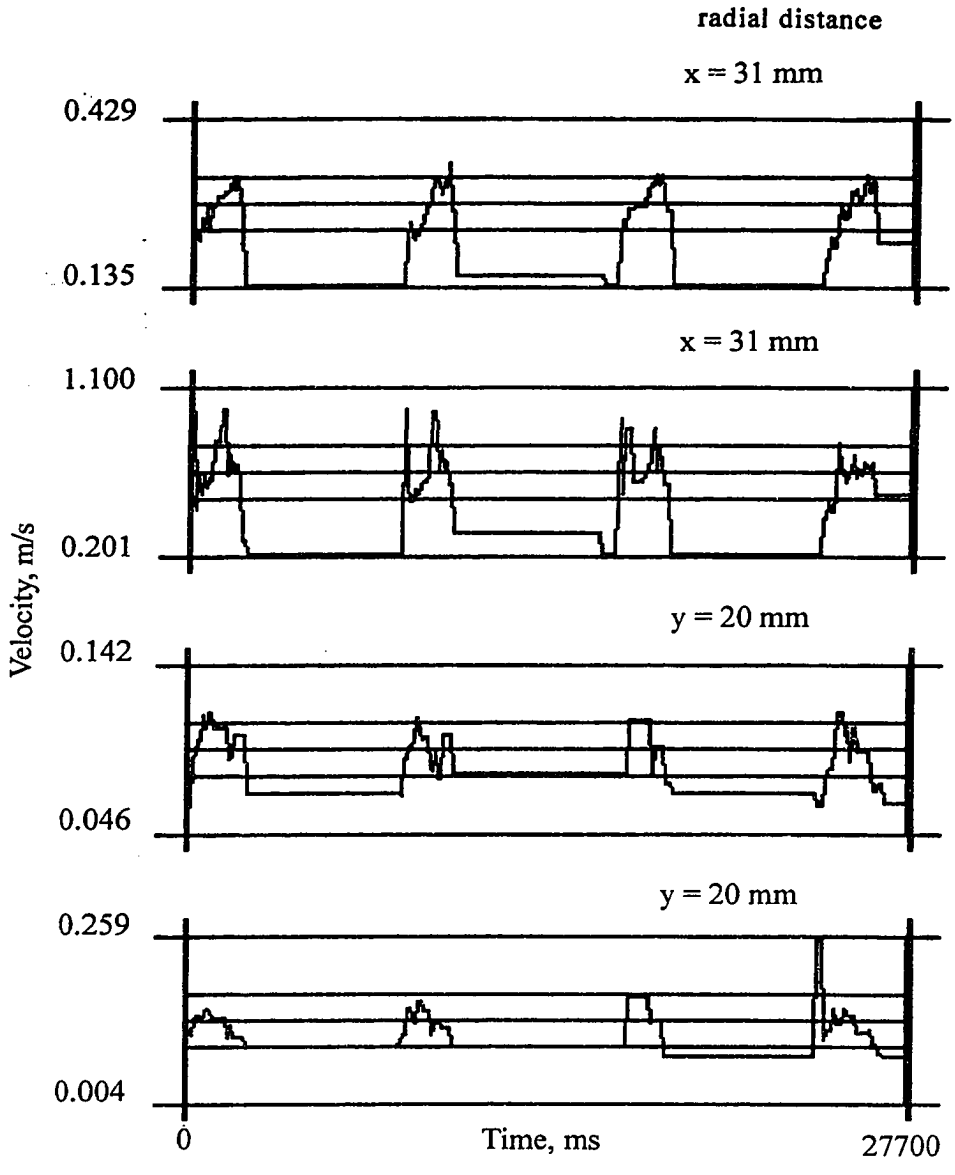

Figure 65. Time-velocity (vertical (u) and horizontal (v) components) histogram for 0.15% xanthan polymer in an intermittently rotating horizontal cylinder simulating a Sterilmatic™ retort system, shown as a function of radial position; 300 rpm, 1.0 cm headspace, y = -15 mm

and glycerol.

Figure 66 shows the velocity response at different radial locations for 1.5% CMC-H solution at 300 rpm. The initial slope of the velocity-time curve indicates that response of the points closer to the wall was faster than that of the points away from the wall. Evidently, the energy that was supplied to the fluid was first extracted from the cylinder wall, and its transfer to the center took time, especially for low viscosity fluids. It is very interesting to note how rapidly the peak tangential velocity drops to 0.3 m/s from 1.25 m/s at two radial measurement points which are only 1.5 cm apart (35 mm and 20 mm).

4.7 Power Spectrum

A turbulent motion can be represented as a super-position of periodic eddies or waves with different length and time scales, and different orientations in space. The process of stresses generation, diffusion and energy transmission between the various scales of mation can be described in terms of interactions between these eddies. However, the interactions are very complex. A particular superposition of harmonic components with differeng frequencies or wavelengths is specified by a function giving the variation of the component intensity with frequency or wavelength. This is called a spectrum function (Reynolds, 1974). The spectrum basically gives us information about the distribution of energy over different length scales, because the different scales play different roles in the dynamics of the motion. This is often expressed by talking of 'eddies of different sizes' (Tritton, 1988). The spectrum curve is often interpreted in terms of the energy associated with eddies of various sizes. Small eddies contribute to large wavenumber components of the spectrum. Spectral analysis was determined via packaged software (FIND, version 4.03, TSI Inc., St. Paul, MN) based on a fast Fourier transform technique.

Figure 67 shows the typical power spectrum vs. frequency plots for water at different rotational radial positions for 300 rpm. As can be inferred from this figure, the

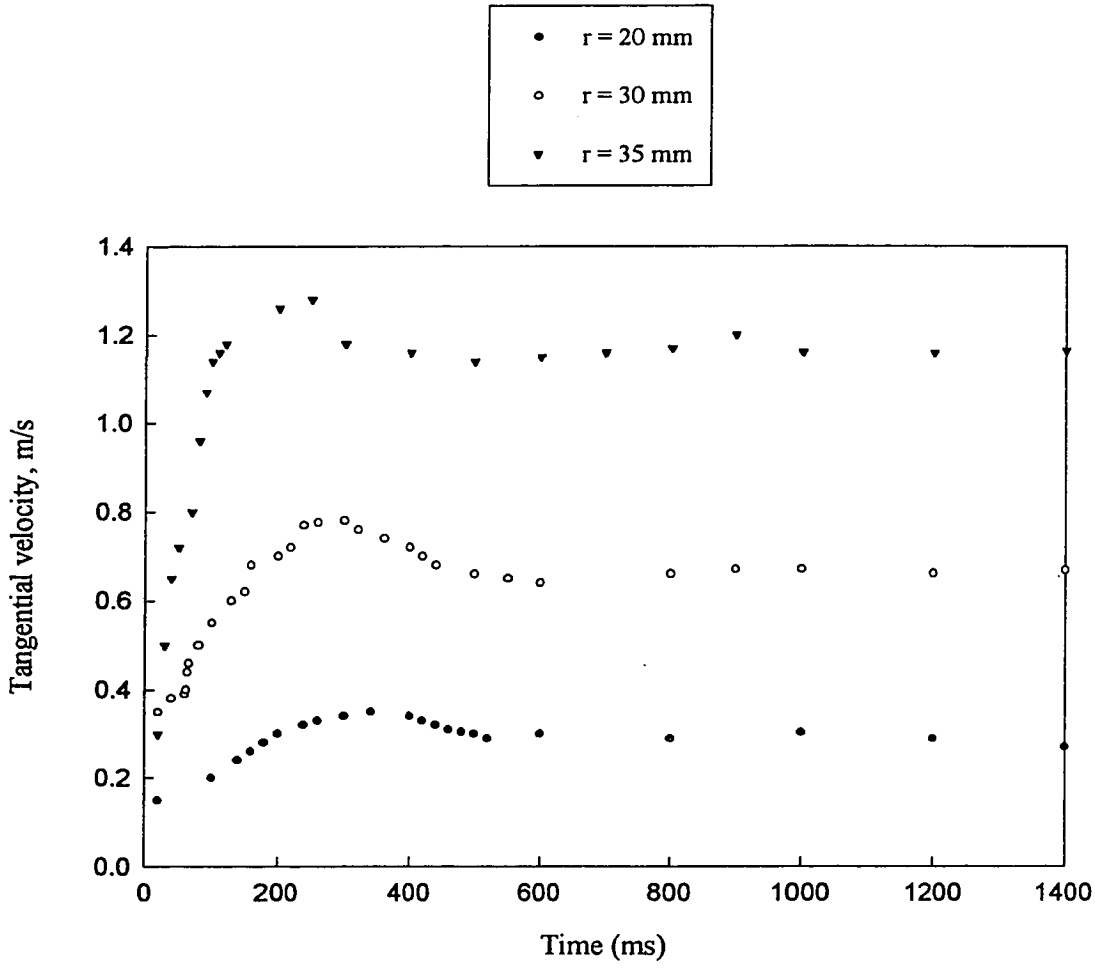

Figure 66. Velocity response of 1.5% CMC-H during accelerating phase at different radial locations; 350 rpm, 0.5 cm headspace, z= 8 mm, y = -15 mm

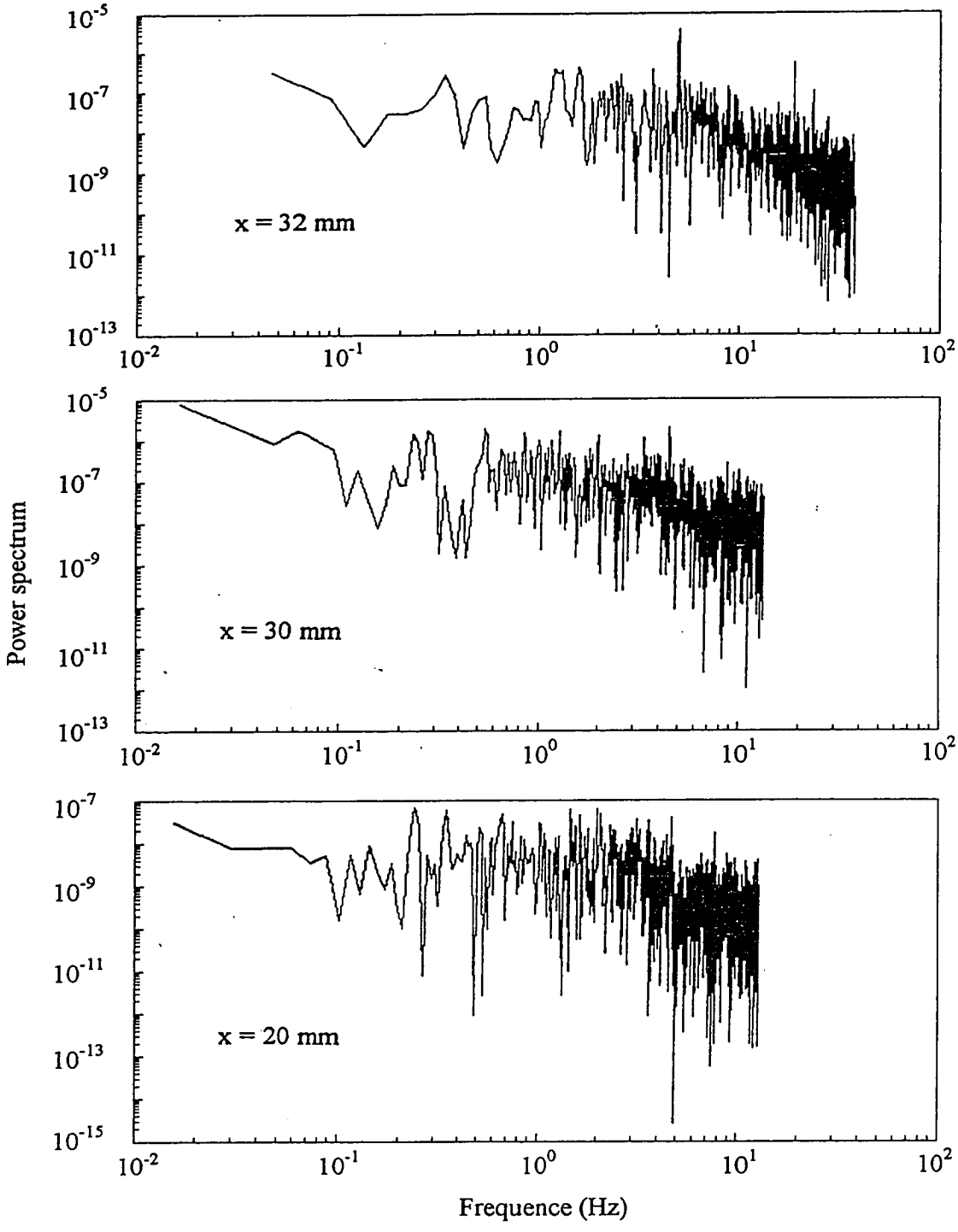

Figure 67. Power spectrum for horizontal velocity component of water in continuous rotation as a function of radial position; 300 rpm, 0.5 cm headspace, y = -15 mm

total energy of the eddies decreased toward the center indicating a decrease in the eddy size. In this case more kinetic energy was transferred to the eddies of the middle frequency range. More chaotic behavior was observed moving in the direction away from the wall towards the center of the container. This is consistent with the results of the turbulence intensity profiles presented in the previous sections.

4.8 Nature of Agitation

In order to predict whether flow was laminar or turbulent, it is necessary to explore the characteristics of the flow when it is laminar and turbulent. Experiments with many fluids in many systems have confirmed that the Reynolds number which is defined as the ratio of the inertial to viscous forces is able to characterize the transition from laminar to turbulent flow (Tritton, 1988). For instance, the flow of a fluid in circular pipe flow is always laminar at Reynolds numbers up to about 2000. However, a critical Reynolds number for axially rotating systems that distinguish between laminar and turbulent flow has not yet been defined. In fact, at even very small rotational velocities, the flow inside the cylinder was turbulent due to the oscillatory motion of the headspace bubble. However, a Reynolds number for this system, analogous to pipe flow, can be calculated assuming the velocity of the container being equal to the tangential velocity at the periphery of the cylinder. The fluid could then be assumed to be moving with the same tangential velocity as the wall of the cylinder. The Reynolds number based on the diameter of the cylinder may be written as:

$$Re = \frac{L_c V \rho}{\mu} \tag{77}$$

where L_c = characteristic length, which in this case is D, the cylinder diameter.

A linear tangential velocity profile has been found in axially rotating pipes in a range of Reynolds number of 600 to 1000 (Reich et al., 1989). A linear increase in tangential velocity for the same system was also observed with increasing rotational

Reynolds number which was also defined as in equation (77). Metzner (1956) defined the generalized Reynolds number for pseudoplastic fluids in pipeline flow (Gerhart and Gross, 1985):

$$GRe' = \frac{D^n V^{2-n} \rho}{8^{n-1} m \left(\frac{3n+1}{4n}\right)^n} \tag{78}$$

Since the velocity of the container may be written in terms of the diameter and speed of rotation, rotational generalised Reynolds number can be written from the above equation.

$$GRe = \frac{D_r^2 N^{2-n} \rho}{8^{n-1} m \left(\frac{3n+1}{4n}\right)^n} \tag{79}$$

Comparing equation (79) for non-Newtonian fluids with the rotational Reynolds number

$$Re = \frac{L_c^2 N \rho}{\mu} \tag{80}$$

for Newtonian liquids, the apparent viscosity term for non-Newtonian fluids can be written as:

$$\mu_a = \frac{m 8^{n-1}}{N^{1-n}} \left[\frac{3n+1}{4n}\right]^n \tag{81}$$

Thus, the apparent viscosity term becomes a function of n, m and N. The apparent viscosities may be used in calculating Reynolds number. The calculated rotational

Reynolds numbers for the liquids are given in Table 4.

Even though the rotational Reynolds numbers were small for non-Newtonian liquids and there are no Reynolds number values for laminar and turbulent flow characterization in partially filled rotating horizontal cylinders, flow could be considered as turbulent. Time-velocity diagrams showed oscillograms of velocity fluctuations, and they were irregular and non-periodic.

4.9 Relationship Between Turbulence Intensity and Rotational Reynolds Number

In order to generalize the results of this study, the parameters that have been measured should be presented in dimensionless form. For this reason, the turbulence intensity which is a direct measure of turbulent kinetic energy and mixing characteristics of the system was plotted against the rotational Reynolds number. Gavish et al. (1978) defined a Reynolds number, Re_g for axially rotating cylinders:

$$Re_g = \frac{\omega r_b^2}{\nu} \tag{82}$$

where r_b is the volume equivalent bubble radius calculated from the headspace measurements assuming that the bubble is spherical, ω is the rotational speed and ν is the kinematic viscosity. The kinematic viscosity of the non-Newtonian fluids, CMC and xanthan polymer were calculated from equation 81. Average radial and tangential turbulence intensities inside the container were plotted against Re_g.

As can be inferred from Equation 82, rotational Reynolds number is composed of all important parameters which characterize the hydrodynamics of the axially rotating systems. For each rotational Reynolds number, the turbulent intensity values were averaged over the measurement domain, representing an averaged mixing behavior at that Reynolds number rather than a spatial variance.

Table 4. Rotational Reynolds numbers for liquids used.

Solution	rpm	GRe
25% glycerol	200	64000
	300	96000
	350	112011
50% glycerol	200	23000
	300	34541
	350	40267
80% glycerol	200	2576
	300	3864
	350	4508
2% CMC-L	200	5573
	300	8397
	350	9808
2% CMC-M	200	1288
	300	2037
	350	2424
1.5% CMC-H	200	466
	300	780
	350	948
0.15% xanthan	200	6018
	300	11616
	350	14902
0.25% xanthan	200	4880
	300	9850
	350	12851

Figure 68 shows the variation of the tangential turbulence intensity with rotational Reynolds number for Newtonian liquids used in the experiments. Two different regions which show different behaviors can be identified in this figure. In the

first region, $0 < Re_g < 1000$, the tangential turbulence intensity increased strongly with increasing rotational Reynolds number. In the second region, $1000 < Re_g < 7000$, tangential turbulence intensity decreased slowly with increasing Re_g. Hence, increasing the Re_g in this region did not increase the tangential turbulence intensity.

Figure 69 shows the variation of the radial turbulence intensity with rotational Reynolds number for Newtonian liquids used in the experiments. In this figure, the effect of Re_g can be may be separated into two different regions. In the first region, $0 < Re_g < 1000$, the radial turbulent intensity increased very rapidly with increasing Re_g. In the second region, one can still observe an increase in radial turbulence intensity with increasing Re_g, but with reduced slope when compared to region I.

The turbulent intensities (TI) were correlated with Re_g, by employing least squares linear regression. For the Newtonian liquids, these correlations are

$$TI_{tangential} = 0.339\ Re_g \qquad (83)$$

for $0 < Re_g < 950$

$$TI_{tangential} = 148.80 - 3.64 \times 10^{-3}\ Re_g \qquad (84)$$

for $950 < Re_g < 7000$ $r^2 = 0.30$

$$TI_{radial} = 0.0468\ Re_g \qquad (85)$$

for $0 < Re_g < 950$

$$TI_{radial} = 28.43 + 1.39 \times 10^{-3}\ Re_g \qquad (86)$$

for $950 < Re_g < 7000$ $r^2 = 0.72$

Figure 70 shows the variation of tangential turbulence intensity with Re_g for non-Newtonian fluids. Figure 70 also indicates two different regions where increases in tangential turbulence intensity can be correlated with two different equations as shown below:

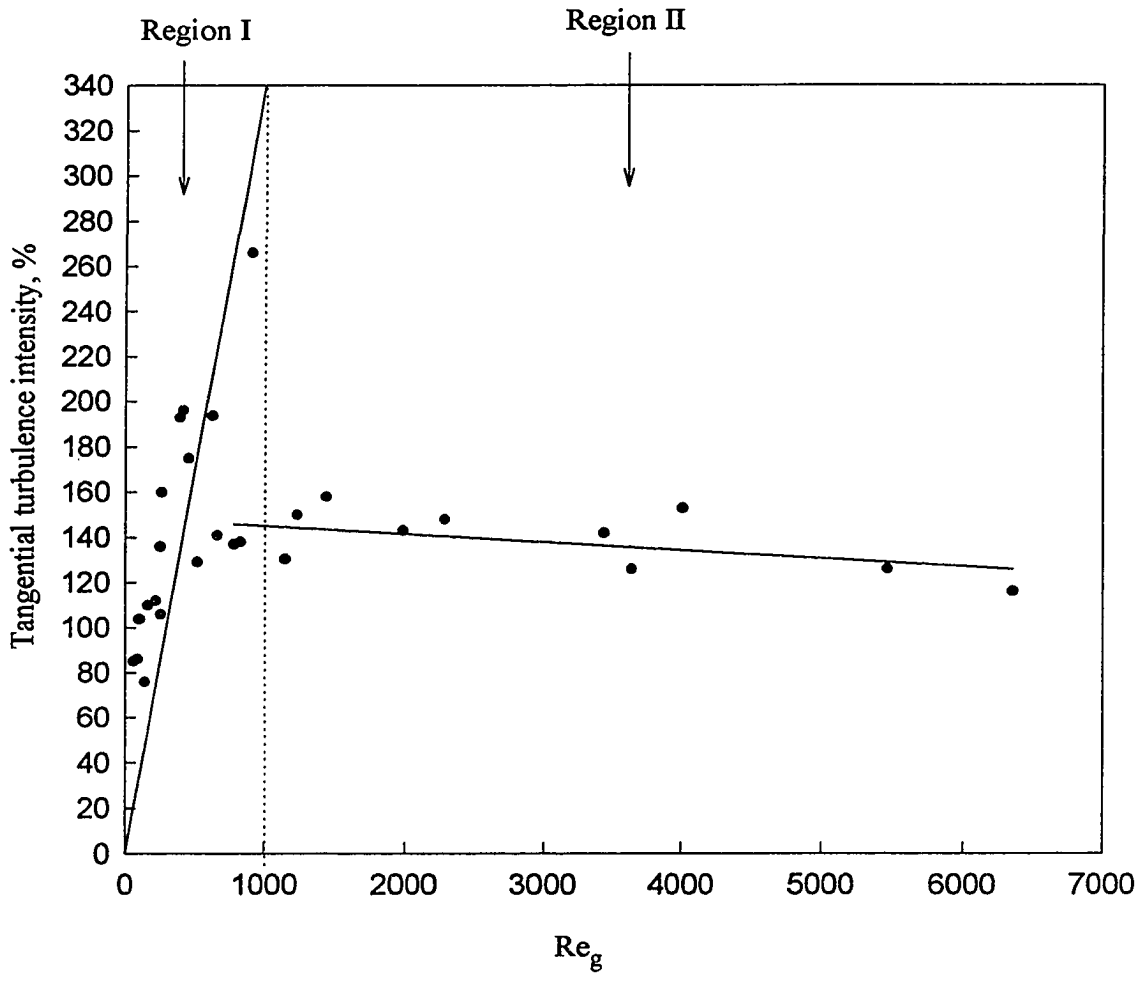

Figure 68. Effect of rotational Reynolds number on tangential turbulence intensity for Newtonian liquids.

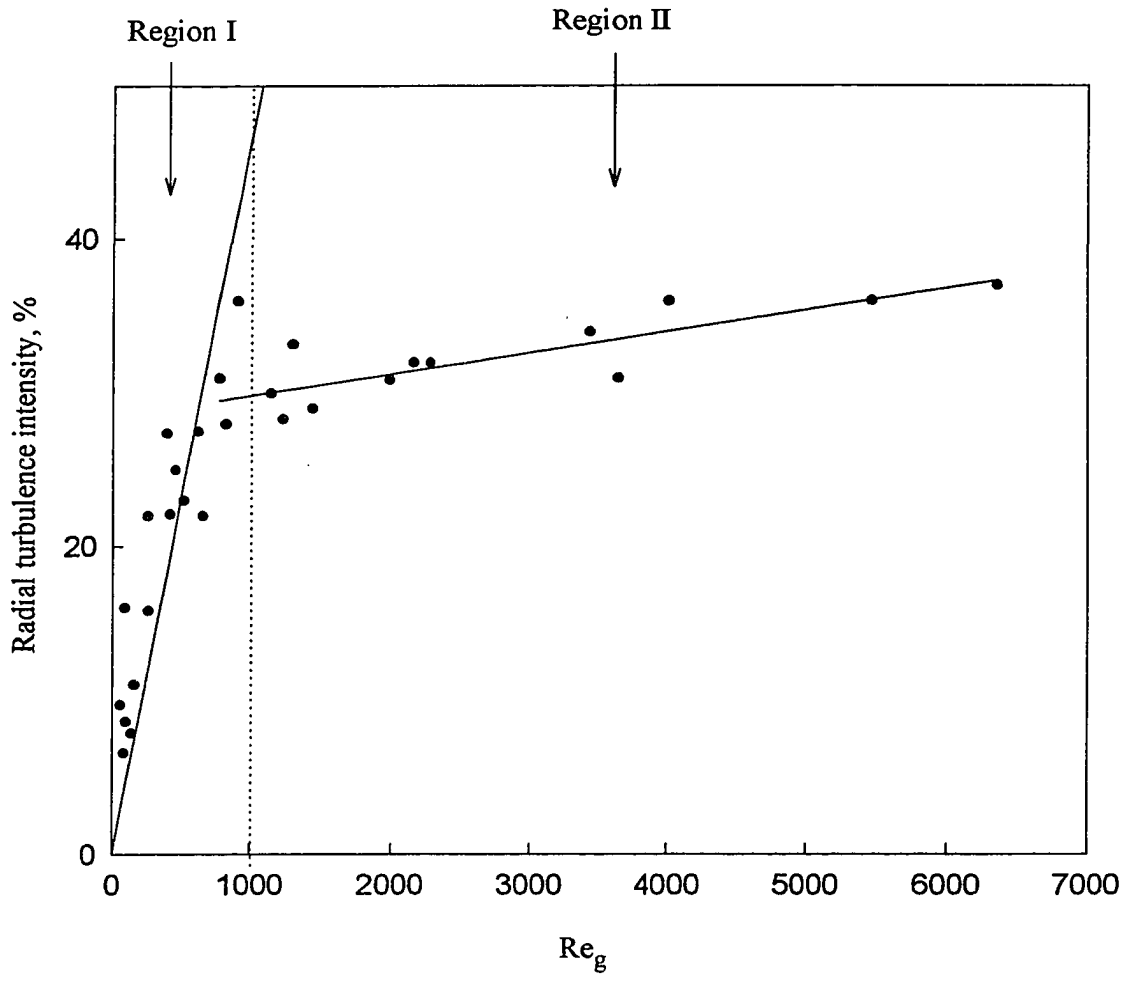

Figure 69. Effect of rotational Reynolds number on radial turbulence intensity for Newtonian liquids.

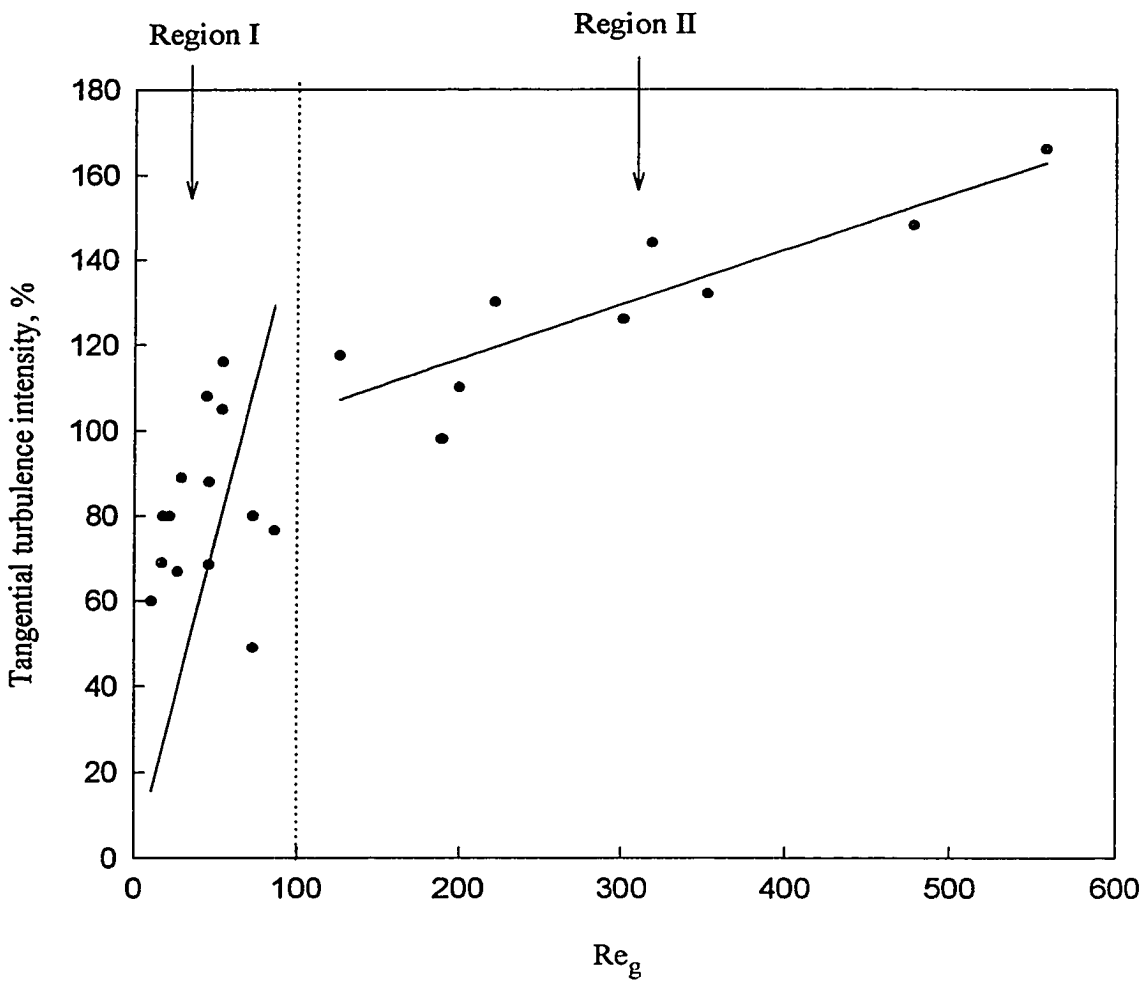

Figure 70. Effect of rotational Reynolds number on tangential turbulence intensity for non-Newtonian liquids.

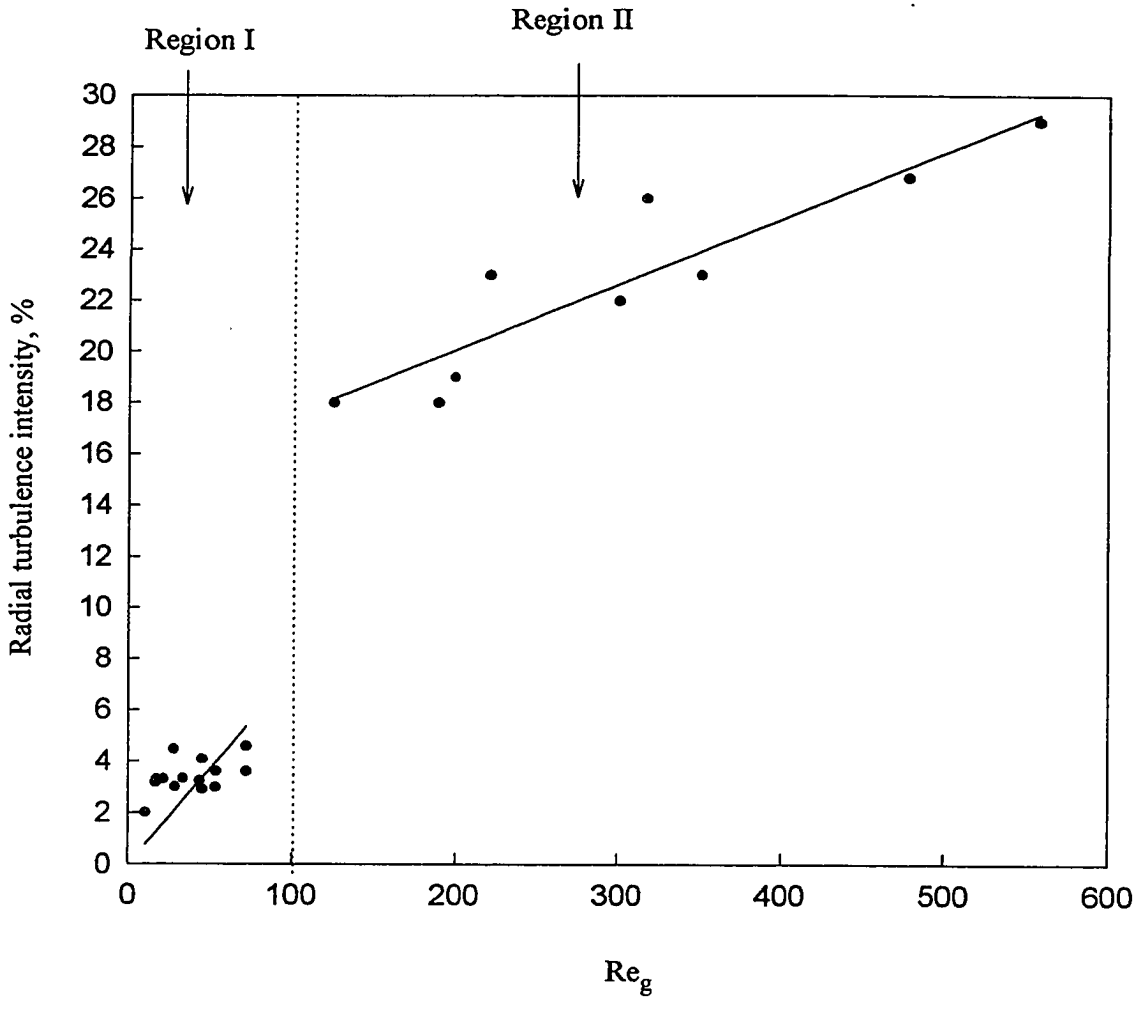

Figure 71. Effect of rotational Reynolds number on radial turbulence intensity for non-Newtonian liquids.

$$TI_{tangential} = 1.497\ Re_g \quad \text{for } 0 < Re_g < 100 \tag{87}$$

$$TI_{tangential} = 90.99 + 0.128\ Re_g \quad \text{for } 100 < Re_g < 600 \quad r^2 = 0.77 \tag{88}$$

The correlation of radial turbulence intensity and Re_g for non-Newtonian fluids was computed and shown below:

$$TI_{radiall} = 0.0729\ Re_g \quad \text{for } 0 < Re_g < 100 \tag{89}$$

$$TI_{radial} = 14.91 + 0.026\ Re_g \quad \text{for } 100 < Re_g < 600 \quad r^2 = 0.84 \tag{90}$$

For non-Newtonian liquids, increasing Re_g increased the tangential turbulence intensity in both regions but with a smaller slope in the second region, $100 < Re_g < 600$ when compared to the first region $0 < Re_g < 100$.

The same analyses were also carried out for the experiments obtained from stop-go runs. Similar trends were observed with higher turbulence intensity values as compared to the continuous rotational mode. Figure 72 shows the variation of the tangential turbulence intensity with rotational Reynolds number for Newtonian liquids used in the experiments. As in the case of the continuous rotational mode, two different regions which show different behaviors can be identified in this figure. In the first region, $0 < Re_g < 1000$, the tangential turbulence intensity increased linearly with increasing rotational Reynolds number. In the second region, $1000 < Re_g < 7000$, one can still observe an increase in the tangential turbulence intensity but with a lower slope as the rotational Reynolds number increases. Figure 73 shows the variation of the radial

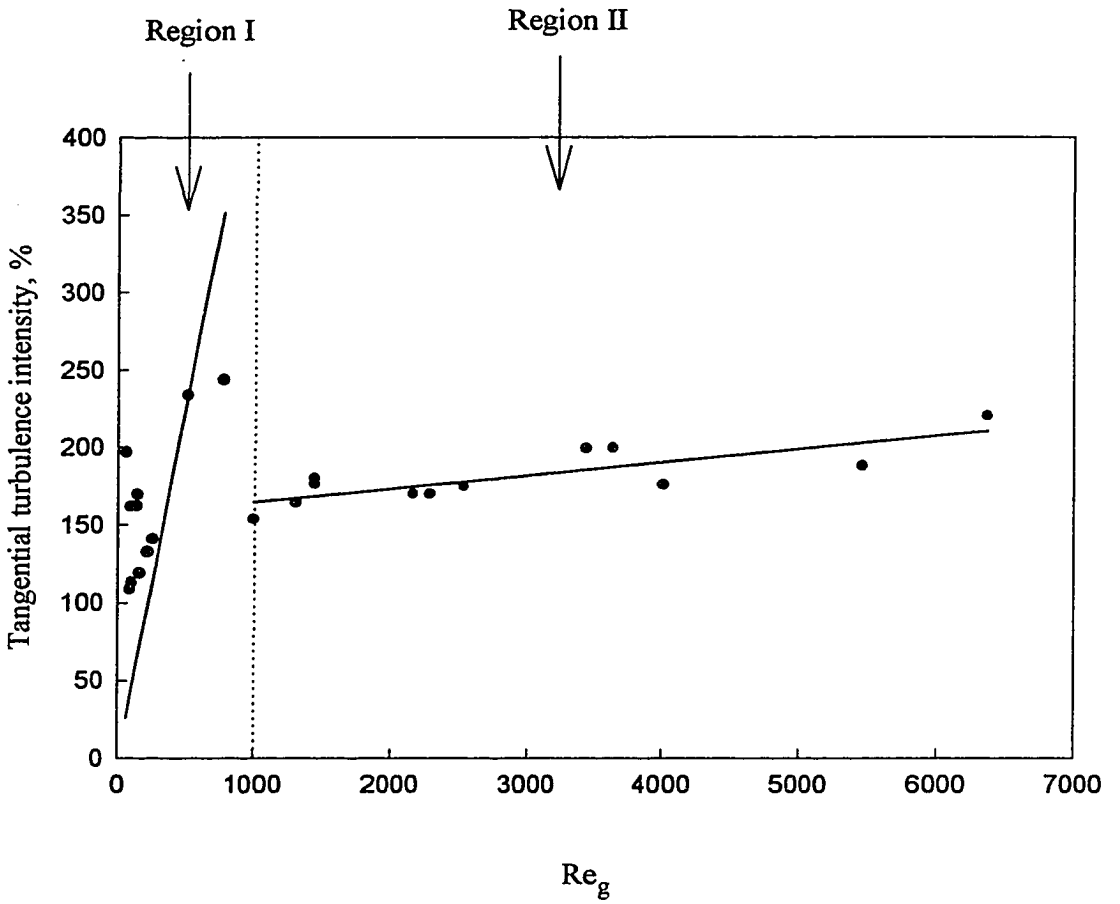

Figure 72. Effect of rotational Reynolds number on tangential turbulence intensity for Newtonian liquids in Steritort simulation.

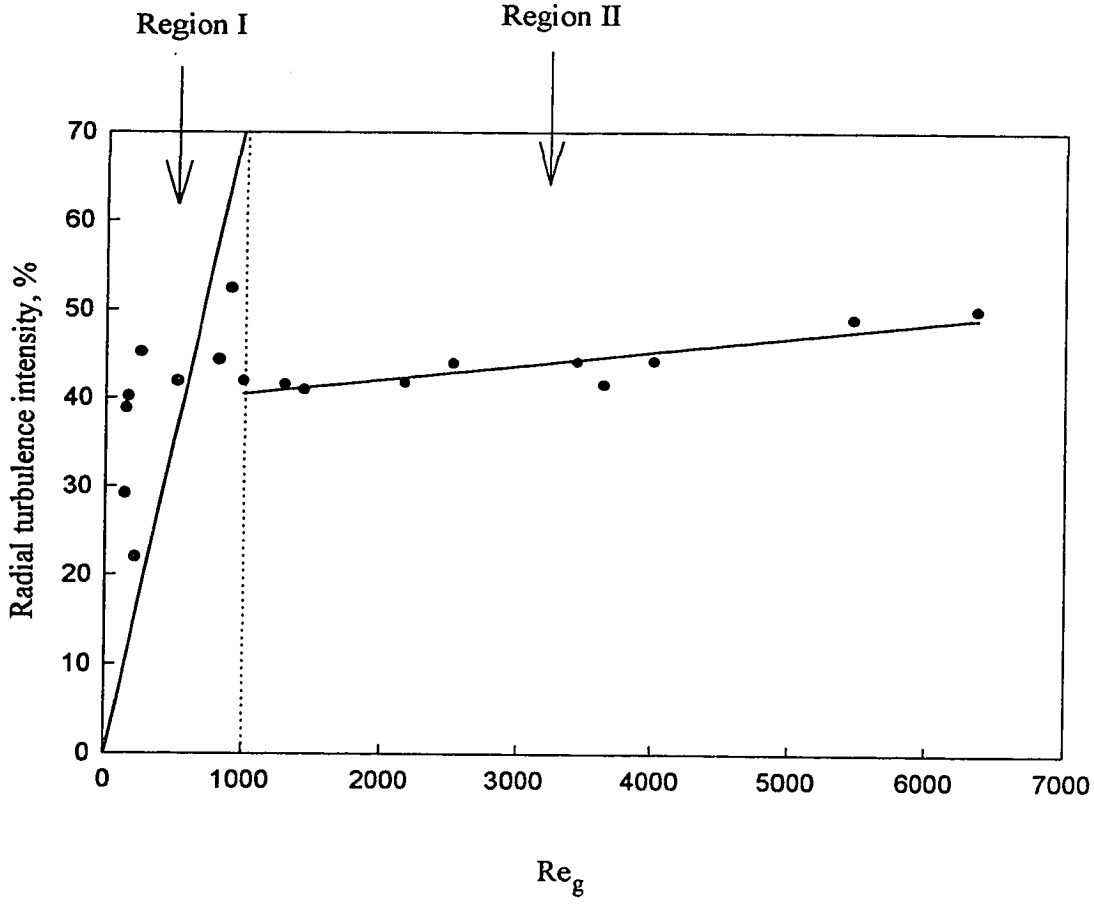

Figure 73. Effect of rotational Reynolds number on radial turbulence intensity for Newtonian liquids in Steritort simulation.

turbulence intensity with rotational Reynolds number for Newtonian liquids which exhibited the same "two-region" pattern as the previous graph. Turbulence intensities were correlated to rotational Reynolds number by employing a linear regression. These correlations are:

$$TI_{tangential} = 0.451\ Re_g \quad \text{for } 0 < Re_g < 950 \tag{91}$$

$$TI_{tangential} = 156.16 + 8.52 \times 10^{-3}\ Re_g \quad \text{for } 950 < Re_g < 7000 \quad r^2 = 0.65 \tag{92}$$

$$TI_{radial} = 0.0709\ Re_g \quad \text{for } 0 < Re_g < 950 \tag{93}$$

$$TI_{radial} = 38.97 + 1.58 \times 10^{-3}\ Re_g \quad \text{for } 950 < Re_g < 7000 \quad r^2 = 0.80 \tag{94}$$

Figures 74 and 75 show the variation of tangential and radial turbulent intensities with rotational Reynolds number for non-Newtonian liquids used in stop-go motion, respectively. The "two-region" behavior is also present in these two figures. In the first region, $0 < Re_g < 100$, both tangential and radial turbulent intensities increased very steeply with increasing rotational Reynolds number. In the second region $100 < Re_g < 600$, both radial and tangential turbulent intensities increased slightly with rotational Reynolds number. The correlations obtained from linear regression analyses are presented below:

$$TI_{tangential} = 2.61\ Re_g \quad \text{for } 0 < Re_g < 100 \tag{95}$$

$$TI_{tangential} = 129.8 + 0.07588\ Re_g \quad \text{for } 100 < Re_g < 600 \quad r^2 = 0.66 \tag{96}$$

$$TI_{radial} = 0.723\ Re_g \quad \text{for } 0 < Re_g < 100 \tag{97}$$

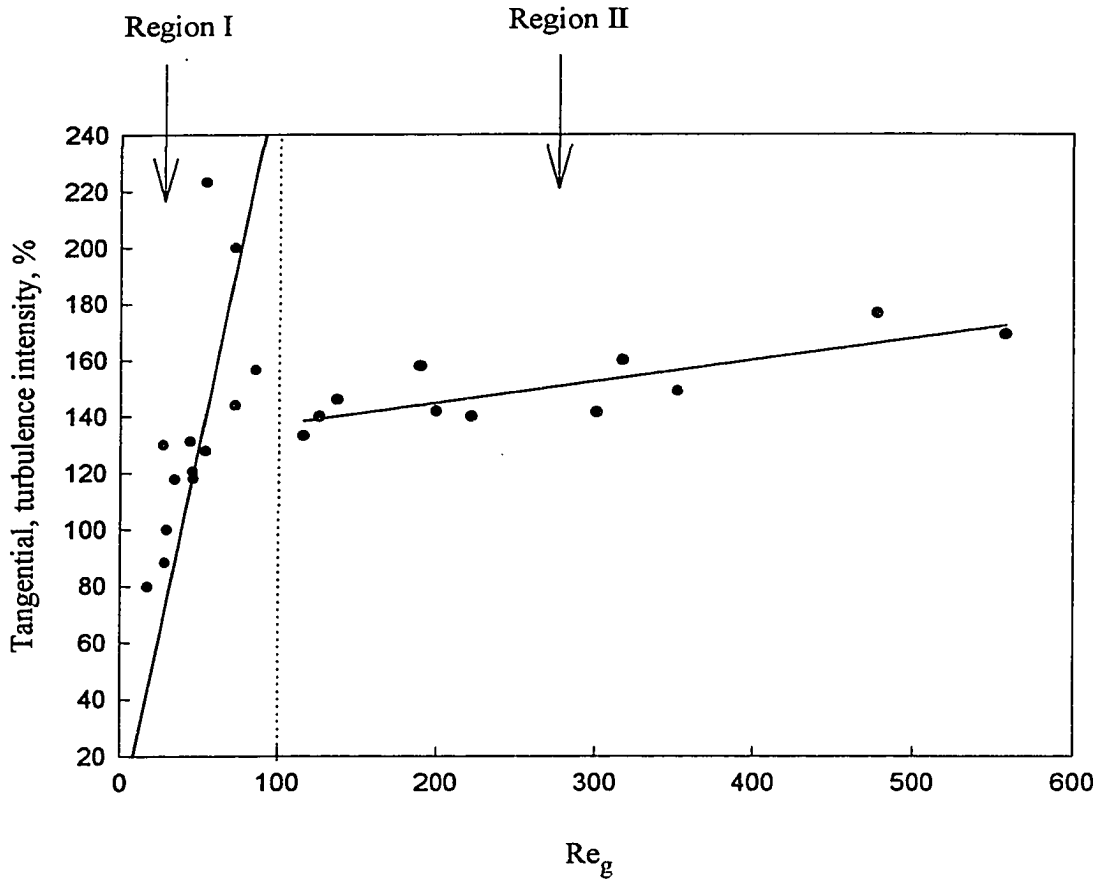

Figure 74. Effect of rotational Reynolds number on tangential turbulence intensity for non-Newtonian liquids in Steritort simulation.

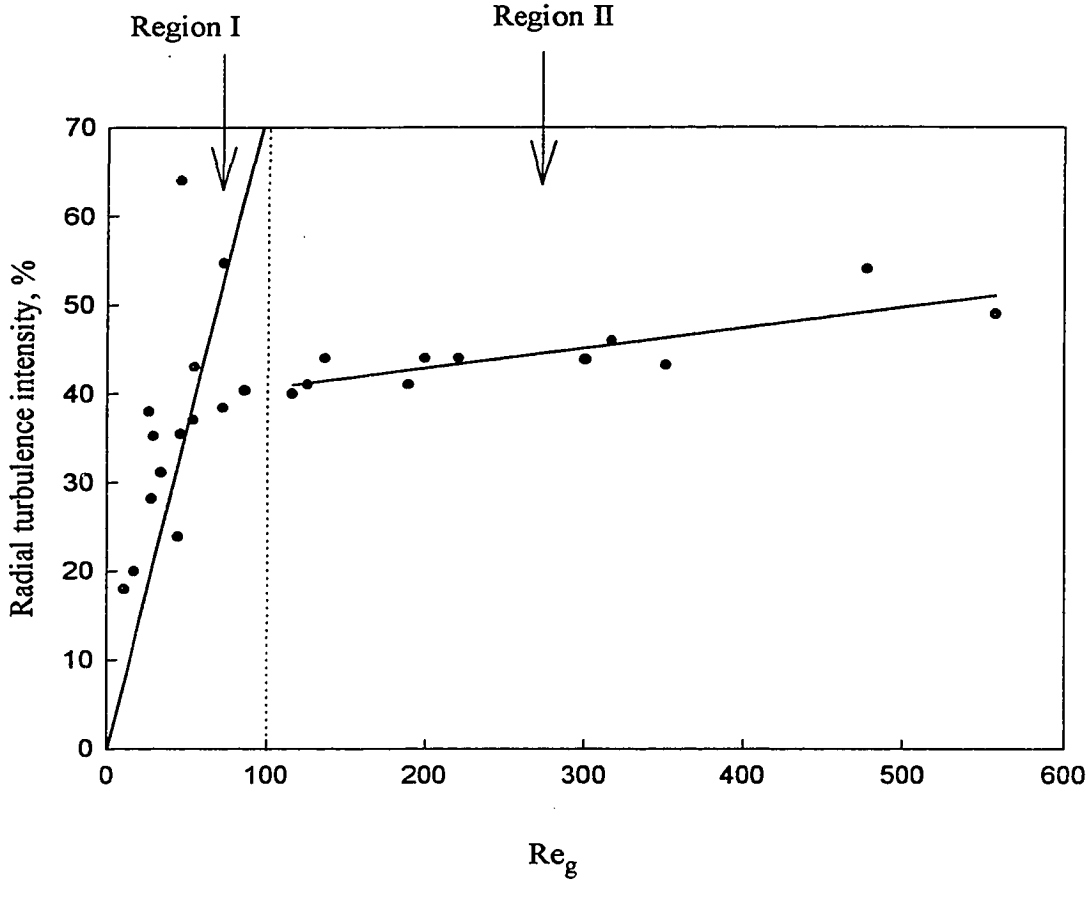

Figure 75. Effect of rotational Reynolds number on radial turbulence intensity for non-Newtonian liquids in Steritort simulation.

$$TI_{radial} = 38.35 + 0.0227\,Re_g \qquad (98)$$

$$\text{for } 100 < Re_g < 600 \quad r^2 = 0.68$$

Similar conclusions were obtained by Anantheswaran and Rao (1985b) for end-over-end agitation systems. The increase in the Reynolds number due to the increase in velocity was found to be greater for non-Newtonian fluids than Newtonian fluids. They stated that low speeds did not improve internal agitation when very viscous fluids were heated because the headspace bubble travelled in a path close to the wall, resulting in poor mixing.

From the above graphs and analyses, the following conclusions can be reached.

a) The turbulent intensity variation with the rotational Reynolds number shows similar trends for Newtonian and non-Newtonian liquids used in the experiments. Two different regions can be identified: one showing a sharp increase in turbulence intensity with increasing rotational Reynolds number, and another that showed a smaller or no increase with rotational Reynolds numbers, and

b) The radial component of turbulence intensity was more sensitive to the change in the rotational Reynolds number than the tangential component for the continuous case. For Newtonian liquids, the increase in the tangential component was limited to the low Re_g region ($0 < Re_g < 1000$). This tendency did not bring any consequences as far as mixing was concerned. Since the tangential turbulence intensity values were one order of magnitude higher than radial turbulence intensity values for both Newtonian and non-Newtonian liquids, this indicated that the major portion of the turbulent kinetic energy came from the tangential component and was dissipated. Hence, mixing in the radial direction should be the main concern in axially rotating cylindrical systems and can be increased by increasing the rotational Re_g.

Although the scope of this study did not cover the heat transfer analysis in axially rotating systems, the above findings show that the turbulent transport of energy as well as momentum may increase with increasing Re_g, especially in the radial direction, leading to a more uniform temperature distribution inside the container.

4.10. Comparison of Continuous and Stop-go Systems

This section compares the results of continuous and stop-go rotation systems for Newtonian and non-Newtonian fluids. Figures 76 and 77 show the Cartesian component of the velocity along the radial direction for continuous and stop-go rotation systems. For both Newtonian and non-Newtonian fluids both x (horizontal) and y (vertical) components of the mean velocity were greater, hence, the resultant velocity for continuous rotation were higher than those for stop- go rotation as the system reached a steady-state in the continuous case. When the container experienced sudden accelerations and decelerations in the stop-go case, the result was lower mean velocities. For water, the differences in the mean velocities were more pronounced due to its low viscosity (Figure 76). With increasing viscosity, the viscous forces became more and more effective, thereby suppressing the effect of inertial forces due to sudden acceleration and deceleration. Thus, the difference in the mean velocities of the continuous and stop-go runs decreased as the viscosity was increased, especially in the center of the cylinder. In the near wall region, the difference was higher when compared to the central region as the fluid in that region experienced the acceleration and deceleration first.

Figures 78 and 79 present the effect of stop-go rotation on the turbulence intensities for water and xanthan polymer. For all of the fluids tested, the turbulence intensities for the stop-go operation were found to be larger than those of the continuous mode. When the simulation system was run in the stop-go mode, extra inertial forces arose due to acceleration and deceleration periods, which, in turn increased the velocity fluctuations. This increase suggested that the local mixing behavior was enhanced.

4.11. Statistical Analyses

Effects of different factors and interaction effects on velocity components were analyzed by analysis of variance. Concentration, rotational speed, amount of headspace, and their interactions were significant ($p<0.05$) influences on tangential and radial

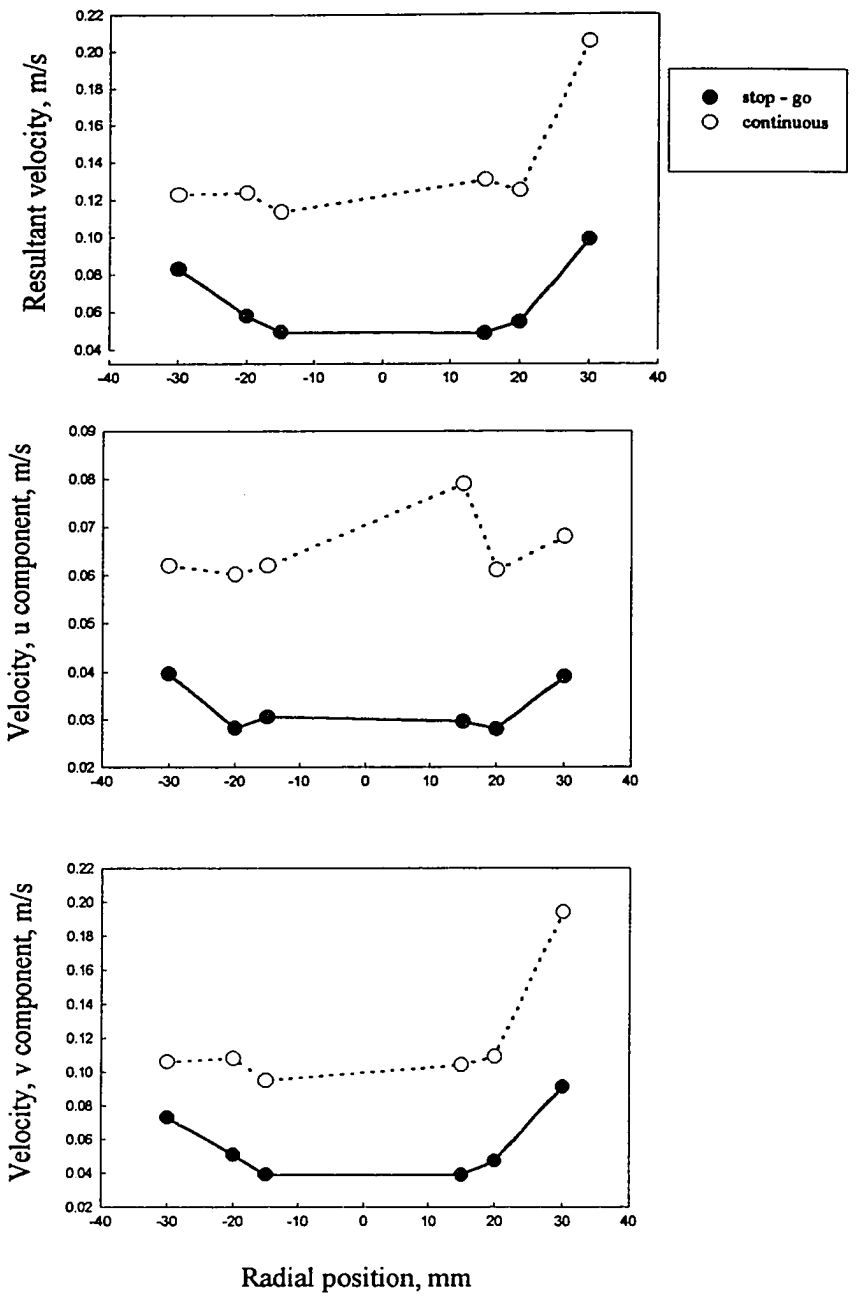

Figure 76. Comparison of velocities of continuous and Steritort™ simulation for water; 200 rpm. 0.25 cm headspace, y = -10 mm

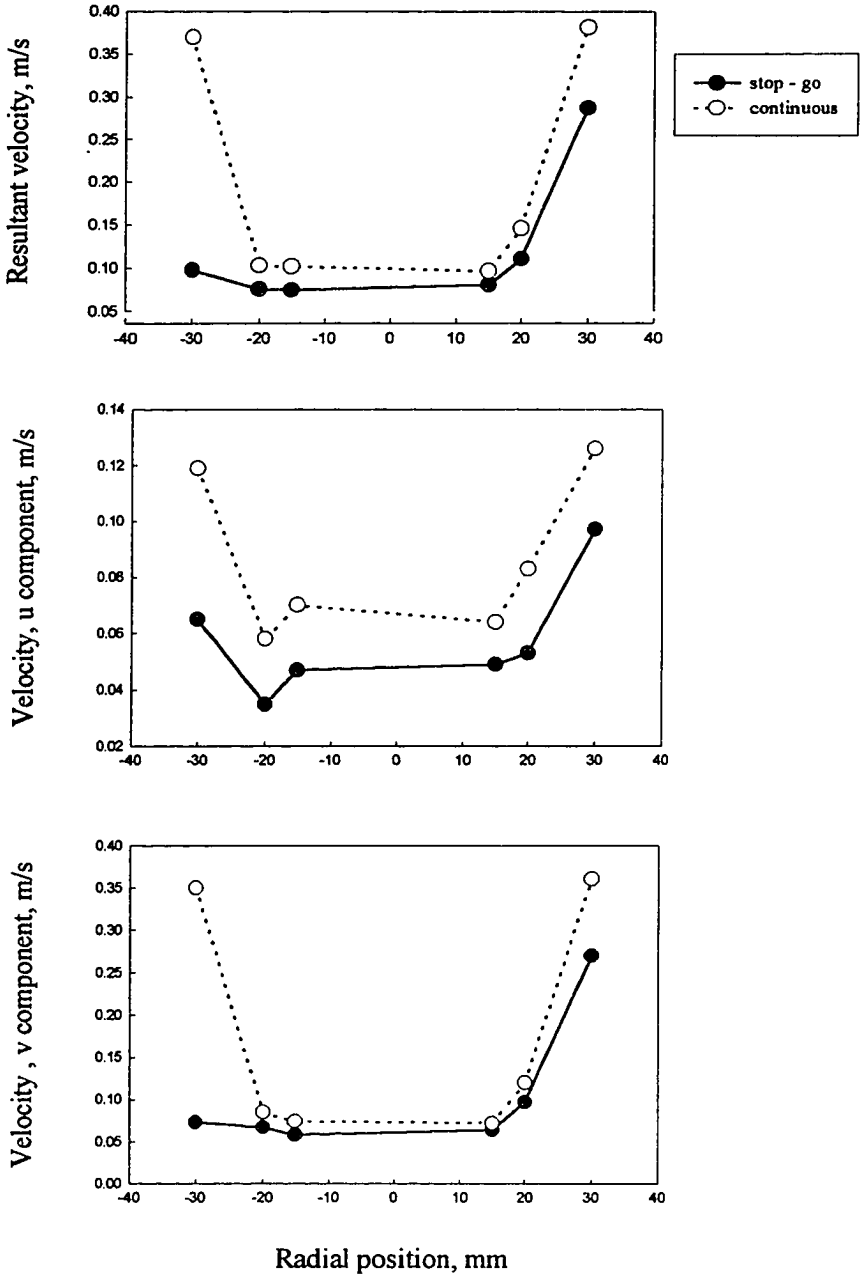

Figure 77. Comparison of velocities of continuous and Steritort™ simulation for 0.15% xanthan polymer; 200 rpm, 0.25 cm, y = -10 mm

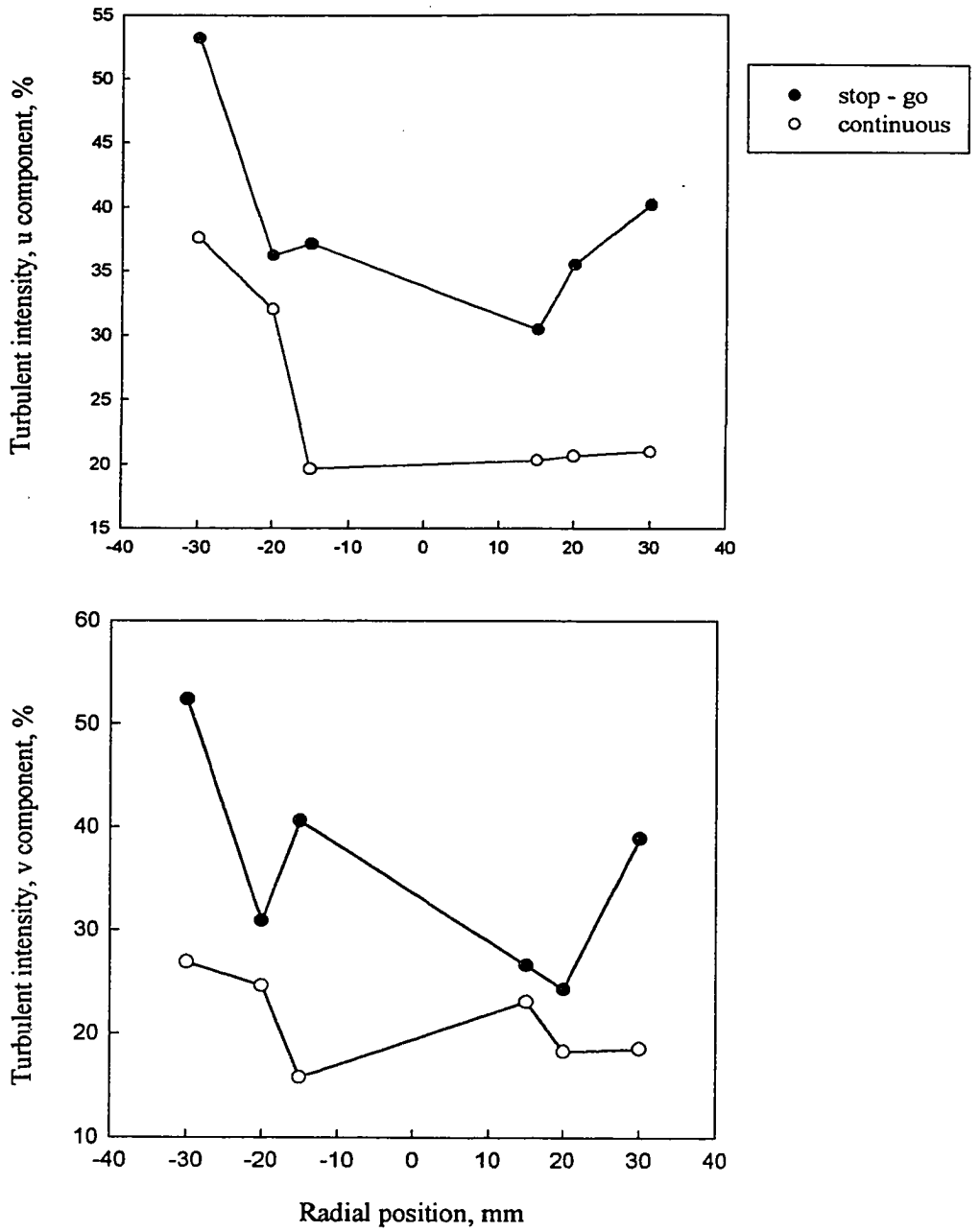

Figure 78. Comparison of turbulence intensities of continuous and Steritort™ (stop-go) simulation for water; 200 rpm, 0.25 cm headspace, y = -10 mm

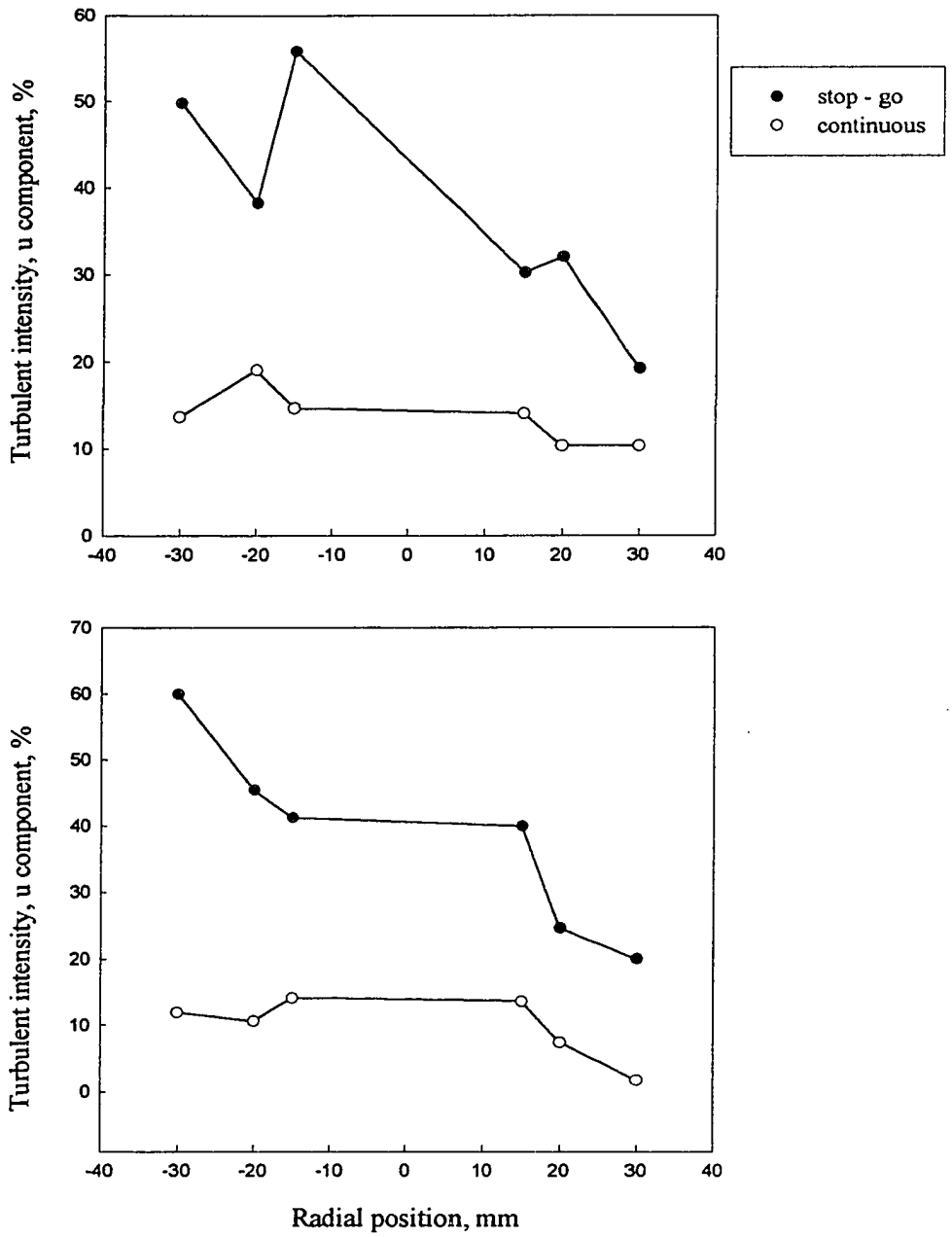

Figure 79. Comparison of turbulence intensities of continuous and Steritort™ simulation for 0.15% xanthan polymer; 200 rpm, 0.25 cm, y = -10 mm

velocity components depending upon the region. These findings are summarized in Table 5. Newtonian and non-Newtonian liquids showed different responses depending upon the region. The radial velocity component of water in region I (see Figure 9) was not significantly affected by the rotational speed; instead, the headspace volume and its interaction with rotational speed were important. The tangential component of the velocity of water was not affected by these two factors in other regions. However, the radial component of the velocity of water in those regions was affected by these two factors and their interactions. Experiments showed that rotational speed did not change the pattern of measured tangential and radial velocities along radial direction.

The radial components of velocity for both glycerol and CMC solutions were significantly ($p<0.05$) affected by all three factors and their interactions. Tangential velocity component of CMC solutions in all regions were not significantly affected by any of the experimental all factors or their interactions. Concentration and its interactions with other factors were significant for the tangential component of velocity for glycerol solution in all regions.

4.12. Relating heat transfer for the systems studied

It is widely accepted that energy in turbulent flows is transported quickly from one place to another by virtue of the eddy activity. However, very close to the wall eddy activity may become negligible. Rapid and random movement of eddies results in rapid transport of energy. Therefore, it is always desirable to have some physical information about flow phenomena to develop a model or calculate the heat transfer to a system.

It is difficult to relate the results of the present study with heat transfer without having temperature profile data for the same system. The velocity gradient was high for Newtonian systems near the wall of the rotating cylinder. We may say that heat transfer would be high in that region due to the high momentum exchange. The velocity gradient in the core was found to be low, hence heat transfer would be small. Increasing concentration slightly improved the velocity gradient, however a small change in the turbulent intensity gradient were observed. In future research, to develop a heat transfer

Table 5. Main effects and interactions for different factors on radial and tangential velocities at different locations inside the cylinder.

	X Y	Water	Glycerol	CMC
R	10 30	d, Nd[1]	all	all
T		all	c, cN[2]	none
R	10 20	Nd	all	all
T		all	c	none
R	10 15	d	c, N, cN, cd, cNd	all
T		none	c, N, d, cNd	none
R	-10 -30	d	all	all
T		d	c,N d, cNd	none
R	-10 -15	Nd	all	(all[3] except cNd)
T		d, Nd	c, Nd, cNd	c, cd[4], Nd, cNd
R	-10 20	d	all	all
T		none	c, Nd	c, cd, Nd, cNd
R	10 30	all	all	all
T		none	cd	none
R	-20 27	all	all	c, N, cd
T		none	cd	none
R	-30 15	all	all	c, N
T		none	N, cN, Nd, cNd	none

where c = concentration, N = rotational speed, d = amount of headspace, R = radial velocity component, T = tangential velocity component, X = axis, Y= abscissa.

[1] Nd shows the interaction between rotational speed and headspace

[2] cN shows the interaction between concentration and rotational speed

[3] All shows the all factors and their interactions

[4] cd shows the interaction between concentration and headspace

correlation equation for Steritort™ type retorts, the effect of natural convection should be added. Since the can rotates about its own axis only during about one-third of a complete rotation, natural convection will be important during the other part of the rotational cycle. This is indicated by time-velocity profiles obtained for several systems studied. By looking at those time-velocity histograms, especially for highly viscous systems, one can say that the contents of the container have little mixing, hence little forced convection takes place.

4.13. Conclusions and Recommendations

LDV measurements have provided information on the velocity characteristics of fluid flow in horizontal axially rotated partially-filled cylinders in two different systems. These findings can be used to provide detailed insight into the flow characteristics of Newtonian and non-Newtonian liquids. To the author's knowledge, this kind of information has not been mentioned in any existing work.

The main conclusions from these studies are as follows:

a) Two main regions of flow were distinguished. The first region was close to the container wall where viscous forces were predominant. The second region covered the large volume throughout the middle of the cylinder and variation of velocity of liquid inside the cylinder location and time was mostly influenced by gravitational and inertial (centrifugal) forces,
b) The turbulence is anisotropic, since all statistical properties and all scales of the motion were independent of the direction, such as intensities of the tangential and turbulence were not equal at a measuring point,
c) With the cylinder rotating, the standard deviations of tangential velocity component were more than 20% of the mean velocity. On the other hand, the standard deviation of the radial component of the velocity was much lower than that of the tangential component,

d) Tangential velocity fluctuations were more important than radial velocity fluctuations for better mixing,

e) Increasing rotational speed increased the mean velocities and turbulence intensities,

f) Increasing headspace, usually improved mixing and caused more random motion in some systems,

g) An increase in the apparent viscosity of fluids significantly suppressed turbulence inside the cylindrical container by decreasing both radial and tangential turbulence intensities,

h) The radial component of velocity at different locations was significantly affected by the different factors studied (concentration, rotational speed and amount of headspace, and their interactions). The tangential component of velocity showed different responses at different locations,

i) Time-velocity plots displayed periodic fluctuations which may be attributed to inherent features of the liquid motion,

j) Distribution of the Reynold stress and correlation coefficient were not greatly affected by rotational speeds or changing headspaces,

k) The mixing characteristics of the system were correlated with rotational Reynolds number which comprised all the parameters relating the hydrodynamics of flow inside the container,

l) The results showed that mixing in the system can be characterized in two different regions, a low rotational Reynolds number region in which the mixing in both radial and axial direction increased very sharply with increasing rotational Reynolds number, and the other region in which mixing was slightly improved or unaffected by the increase in rotational Reynolds number,

m) Velocity has three components in x, y and z directions. It would be highly desirable to measure 3-components using frequency shifters. This would require a three-component LDV system,

n) It would also be interesting to study the effect of can aspect ratio for similar systems, since the aspect ratio may affect the flow patterns in the container,

o) It would further be interesting to use the LDV to measure the flow at different conditions especially in a wide range of rotational speeds to find and define the critical Reynolds number (if it exists) for transition from laminar to turbulent flow,

p) A heat transfer study could be carried out on the same cylinder to get the temperature distribution and find out a heat transfer correlation using available velocity data. Data would also serve as a database for comparison of the solution of the three-dimensional transport equations (mass, momentum and energy).

REFERENCES

Anantheswaran, R.C. 1984. Heat penetration to model fluid foods in cans during end-over-end rotation. Ph.D. thesis. Cornell University, Geneva, NY.

Anantheswaran, R.C. and Rao, M.A. 1985a. Heat transfer to model Newtonian liquids foods in cans during end over end rotation. J. Food Eng. 4:1-19.

Anantheswaran, R.C. and Rao, M.A. 1985b. Heat transfer to model non-Newtonian liquid foods in cans during end-over-end rotation. J. Food Eng. 4:21-35.

Arpaci, V.S. and Larsen, P.S. 1984. Convection Heat Transfer. Prentice-Hall, Inc., Englewood Cliffs, NJ.

Ball, C.O. and Olson, F.C.W. 1957. Sterilization in Food Technology, McGraw-Hill Book Co., Inc., New York, NY.

Bagley, E.B. and Christianson, D.D. 1982. Swelling capacity of starch and its relationship to suspension viscosity-effect of cooking time, temperature and concentration. J. Texture Studies 13:115-126.

Berry, M. R., Savage, R. A. and Pflug, I.J. 1979. Heating characteristics of cream-style corn processed in a Steritort: Effects of headspace, reel speed and consistency. J. Food Sci. 44:831-835.

Berry, M.R. and Dickerson, R.W. 1981. Heating characteristics of whole kernel corn processed in a Steritort. J. Food Sci. 46:889-895.

Berry, M.R. and Bradshaw, J.G. 1982. Heat penetration for sliced mushrooms in brine processed in still and agitating retorts with comparisons to spore count reduction. J. Food Sci. 47:1698-1704.

Berry, M.R., Bradshaw, J.G. and Kohnhorst, A.L. 1985. Heating characteristics of ravioli in brine and in tomato sauce processed in agitating retorts. J. Food Sci. 50:815-822.

Blaisdel, J. L. 1963. Natural convection heating of liquids in un-agitated food containers. Ph.D. thesis. Michigan State University, East Lansing, MI.

Cannon, J.N. and Kays, W.M. 1969. Heat transfer to a fluid flowing inside a pipe rotating about its longitudinal axis. J. Heat Trans. 91:135-139.

Carslaw, H.S. and Jaeger, J.C. 1959. Conduction of Heat in Solids. 2nd ed. Clarendon Press, Oxford, GBR.

Chandrasekaran, M., Marcroff, M., Bakalis, S. and Karwe, M.V. 1997. Application of Laser Doppler Anemometry in understanding food processing operations. Trends Food Sci. Technol. 8:369-375.

Chang, S.Y. and Toledo, R.T. 1989. Heat transfer and simulated sterilization of particulate solids in a continuously flowing system. J. Food Sci. 54:1017-1023,1030.

Chen, C.J. and Jaw, S.Y. 1998. Fundamentals of turbulence modelling. Taylor and Francis Publishers, Washington. DC.

Cheng, R. K. and Ng, T. T. 1983. Velocity statistics in premixed flames. Combustion and Flame 52: 185-202.

Christiansen, E.B. and Craig, S.E. 1962. Heat transfer to pseudoplastic fluids in laminar flow. A.I.Ch.E.J. 8:154-160.

Clifcorn, L.E., Peterson, G.T., Boyd, J.M. and O'Neil, J.H. 1950. A new principle for agitating in processing of canned foods. Food Technol. 4(11):450-460.

Conley, W., Kaap, L. and Schuhmann, L. 1951. The application of end over end agitation to the heating and cooling of canned food products. J. Food Technol.5:457-460.

de Ruyter, P.W. and Brunet, R. 1973. Estimation of process conditions for continuous sterilization of foods containing particulates. Food Technol. 27 (7):44-46,48,50-51.

Drain, L.E. 1980. The Laser Doppler Technique. John Wiley and Sons, New York, NY.
Duquenoy, A. 1980. Heat transfer to canned liquids. Proc. of 2nd Int. Congress Eng. Food and 8th European food symposium held at Helsinki, Finland. Applied Sci. Pub. Essex, GBR.1:483-489.

Durst, F., Melling, A. and Whitelaw, J. H. 1981. Principles and Practices of Laser Doppler Anemometry, Academic Press, New York, NY.

Eisner, M. 1988. Introduction into the Technique and Technology of Rotary Sterilization. Private Author's Edition, Milwaukee, WI.

Elder, R.L. and Forster, C.P. 1984. Laser Anemometry for flow measurement in small centrifugal compressors. Second International Symposium on Applications of Laser Anemometry to Fluid Mechanics. Lisbon, PRT. July 2-5.

Elias, C.B., Desai, R.B., Patole, M.S., Joshi,J.B. and Mashelkar, R.A. 1995. Turbulent shear stress effect on mammalian cell culture and measurement using Laser Doppler Anemometer. Chem. Eng. Sci. 50:2431-2437.

Fagerson, I.S. and Esselen, W.B. 1950. Heat transfer in commercial glass containers during thermal processing. Food Technol. 4:411-415.

Gavish, J., Chadwick, R.S., and Gutfinger, C. 1978. Viscous flow in a partially filled rotating horizontal cylinder. Israel J. Technol. 16:264-272.

Gerhart, P.M. and Gross, R.J. 1985. Fundamentals of Fluid Mechanics. Addison-Wesley Publishing Co. Reading, GBR.

Goldstein, R.J. and Adrian, R.J. 1971. Measurements of fluid velocity and gradient using laser Doppler techniques. Rev. Sci. Instrum.42:1317-1320.

Greenspan , H.P. 1976. On a rotational flow distributed by gravity. J. Fluid Mech.104: 335-351.

Hassan, B.H. 1984. Heat transfer coefficients for particles in liquid in axially rotating cans. Ph.D. thesis. University of California, Davis, CA.

Hiddink, J. 1975. Natural convection heating of liquids, with reference to sterilization of canned food. Center for Agricultural Publishing and Documentation, Wageningen, NDL.

Hotani, S. and Mihori, T. 1983. Some thermal engineering aspects of the rotation method in sterilization. In: Heat Sterilization of Food. T. Motohiro and K. Hayakawa, Eds. Koseisha-Koseikaku Co., Ltd. Tokyo, JPN.

Houtzer, R.L. and Hill, R.C. 1977. Effect of temperature deviation on process sterilization value with continuous agitators. J. Food Sci. 42:775-777.

Javier, R.A., Naveh, D., Peristein, E. and Kopelman, I.J. 1985. Convective heating rate parameters of model solutions in an agitating retort simulator. Lebensm-Wiss. u-Technol.18:311-315.

Jaworski, Z., Nienow, A.W., Koutsakos, E., Dyster, K. and Bujalski, W. 1991. LDA study of turbulent flow in baffled vessel agitated by a pitched blade turbine. Chem. Eng. Res. Des. 69:313-320.

Jones, A.T. Pflug, I.J., and Blanchett, R, 1980. Effect of fill weight on the F-value delivered to two styles of green beans processed in a Sterilmatic retort. J. Food Sci. 45:217-220.

Karwe, M.V., and Sernas V. 1996. Application of Laser Doppler Anemometry to measure velocity distribution inside the screw channel of a twin-screw extruder. J. Food Process Eng. 19:135-152.

Kays, M.W. and Crawford, M.E. 1980. Convective Heat and Mass Transfer. McGraw-Hill Book Company, New York, NY.

Koutsakos, E. and Nienow, A.W. 1989. Effects of rheological properties of simulated fermentation broths on flows in stirred bioreactors: a laser anemometry study In: Rheology of Pharmaceutical and Biological Material with General Rheology Carter, R.E., ed. pp. 284-303, Elsevier Science Publishing Ltd., Essex, GBR.

Ladeinde, F. and Torrance, K.E. 1991. Convection in a horizontal cylinder with radial and normal gravity forces. J. Fluid Mech. 228:361-385.

Lekwauwa, A, N. and Hayakawa, K. I. 1986. Computerized model for the prediction of thermal responses of packaged solid liquid food mixture undergoing thermal processes. J. Food Sci. 51:1042-1049,1056.

Lenz, M. K. and Lund, D.B. 1978. The lethality-Fourier number method. Heating rate variations and lethality confidence intervals for forced convection heated foods in containers. J. Food Proc. Eng. 2:227-271.

Lopez, A. 1987a. A Complete Course in Canning and Related Processing. Book I. The Canning Trade, Inc., Baltimore, MD.

Lopez, A. 1987b. A Complete Course in Canning and Related Processes. Book II. The Canning Trade, Inc., Baltimore, MD.

Marvin, J.G. 1983. Turbulence modelling for computational aerodynamics. AIAA J. 21: 941-955.

McLaughlin, D.K. and Tiederman, W.G. 1973. Biasing correcting for individual realization of laser anemometer measurements in turbulent flows. Phys. Fluids 16:2082-2088.

Menon, R., and Lai, T. W. 1991. Key considerations in the selection of seed particles for LDV particles. In: Laser Anemometry, Advances and Applications, vol. 1. Dybbs, A and Ghorashi, B. (eds.). The American Society of Mechanical Engineers. New York, NY. pp. 719-730.

Merson, R.L., Leonard, S.J., Mejia, E. and Heil, J. 1980. Temperature distributions and liquid side heat transfer coefficients in model liquid foods in cans undergoing flame sterilization heating. J. Food Proc. Eng. 4:85-98.

Metzner, A.B. 1956. Non-Newtonian technology: Fluid mechanics, mixing and heat transfer. Advan. Chem. Eng.1:78-153.

Naveh, D. and Kopelman, I.J. 1980. Effect of some processing parameters on the heat transfer coefficients in a rotating autoclave. J. Food Proc. Pres. 4: 67-77.

Ozisik, M.N. 1980. Heat Conduction. John Wiley and Sons, New York, NY.

Parchomchuk, P. 1977. A simplified method for agitation processing of canned foods. J. Food Sci. 42:265-268.

Peralta Rodriguez, R.D. and Merson, R.L. 1982. Heat transfer and chemical kinetics during flame sterilization. In: Food Process Engineering, Schwartzberg, H.G., Lund, D. and Bomben, J.L. (Eds.). AIChE Symposium Series. No. 218. Vol.78: 58-67.

Pflug, I.J. 1982. Measuring the integrated time temperature effect of a heat sterilization process using bacterial spores. In: Food Process Engineering, Schwartzberg, H.G., Lund, D. and Bomben, J.L. (Eds.). AIChE Symp. Series, No. 218, Vol 78: 68-75.

Plattern, J.K., Villers, D. and Lhost, O. 1986. LDV study of some free convection problems at extremely slow velocities: Sole driven convection and Marangoni convection. Third International Symposium on Applications of Laser Anemometry to Fluid Mechanics. Lisbon, PRT. July 7-9.

Quast, D.G. and Siozawa, Y.Y. 1974. Heat transfer rates during heating of axially rotated cans. Proc. IV Int. Congress Food Sci. and Technol. Vol.IV, pp. 458-468.

Rao, M.A. and Anantheswaran, R.C.1988. Convective heat transfer to fluid foods in cans. Adv. Food Res. 32:39-84.

Reich, G., Weigand, B. and Beer, H. 1989. Fluid flow and heat transfer in an axially rotating pipe-II. Effect of rotation on laminar pipe flow. Int. J. Heat Mass Transfer 32:563-574.

Reynolds, A.J. 1974. Turbulent Flows in Engineering. John Wiley & Sons. London, GBR.

Rotstein, E., Saguy, I. and Valentas, K.J. 1988. Heat processing of viscous materials in axially rotating cans. An engineering model. Intl. Symposium on Progress in Food Preservation Process, vol.1. 41. Brussels, BEL, April 12-14.

Schlichting, H. 1987. Boundary-Layer Theory. McGraw-Hill, Inc. New York, NY.

Singler, T.J. 1989. Boundary layer measurements at an internal free surface in a partially filled horizontal and rapidly-rotating cylinder. J. Fluids Eng. 111: 457-463.

Soule, C.L. and Merson, R.L. 1985. Heat transfer coefficients to Newtonian liquids in axially rotated cans. J. Food Eng. 8:33-46.

Speers, R.A. and Tung. M.A. 1986. Concentration and temperature dependence of flow behavior of xanthan gum dispersions. J. Food Sci. 51:96-98,103.

Stoforos, G.N. and Merson, R.L. 1990. Estimating heat transfer coefficients in liquid particulate canned foods using only liquid temperature data. J. Food Sci. 55:478-483,521.

Stumbo, C.R. 1973. Thermobacteriology in Food Processing. Academic Press, New York, NY.

Teixeira-Neto, R.O. 1982. Heat transfer to liquid foods during flame sterilization. J. Food Sci. 47:476-481.

Tritton, D.J. 1988. Physical Fluid Dynamics. Oxford Science Publications, New York, NY.

Tung, M.A. 1989. Concepts in Rheology- unpublished lecture notes, Technical University of Nova Scotia, Halifax, NS.

Watson, E.L. and Harper, J.C. 1987. Elements of Food Engineering. 2nd Ed. Van Nostrand Reinhold Company Inc., New York, NY.

Wedemeyer, E.H. 1964. The unsteady flow within a spinning cylinder. J. Fluid Mech. 20: 383-399.

Whitaker, S. 1976. Elementary Heat Transfer Analysis. Pergamon Press, Inc. NewYork, NY.

Zaman, S., Rotstein, E. and Valentas, K. J. 1991. Can material influence on the performance of rotating cookers. J. Food Sci. 56: 1718-1724.

APPENDIX

TERMS AND FUNCTIONS OF LDV COMPONENTS

LASER

Purpose : provides a stable, coherent light source

Type : Lexel Model 95-2 , 2W Argon ion

Features : multiline operation, beam diameter = 1.2 mm

BEAM COLLIMATOR

Purpose : controls the divergence of the laser beam

Type : TSI model 9108-1

COLOR SEPARATOR

Purpose : separates the beams at different wavelengths, and reflects the beams to polarization rotator and beam splitters

Type : TSI Color separator, model 9105

Features : 2 strong beams, blue at 488.0 nanometers and the green beam at 514 nanometers are being selected

BEAM SPLITTER

Purpose : splits the laser beam into two parallel beams each 25 millimetres from the optical axis.

Type : TSI model 9115-1

Features : intensity is equally divided (50:50) in the dual beam mode

FREQUENCY SHIFT SYSTEM

Purpose : allows measurement of flow reversals, high turbulent intensity, low velocity flows by shifting the frequency of one of the beams splitter

Type : TSI model 9180

Features : contains Bragg shift to accomplish the frequency shift

RECEIVING ASSEMBLY

Purpose : focuses the scattered light collected by the receiving lens onto the photodetector aperture

Type : TSI model 9140

Features : has x-y adjustments on the photodetector mount front lens of assembly is adjustable to optimize the focus

PHOTOMULTIPLIER SYSTEM

Purpose : converts the scattered light into electrical signals voltage, which are sent to the signal processor.

Type : TSI model 9160

BEAM STOP

Purpose : blocks off all beams produced by the Bragg cell except the high intensity shifted beam to be used

Type : TSI model 9181-4

Features : has two sets of stops at 90 degrees to each other

BEAM SPACER

Purpose : reduces the 50 mm beam spacing (produced by the beam splitter) to a spacing of 35 mm.

Type : TSI model 9113-35

Features : consists of two fixed rhombic prisms

BEAM EXPANDER

Purpose : expands the incident beam diameter 3.75 times which results in a decrease in measuring volume length and diameter and an improvement in signal-to-noise ratio

Type : TSI model 9189

TRANSMITTING (FOCUSSING) LENS

Purpose : focuses the beams exiting the beam expander

Type : TSI model 9169-450 Features: focal length = 480 mm
focal distance = 458 mm also acts as receiving lens for scattered light

SIGNAL PROCESSOR

Purpose : processes signals from the photodetector, i.e., accurately and quickly measures the dominant frequency of a Doppler signal or burst

Type : TSI model 650

DATA PROCESSOR

Purpose : processes the binary digital output of the signal processor and displays the velocity measurement

Type : PC 486/dx2 66

Features : Find software (revision 4.03) developed by TSI